University of Alberta

Biological Cell Electrophoresis on Microfluidic Chips

by

Rubin Ma

A thesis submitted to the Faculty of Graduate Studies and Research in partial fulfillment of the requirements for the degree of

Master of Science

in

Micro-Electro-Mechanical Systems (MEMS) and Nanosystems

Department of *Electrical and Computer Engineering*

Edmonton, Alberta, Canada

Spring 2006

Library and Archives Canada

Published Heritage Branch

395 Wellington Street
Ottawa ON K1A 0N4
Canada

Bibliothèque et Archives Canada

Direction du Patrimoine de l'édition

395, rue Wellington
Ottawa ON K1A 0N4
Canada

Your file Votre référence
ISBN: 0-494-13847-5
Our file Notre référence
ISBN: 0-494-13847-5

NOTICE:
The author has granted a non-exclusive license allowing Library and Archives Canada to reproduce, publish, archive, preserve, conserve, communicate to the public by telecommunication or on the Internet, loan, distribute and sell theses worldwide, for commercial or non-commercial purposes, in microform, paper, electronic and/or any other formats.

The author retains copyright ownership and moral rights in this thesis. Neither the thesis nor substantial extracts from it may be printed or otherwise reproduced without the author's permission.

AVIS:
L'auteur a accordé une licence non exclusive permettant à la Bibliothèque et Archives Canada de reproduire, publier, archiver, sauvegarder, conserver, transmettre au public par télécommunication ou par l'Internet, prêter, distribuer et vendre des thèses partout dans le monde, à des fins commerciales ou autres, sur support microforme, papier, électronique et/ou autres formats.

L'auteur conserve la propriété du droit d'auteur et des droits moraux qui protège cette thèse. Ni la thèse ni des extraits substantiels de celle-ci ne doivent être imprimés ou autrement reproduits sans son autorisation.

In compliance with the Canadian Privacy Act some supporting forms may have been removed from this thesis.

While these forms may be included in the document page count, their removal does not represent any loss of content from the thesis.

Conformément à la loi canadienne sur la protection de la vie privée, quelques formulaires secondaires ont été enlevés de cette thèse.

Bien que ces formulaires aient inclus dans la pagination, il n'y aura aucun contenu manquant.

Canada

Abstract

This thesis presents novel techniques towards biological cell separations on microfluidic chips. Specifically, the feasibility of the separation of single biological cells solely based on their difference of electrophoretic mobilities was demonstrated on microfluidic chips using red blood cells, yeast cells, and microspheres. This work also demonstrated a "true" electrophoretic separation of cells on microfluidic chips for the first time. The identification of bacterial cells (*e.g., E. coli* O157) based on immuno-fluorescence labeling and CE was also studied. We also developed methods for microchip performance assessment and microchip rejuvenation that were useful for all glass chip-based research on microfluidics. We are among the first to demonstrate these techniques on microfluidic devices, and these increase the potential for the development of low cost, high efficiency, and portable devices in the field of the life sciences and environmental monitoring.

Acknowledgements

I would like to express my sincere gratitude and appreciation to my supervisor, Professor Chris Backhouse, for providing me with the great opportunity to work in the research area of microdevices and nanotechnology. His guidance, mentorship, encouragement and support in the past two years have enabled me to be a researcher with great enthusiasm and confidence. I would also like to acknowledge the financial support from a grant awarded to Dr. Backhouse from the Natural Science and Engineering Research Council (NSERC) of Canada.

Researchers and technicians at the Backhouse lab all are excellent people. It was a great experience for me working with them for two years. Especially, I would like to extend my gratitude to Dammika Manage, Alex Stickel for their assistance with lab equipment and supplies, Vincent Sieben and Yao Zheng for their help with fluorescence microscopy and many valuable discussions. I also appreciate the help from Jana Lauzon from the Pilarski lab for her instruction on biohazard handling.

Table of Contents

Chapter 1 Introduction

1.1 Microfluidics 2

1.1.1 Shrinking of Channel Dimensions 2

1.1.2 Electrokinetic Phenomena in Microchannels 2

1.1.3 Coating of Microchannels 4

1.2 Cell Separation Techniques on Micron Scale Devices 5

1.2.1 Dielectrophoresis (DEP) 5

1.2.2 Microfiltration 6

1.2.3 Microchip-Based Flow Cytometry 6

1.3 Capillary Electrophoresis of Cells 7

1.3.1 Basics of Cell CE 7

1.3.2 Definition of "True" Separations 9

1.3.3 Opportunities and Challenges for On-chip Separations 11

1.4 Scope of This Thesis 12

1.5 References 12

Chapter 2 Rapid Performance Assessment Method for Microfluidic Chips

2.1 Introduction 15

2.2 Materials and Methods 16

2.2.1 Reagents 16

2.2.2 Microchips and Microfluidic Tool Kit 17

2.2.3 Microchip Loading 17

2.2.4 DNA Sample Injection and Separation 18

2.2.5 Flow Check Method 19

2.3 Results and Discussions 21

2.4 Conclusions 26

2.5 References 26

Chapter 3 Microchip Rejuvenation

3.1 Introduction 28
3.2 Materials and Methods 31
3.2.1 Reagents and Solutions 31
3.2.2 Microchip and Microfluidic Tool Kit 32
3.2.3 Microchip Treatments 32
3.2.4 Microchip Evaluation 33
3.2.5 Accelerated Microchip Aging 33
3.3 Results and Discussions 34
3.3.1 Establishment of the Microchip Rejuvenation Protocol 34
3.3.2 Long-term Use and Stability of Microchips 39
3.4 Conclusions 41
3.5 References 42

Chapter 4 Stability Study of CE on Microchips

4.1 Introduction 44
4.2 Materials and Methods 46
4.2.1 Reagents 46
4.2.2 Microchips and Microfluidic Tool Kit 47
4.2.3 Voltage Programs and Positioning of the Electrodes 47
4.2.4 Chemical Treatments of Platinum Electrodes 48
4.2.5 Stability of Mobilities of Single Microparticles 48
4.3 Results and Discussions 49
4.3.1 Typical Current Changing Patterns 49
4.3.2 Start Point of Electrode Surface Conditions 50
4.3.3 Effect of Electrode Positions 51
4.3.4 Effect of Electrode Materials 53
4.3.5 Stability of CE of Single Microparticles 55
4.4 Conclusions 58
4.5 References 58

Chapter 5 Electrophoretic Separation of Biological Cells on Microfluidic Chips

5.1 Introduction 60
5.2 Materials and Methods 64
5.2.1 Reagents 64
5.2.2 Latex Beads and Cells 65
5.2.3 Staining of Cells 66
5.2.4 Microchip and Microfluidic Tool Kits (μTK) 66
5.2.5 Injection and Separation of Cells on Microchips 67
5.2.6 Fluorescence Microscopy 68
5.3 Results and Discussions 69
5.3.1 Injection of Cells 69
5.3.2 Forming of Sample Plugs 73
5.3.3 LIF Detections of Cells 77
5.3.4 Separation of Cells 80
5.3.4.1 Separation of Latex Beads and Yeast Cells 81
5.3.4.2 Separation of RBCs and Yeast Cells 83
5.3.4.3 CE Buffer Selection for Human Blood Cell Separation 89
5.4 Conclusions 90
5.5 References 91

Chapter 6 Preliminary Work Towards Selective Identification of Bacterial Cells on Microfluidic Chips

6.1 Introduction 94
6.2 Materials and Methods 97
6.2.1 Reagents 97
6.2.2 Bacteria Washing and Labeling 97
6.2.3 Microchips and Microfluidic Tool Kit 98
6.2.4 Microchip Loading 99
6.2.5 Fluorescence Microscopy 99

6.3 Results and Discussions 99
6.3.1 Separation of FAbs 99
6.3.2 Detection of *E. coli*-FAb Conjugates 107
6.3.3 Specificity of the FAbs 112
6.4 Conclusions 113
6.5 References 114

Summary 116

List of Figures

Figure 1.1 Schematic description of cell separations. A) True separation of two populations of cells in the channel; B), C) false separations of cells in the channel.. 9

Figure 2.1 Diagram of a double cross microchip and the schematic drawing of sample manipulation: a) injection; b) separation. 17

Figure 2.2 Microchips with good resolution in reproducible injection/separations (A) and consistent re-injection returning times (B): t_1=2.69s, t_2=3.04s, t_3=3.13s. Y-axis is relative fluorescence intensity unit (RFU). 22

Figure 2.3 Microchips showing low signal intensity (A) and progressive increasing of re-injection returning times (B): t_1=3.94s, t_2=5.92s, t_3=9.33s 23

Figure 2.4 Microchips with poor resolution (A) and consistent re-injection returning times (B): t_1=2.93s, t_2=3.33s, t_3=3.42s 24

Figure 2.5 Microchips with rising baseline (A) and progressive reducing re-injection returning times (B): t_1=2.0s, t_2=1.3s, t_3=1.0s 25

Figure 2.6 Re-injection profile (unit of Y axis is relative fluorescence unit, RFU): All wells were disconnected in steps 7 and 11 of Table 2.2. The re-injection returning times were t_1=3.14s, t_2=3.5s, t_3=3.665s, similar behavior to that when electrophoretic separations were done (*e.g.* Figure 2.4B). Since no electrophoresis actually took place during the 'separation stage' there was no EOF and the consistent shift in return time for all but the first re-injection suggests that EOF did not play a role 25

Figure 3.1 Series of electropherograms of a representative microchip showing the effectiveness of chemical treatments. (a) A typical aged chip before chemical treatments; (b) the chip was treated with the hot H_2SO_4 process, refilled with new polymer solution and evaluated; (c) the chip from (b) was rinsed with 1 M NaOH, filled with new polymerand evaluated; (d) the chip from (c) was rinsed with 1 M HCl, filled with new polymer and evaluated; (e) the chip from (d) was treated with hot H_2SO_4, 1 M HCl rinsing, filled with new polymer and evaluated. 35

Figure 3.2 Resolution (250/300 bp) change following accelerated microchip aging. 40

Figure 4.1 Positioning of the electrodes in wells (top view) for the study of electrode position effect on electrophoresis stability 47

Figure 4.2 A typical pattern of electric current change with time. Platinum electrodes were used. Refer to section 4.2.2 for electrophoresis conditions. Current data acquisition frequency was 25 Hz. Data smoothing was performed using DPlot (version 2.0.1.4, HydeSoft computing, Vicksburg, MS, USA). Smoothing window was 100. The current measurement quantization was 100 nA (Quantized by resolution of ADC). 49

Figure 4.3 Current changing patterns after two different chemical treatments to platinum electrodes. Data smoothing was performed using DPlot (version 2.0.1.4, HydeSoft computing, Vicksburg, MS, USA). Smoothing window was 100. The current measurement quantization was 100 nA (Quantized by resolution of ADC). 50

Figure 4.4 Electric current changes with electrophoresis time. The reagent was 5GS10G. The electric field was 760 V/cm. The electrode material was nickel. Data smoothing was performed using DPlot (version 2.0.1.4, HydeSoft computing, Vicksburg, MS, USA). Smoothing window was 100. The current measurement quantization was 100 nA (Quantized by resolution of ADC). 51

Figure 4.5 A) Electropherogram obtained using platinum electrodes and definition of the curve features; B) Electropherogram obtained using nickel electrodes. Data smoothing was performed using DPlot (version 2.0.1.4, HydeSoft computing, Vicksburg, MS, USA). Smoothing window was 100. The current measurement quantization was 100 nA (Quantized by resolution of ADC). 54

Figure 4.6 Derived data from current changing curves: electric current increasing rate (h/w) against triangle area (A) 55

Figure 4.7 Typical patterns of the velocity changes of 9.6 μm single beads. Electric field was 470 V/cm. The trangle symbol represents the data point of a bead in 0.5×TBE and 5% GeneScan polymer; The circle symbol represents a bead in 1×TBE and 5% GeneScan polymer; The squre symbol represents a bead in 2×TBE and 5% GeneScan polymer. Platinum electrodes were used. 57

Figure 4.8 Velocity change with time of a latex bead when the buffer was replenished. Reagent in the channel was 0.5×TBE and 5% GeneScan polymer. Electric field was 470 V/cm. Platinum electrodes were used. 57
Figure 5.1 Diagram of a single cross microchip (Type A) 67
Figure 5.2 FEMLAB simulation of the electric field in the sample well and around inlet of the injection channel. The sample well was connected to ground; the sample waste well was connected to 0.4 kV. The conductivity of the fluid in the channel and well was assumed to be 0.1 S; its relative permittivity was assumed to be 80. A) 2D simulation, B) 3D simulation. 71
Figure 5.3 FEMLAB simulation of the electric field at the intersection of the channels. Arrows show the current direction, which is opposite to the direction of the cell migration. The buffer well was connected to ground; the buffer waste well was connected to 2.5 kV. A) the sample well and the sample waste well were floating; B) the sample well and the sample waste well were connected to 220 V. The conductivity of the buffer in the channel was assumed to be 0.1 S, the relative permittivity 80. 72
Figure 5.4 Images of cells during the injection and separation. A) Cells were injected from the sample well to the sample waste well under an electric field of 100 V/cm. B) One second later, cells were moved from the sample well to the buffer waste well to form a sample plug under an electric field of 298 V/cm. C) Another second later, a plug of cells migrated from the buffer well towards the buffer waste well under an electric field of 272 V/cm. D) Cells in the channels after one more second of the separation. No pullback voltage applied. Microscope objective magnification: 20×; halogen lamp voltage: 1.5 V. 76
Figure 5.5 Electropherograms of RBCs in 3 separation runs. The reflected light signal of RBCs (near 37 s) was detected by the optical system of the μTK. Separation electric field was 217 V/cm, with pullback voltages of 0.4 kV. Detected at 5 mm from the intersection. PMT gain was 0.8 V. 78

Figure 5.6 RBC band after a 50s separation of the run #3 in Figure 5.5. The estimated mobilities of the RBCs were 6.2+/-0.5 $\times 10^{-5}$ $cm^2.v^{-1}.s^{-1}$. Picture was taken by a Nikon Coolpix 995 camera. Microscope magnification was 100×. 78

Figure 5.7 Electropherograms of RBCs in 3 separation runs. RBCs were incubated with To-Pro-3 prior to CE. Separation electric field was 217 V/cm, with pullback voltages of 0.4 kV. Detected at 5 mm from the intersection. PMT gain was 0.8 V. 79

Figure 5.8 Electropherograms of yeast cells. Cells were stained by 5 μM To-Pro-3 iodide prior to CE. Separation electric field was 235 V/cm (with pullback voltage of 0.2 kV). PMT gain was 0.6 V. Detected at 5 mm from the intersection. 80

Figure 5.9 Image of yeast cells (non-stained) and 4 μm latex beads (non-stained) during a 5s electrophoretic separation. The 8 dark dots in the channel are 4 μm latex beads; the 2 bright dots in the channel are yeast cells. The separation medium was 5GS1TBE; the separation electric field was 117 V/cm, with pullback of 120 V. Yeast concentration in the sample well was 10 mg/ml initially; latex beads concentration in the sample well was 6 ×107 ea per milliliter. Pictures were taken by a Nikon Coolpix 995 camera mounted on a microscope (magnification, 100×)..... 82

Figure 5.10 Electropherograms of yeast cells and 4 μm beads. Cells and beads were incubated with 5 μM To-Pro-3 iodide for 10 minutes; the separation medium was 5GS1TBE; the separation voltage was 2 kV (with pullback 0.2 kV); PMT gain was 0.6 V; detected at 5 mm from the intersection..... 83

Figure 5.11 Images of RBCs and yeast cells during a separation run. Separation electric field was 217 V/cm with pull back voltage of 0.8 kV. Microscope objective magnification: 20×; halogen lamp voltage: ~1.5 V. 85

Figure 5.12 RBCs and yeast cells in the separation channel after a 25-second separation under an electric field of 217 V/cm. A) Images of the cells under a bright field; B) fluorescent images of the cells. Microscope objective magnification: 20×; reflector for the fluorescent image: Cy5, TOPRO3; exposure time for the fluorescent image:1s. 87

Figure 5.13 Electropherograms of the separations of RBCs and yeast cells. Yeast cells and RBCs were incubated with 10 μM To-Pro-3 iodide for 10 minutes before the CE. The separation medium was 5GS10G; the separation voltage was 2 kV; PMT gain was 0.8 V; detected at ~300 μm from the intersection. 87

Figure 6.1 Electropherogram of the FAbs separations on a microchip. The concentration of the FAbs was 0.125 μg/ml (1000x dilution of the stock suspension). PMT gain was 0.8 V. Separation DC field was 706 V/cm. Detection point was 4 cm from the intersection. 100

Figure 6.2 Electropherograms of the separation of the FAbs in 3 consecutive runs. A) The 1st run; B) the 2nd run; C) the 3rd run. The concentration of the FAbs was 12.5 μg/ml. PMT gain was 0.6 V. Separation DC field was 706 V/cm. Detection point was 4 cm from the intersection. 102

Figure 6.3 Electropherograms of the separation of the FAbs in 3 consecutive runs. A) The 1st run; B) the 2nd run; C) the 3rd run. The concentration of the FAbs was 0.125 μg/ml. PMT gain was 0.8 V. Separation DC field was 706 V/cm. Detection point was 4 cm from the intersection. The chip was not rejuvenated after the runs. 103

Figure 6.4 Electropherograms of the FAbs under various DC field intensities. The concentration of the antibody was 0.125 μg/ml. PMT gain was 0.8 V. Detection point was 1 cm from the intersection. Separation DC fields were 706, 529 and 353 V/cm. 103

Figure 6.5 Schematic diagram of preparation of antibody fragments, redrawn from [28]. 105

Figure 6.6 SDS-PAGE analysis of purified monoclonal antibody (anti- *E.coli*). Lane 1, non-denatured protein sample; lane 2, denatured protein sample (the reducing agent was 100 mM dithiothreitol). The resolving gel contains 12% (v/v) acrylamide, 0.39 M Tris (pH 8.8), 0.1% (v/v) SDS, 0.1% (v/v) ammonium persulfate, and 0.04% (v/v) TEMED (N,N,N',N'-tetramethylethylenediamine). The stacking gel contains 5% (v/v) acrylamide, 0.13 M Tris, 0.1% (v/v) SDS, 0.1% (v/v) ammonium persulfate, and 0.1% (v/v) TEMED. The electrophoresis buffer contains 0.025 M Tris, 0.25 M glycine (pH 8.3), and 0.1% (v/v) SDS. (Picture courtesy of the Suresh lab) 107

Figure 6.7 A) Schematic description of the microchip during injection of the labeled cells. Arrow in the channel indicates the cell migration direction. B) Electropherogram of the injection. PMT gain was 0.8 V. Detection point was at 150 μm from the sample well. C) Fluorescence images of the labeled cells in the injection channel under the fluorescence microscope. Microscope objective magnification: 40×; reflector for the fluorescent image: Cy5, TOPRO3; exposure time for the fluorescent image: 1 s..... 109

Figure 6.8 A) Schematic description of the microchip during the separation of the FAb labeled *E. coli*. The arrow indicates the direction of the cell migration. B) Electropherogram of the separation of the labeled *E. coli*. Separation medium was 5GS1TBE; the separation DC field was 235 V/cm, with pullback voltages of 220V; PMT gain was 0.8 V; detection point was 5 mm from the intersection. 110

Figure 6.9 Images of To-Pro-3 stained *E. coli* cells in the separation channel after a second separation. Separation medium was 5GS1TBE. Separation voltage was 2.5 kV with pullback 250 V. *E. coli* cells were incubated with 10 μM To-Pro-3 for 5 minutes. Microscope objective magnification: 40×; reflector for the fluorescent image: Cy5, TOPRO3; exposure time for the fluorescent image: 1 s. 111

Figure 6.10 Figure 6.10 A) Fluorescence of yeast cells after incubation with the stock FAbs. B) Image of the yeast cells in a bright field. Microscope objective magnification: 20×; reflector for fluorescent image: Cy5, TOPRO3; exposure time for fluorescent image: 1 s; halogen lamp voltage for bright field image: 1.5 V..... 112

List of Abbreviations

Abbreviation	Description
bp	Base pair
CE	Capillary electrophoresis
CZE	Capillary zone electrophoresis
DEP	Dielectrophoresis
DMF	N,N-dimethylformamide
DNA	Deoxyribonucleic acid
E. coli	Escherichia coli
EDL	Electric double layer
ELISA	Enzyme-linked immunosorbent assay
EOF	Electroosmosic flow
FAb	Fluorescence-tagged antibody
FACS	Fluorescence-activated cell sorting
FEP	Fluorinated ethylene-propylene
FWHM	Full width at half maximum
HEC	Hydroxyethylcellulose
HPMC	Hydroxypropylmethylcellulose
LIF	Laser induced fluorescence
MCE	Microchip-based capillary electrophoresis
MEMS	Micro electro mechanical systems
MPS	Microchip performance assessment
μTAS	Micro total analysis systems
μTK	Microfluidic tool kit
PBS	Phosphate buffered saline
PCR	Polymerase chain reaction
PDMS	Polydimethysiloxane
PEO	Poly(ethylene) oxide

Abbreviation	Description
PMMA	Polymethylmethacrylate
PMT	Photomultiplier tube
Pt	Platinum
PVP	Poly(vinylpyrrolidone)
RBC	Red blood cells
RFU	Relative fluorescence unit
RSD	Relative standard deviations
SDS-PAGE	Sodium dodecyl sulphate - Polyacrylamide gel electrophoresis
Si	Silicon
SIMS	Secondary ion mass spectrometry
TBE	Tris-boric acid-EDTA
TEMED	N,N,N',N'-tetramethylethylenediamine
TFFF	Thermal field-flow fractionation
UV	Ultra violet

List of Notations

Notation	Description
ν	Migration velocity of molecules in CE
μ	Electrophoretic mobility
λ	Thermal conductivity of a material
ρ	Thermal density of a material
Q	Net charge of particles
E	Electric field
f	Frictional coefficient
R	Radius of a particle
η	Viscosity

Chapter 1

Introduction

In the past years, microchips as applied to Miniaturized Total Analysis Systems [1], or μTAS, have benefited from the well-established fabrication technology of microelectronics and been applied to analysis in many different biological areas (*e.g.*, [2-4]).

Since an impressive demonstration of cell manipulations on microchips by Li and Harrison [5], microchip devices have become increasingly attractive for cellular analysis. As it is feasible to manipulate cells in microchannels, the sample preparation step coupling to other processing steps for molecular diagnostics [6] could be integrated into a single platform. The potential benefits of this integration include not only improved efficiency, but also reduced risk of sample contamination, and therefore improved sensitivity and accuracy of the analysis. Additionally, microchip-based techniques for the separation and identification of cells of interest (*e.g.*, bacterial cells, or cancer cells) have great potential to improve analysis time, system automation and cost. This is of significant importance for many fields, especially medical diagnostics, food monitoring, and environmental water testing.

This thesis presents a study of the separation of biological cells on microchips. In this work, we demonstrated on-chip manipulations and separation of a variety of biological cells, including *saccharomyces cerevisiae*, red blood cells (RBC), and *Escherichia coli* cells, at the single cell level on glass microchips. We have proved that the selection of particular cells of interest on a microchip, based solely on the difference of their electrophoretic mobilities, is feasible and promising.

This chapter commences with a brief description of some major concepts in the field of microfluidics. Then we give an overview of the state-of-art techniques for cell separations based on microdevices. As the central technology, microchip-based capillary electrophoresis (MCE) is specifically introduced in the next section. At the end of the chapter, we give a general description of the following chapters in this thesis.

1.1 Microfluidics

1.1.1 Shrinking of Channel Dimensions

As summarized in [7], besides the practical advantages such as portability and reduced reagents, the principle advantages of microfluidic devices relate to improved analytical performance. First, the shrinking of the channel dimensions results in significant reduction of both molecular and thermal diffusion times. Additionally, since small channels have larger surface to volume ratio, better heat dissipation is obtained, and this makes it possible to apply higher voltages. Moreover, since the fluid flow is laminar in small channels, band broadening from turbulence is avoided. All these features of microchips result in potentially improved efficiencies of the analysis.

On the other hand, shrinking of channel dimensions also gives rise to some problems. For instance, the interface between the microchannel and outside world become difficult as the cross-sectional dimensions shrink. Additionally, the interactions between the channel wall and samples under analysis become more significant [8]. Therefore, surface modifications become more critical for microfluidic devices.

1.1.2 Electrokinetic Phenomena in Microchannels

Microfluidic flows are readily manipulated by many kinds of external forces such as pressure, electric, magnetic, and capillary force [9]. The common method for moving reagents in the channels of microchips is electrokinetic transport. This involves two important phenomena: electroosmosic flow (EOF) and electrophoresis.

Electroosmosis refers to the bulk movement of an aqueous solution passing a stationary solid surface due to an externally applied electric field. At the interface between a glass surface and aqueous solution, silanol molecules (SiOH) on the glass surface react with free hydroxyl ions (OH^-) in the aqueous solution, forming $Si(OH)^{2-}$ and leaving the glass surface negatively charged. Free H^+ ions in the water are attracted by the negatively charged surface of glass and therefore accumulate near the surface. As a result, an electrical potential gradient arises near the interface, although the interiors of both the glass and the liquid remain electrically neutral. The region containing this electrical potential gradient is called the electric double layer (EDL) [10]. An imaginary

surface separating the thin layer of the liquid bound to the solid surface and showing elastic behavior from the rest of liquid showing normal viscous behavior is called the shear plane (slipping plane). The electric potential at the shear plane is called zeta potential. Similar electrochemical reactions occur at most liquid-solid interfaces as well as at other phase interfaces (*e.g.*, solid-gas). When an electric field is applied along the channel, the ions in the double layer move towards the electrode of opposite polarity. This creates motion of the fluid near the walls and transfers via viscous forces into convective motion of the bulk fluid. If the channel is open at the electrodes, the velocity profile is uniform across the entire width of the channel. If the electric field is applied across a closed channel (or a backpressure exists that just counters that produced by the pump), a recirculation pattern forms in which fluid along the center of the channel moves in a direction opposite to that at the walls [9].

Another electrokinetic phenomenon known as "electrophoresis" also occurs in the channels upon application of an electric field. Electrophoresis is the movement of charged molecules or particles in a stationary solution under an electrical field. It can be used to move molecules/particles in solution or to separate molecules with very subtle difference in mobilities. The velocity of a particle per unit of the applied electric field is its electrophoretic mobility μ ($cm^2\ V^{-1}s^{-1}$), which is a characteristic of individual particles and can be used as a basis of separation and purification. The electrophoretic mobility is given by [11],

$$\mu = v / E \qquad (1)$$

where v is the apparent velocity of the particle ($cm.s^{-1}$), E is the electric field ($V.cm^{-1}$).

Without effective suppression, EOF and electrophoresis generally occur at the same time in channels. Since EOF generates an essentially uniform velocity profile across the entire width of the open-ended channel, as compared to the parabolic profile seen in pressure-driven flow, the leading and trailing edge of an injected sample plug, and subsequently separated analyte zones, are flat [7, 12]. Therefore, EOF pumping was utilized as one of major approaches for cell transport in the literature [5, 13]. However, when the EOF flow is constrained at the ends of a channel, a pressure drop builds up along the channel so as to recirculate part of the fluid through the channel [9]. Additionally, bare capillary walls may show electrical heterogeneities because of defects

in the surface treatment, or by adsorption of some chemical species. When an electric current runs through a heterogeneous channel, the EOF mobility varies along the channel, triggering pressure gradients and nonuniform flows, such as recirculating rolls and multidirectional flows, within the bulk fluid [14]. As mentioned above, the effects of EOF could be more serious in microchannels due to the shrinkage of the channel dimensions. In Chapter 2, we will demonstrate a technique to monitor the flow during electrophoresis.

1.1.3 Coating of Microchannels

As discussed above, the surface modification of the microchannel is critical for microchip electrophoresis in terms of controlling electro-osmotic flow (EOF) and reducing reagent-wall interactions [15]. As summarized in [16], a variety of approaches and techniques for microchannel coating have been developed. These surface modification methods can be generally divided into two groups, (1) permanent coatings of the microchannel surface with a covalently bonded polymer layer, and (2) dynamic coatings by adsorption of a hydrophilic polymer coating to the microchannel wall. The covalent modification of microchannel surface is laborious and time-consuming [17]. In contrast, dynamic coating is much simpler. Moreover, some dynamic coating polymers [18, 19], GeneScan® polymer for instance, also serve as a sieving matrix for electrophoretic separations.

However, the dynamic coatings require regeneration after a number of consecutive runs due to unavoidable degradations of the coating during electrophoresis [20]. Fung and Yeung were the first who reported that the polymer coating on the surface of fused silica CE columns could be regenerated for DNA separation through 0.1M HCl flushing after each run [21]. Chiari *et al.* reported another coating regeneration process involving a 10-minute flushing with 0.1M NaOH [22], after which 50 reproducible runs were achieved. Despite the existence of such methods, a standard practice in the life sciences is to discard the capillary after a certain number of runs (*e.g.,* 100 runs, ABI [23]). However, this lifetime is dictated by the samples being run - *i.e.* contamination can greatly shorten the lifetime. This "aging" of microchip can introduce artifacts in electrophoretic analyses. The assessment of microchip performance and rejuvenation of "aged" microchip are two major topics that must be addressed in order to achieve

repeatable electrophoresis. In Chapter 3, we will introduce a rejuvenation method for microchips.

1.2 Cell Separation Techniques on Micron Scale Devices

The separation of cells would enable the identification of rare, abnormal cells in large populations, thus potentially providing early disease detection and prevention. Besides its importance in life sciences, cell separation techniques are also of vital importance in environmental monitoring (*e.g.*, bacteria in freshwater). In the past, the separation of cells has involved two general approaches, single cell methods and fractionation methods. Single-cell techniques, such as flow cytometry [24], rely on spatially isolating microorganisms from mixed populations. Fractionation techniques, such as selective culture, differential centrifugation, filtration, and adsorption methods, operate at the population level and separate mixtures into subpopulations based on biological, chemical, and/or physical differences between individual groups of cells. Both conventional single-cell techniques and fractionation techniques employ expensive equipment, or are labor intensive. An efficient, convenient, and cost effective technique is required.

There are several reasons making microfluidic devices and systems attractive for analysis of single cells [25], including the possibility of easy integration of analytical protocols into a single platform, the availability of multiple methods for cell manipulations, and the potential of high efficiencies. Several concepts or techniques for the separation of cells on micro devices have been reported in the literature. Among those techniques, dielectrophoresis, micro-filtration, and microchip-based flow cytometry are popular and are briefly described below.

1.2.1 Dielectrophoresis (DEP)

All types of cells exhibit exclusive physiological and morphological states which give them particular dielectric fingerprints [26]. The dielectric properties of cells vary in accordance to the magnitude and frequency of the applied electric voltage, the dielectric characteristic of the suspending medium and the geometry of the electrodes. Under the appropriate set of conditions, any bio-particle will react in one of two opposite ways, either migrate into strong electric fields or move into weak electric fields. DEP, which

utilizes the interaction of intrinsic dielectric properties of the cells and the applied inhomogeneous electric filed, has become an active cell separation and sorting technique.

Studies on DEP techniques have been reported in the literature attempting to distinguish cells by their age, anomalies, history in culture media, or hemophilic traits [27, 28]. Although the DEP technique is not limited to differentiating based on cell sizes and it does not require cell staining for detection, it requires buffers with specific low conductivity, and therefore, the original sample has to be pre-treated or diluted with appropriate chemicals to obtain the desired conductivity. Moreover, the sensitivity and efficiency of DEP are affected by electro-dynamic flow and cell-cell interactions in the presence of inhomogeneous fields [29]. These limitations make it challenging for the future integration of cell analysis on a Lab-on-a-chip device.

1.2.2 Microfiltration

Cell filtration techniques are based on using the size difference of cells to separate them by means of physical barriers. The physical barriers are usually porous membranes or hollow fibers [30]. For instance, porous membranes can retain cells bigger than their pore sizes but let smaller cells go through. Micro-filtration [31, 32] relies on microfabricated structures such as arrays of posts, tortuous channels, comb-shaped filters, etc.

An advantage of this technique is that it does not require specific buffer conditions. However, it does require a size difference between desirable and undesirable cell types. Besides, the success of the separation often depends on other factors like the cell deformability, cell concentration, viscosity of the medium, and the driving force [33]. Moreover, fouling and clogging problems also hinder the application of this technique.

1.2.3 Microchip-Based Flow Cytometry

Flow cytometry is used to measure certain physical or chemical properties of cells as they pass by in single file. Commercialized flow cytometers have been available in the market for years. They realize cell sorting through measuring differences in fluorescence with high accuracy. In order to generate single file of cells, hydrodynamic focusing in a sheath fluid is employed in flow cytometers. Optical signals are collected as the particles (*e.g.*, cells) pass the detector. To sort, the jet is broken into droplets by a nozzle, and droplets

containing chosen particles are electrostatically deflected. A throughput on the order of 10^4 cells/s is common with available instruments. Using several antibodies tagged with different fluorescent labels, scientists can measure several variables in a cell population simultaneously. This multiparametric method eliminates several separate runs to measure more than one parameter. Coupling the fluorescence staining to flow cytometry, Fluorescence-Activated Cell Sorting (FACS) has become a powerful technique for cell sorting.

Microfabricated cytometers have been reported in the literature in recent years. For instance, Fu *et al.* reported a microfabricated FACS device [34], which was demonstrated with sorting of microbeads and *E. coli* cells using electrokinetic flow. The disposable sorting device is fabricated using soft lithography, which enables the design and fabrication to be inexpensive and flexible. However, the throughput of the device is only about 20 cells/s. Another microfluidic device for cytometry of fluorescently labeled *E. coli* samples was reported by McClain *et al.*[35]. The channels of the device were coated in order to reduce cell adhesion and suppress the electroosmotic flow. The throughput of the device was about 30~80 cells/s. An impressive electrokinetic focusing technique that confines cells spatially by application suitable voltages was introduced by McClain *et al.* in the report. Similarly, the sheath flow concept of conventional flow cytometry is also accomplished in the LabChip (Caliper Life Science, Hopkinton, MA, USA) by using buffer flows moving from side channels into the cell-transporting channel. This flow-pinching method facilitates single file particle detection without the worry of channel clogging, a complication associated with the alternative method of focusing by narrowing the channel dimension.

1.3 Capillary Electrophoresis of Cells

1.3.1 Basics of Cell CE

The surface of biological cells (*e.g.*, bacteria) contain a variety of charged polymers, such as sialic acid, polysaccharides, lipopolysaccharides, and proteins, and these contain an array of ionizable groups such as carboxyl, phosphate, sulfate, and amino moieties [36]. Most cell surfaces contain both positively and negatively charged groups and tend to be

amphoteric, with a net positive charge at low pH and a net negative charge at high pH. In liquid media, the charged surface polymers interact with counter ions from the surrounding media to produce an electric double layer, which determines the zeta potential of the cell [37]. The zeta potential is influenced by many factors, such as the cell type, age, and properties of the surrounding media including the pH, ionic strength, and chemical composition [37, 38].

According to the principles of electrophoresis [39], when DC electric field (E) is applied along the separation channel, a force equal to QE (where Q is the net charge of the cell) will act on the cell. When the cell is set to move from rest, a frictional force $f(dx/dt)$ (where f is the frictional coefficient and dx/dt is the velocity of the cell) will act in the opposite direction (Stokes' law [39]). According to Newton's second law, the following equation will hold for an isolated particle in a perfect insulator [39]:

$$m\frac{d^2x}{dt^2} = QE - f\frac{dx}{dt} \qquad (2)$$

where m is the mass of the particle, Q is the net charge of the particle, E is the electric field applied, f is the frictional coefficient, dx/dt is the velocity of the particle. The equation (1) can be solved as:

$$\frac{dx}{dt} = \frac{QE}{f}\left(1 - \exp\left[-\left(\frac{f}{m}\right)\right]t\right) \qquad (3)$$

For spherical particles f is equal to $6\pi\eta R$, where R is the particle radius and η is the viscosity. For instance, a 4-μm polystyrene microsphere has the frictional coefficient

$f = 6\pi\eta R = 3.35 \times 10^{-5}$ gram/s, where η is assumed 0.89 cP (centi-Poise, 1 cP = 10^{-2} gram. cm $^{-1}$. s $^{-1}$), the η of water at 25 °C [40]. Refer to Table 1.1 for the viscosity data of some materials.

$m = \rho(4/3)\,\pi R^3 = 3.5\times 10^{-11}$ g, where ρ is assumed 1.055 $gram/cm^3$ [41].

Since the value of $f/m \approx 1\times 10^6$, the value of exp $(-f/m)t$ decreases to $1/e$ in about 10^{-6} sec., and therefore for periods longer than about 10^{-5} sec., equation (2) reduced to

$$\frac{dx}{dt} = \frac{QE}{f} \qquad (4)$$

Therefore, the migration velocity of cells is proportional to the charge-to-size ratio in a certain electrophoretic medium. The cell accelerates rapidly until the electric force is

balanced by the frictional force in a very short time (*e.g.*, $< \sim 10^{-5}$ seconds for a 4 μm latex bead).

The electrophoresis of cells is one of the earliest techniques to separate cells and study events at the level of the membranes of single cells. The intensity of this surface charge varies with the type of cell, and this allows separation of cells based on migration mobility in an electric field in large-scale systems. Since the 1920s [42], generations of scientists have been trying to improve the techniques of cell CE by introducing new instruments and developing new protocols. Using this approach, the separation of one population of cells from others is on the basis of difference of their electrophoretic mobilities, no matter if there is distinct size or density range from others [43, 44]. However, these conventional separation techniques require expensive equipment and are labor intensive, which results in the failure of these electrophoresis techniques to be widely used.

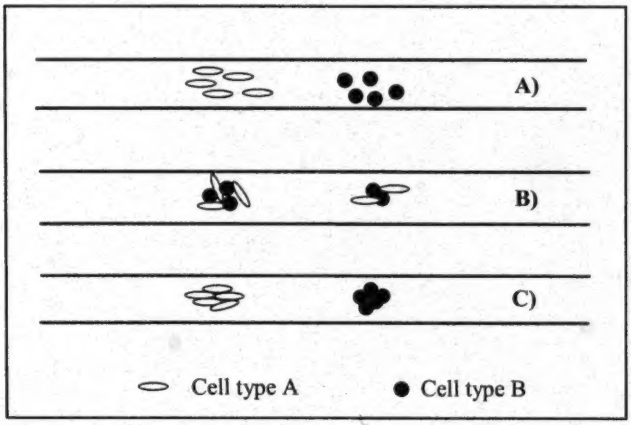

Figure 1.1 Schematic description of cell separations. A) True separation of two populations of cells in the channel; B), C) false separations of cells in the channel

1.3.2 Definition of "True" Separations

A mixture of different types of cells may be separated into fractions in the separation channel. An apparent separation may be suggested by the separated peaks in the electropherogram (a plot of signal (*e.g.*, fluorescence) intensity over time). Unfortunately, the apparent separation based on the electropherogram may be a false separation in terms of the purity and the repeatability of the mobility of cells in each fraction. As shown in Figure 1.1A, if each fraction of the separation is reliably composed of only one type of

cells (without clumping), we consider the separation to be a true separation (*i.e.*, it could be used to provide meaningful information). The "true separation" has been clearly established in macroscopic CE (but not on microchips) [36]. If each fraction of the separation is an agglomeration of different type of cells (as shown in Figure 1.1B), we consider the separation to be a false separation (*i.e.*, any peaks are likely the result of random clumping events and provide little if any information on the cells themselves). In case that each fraction is an agglomeration of only one type of cells (as shown in Figure 1.1C), the apparent mobility of each fraction is not repeatable due to the size of the agglomeration may change with the cell numbers in the clump. We consider the separation in Figure 1.1C to be another type of false separation.

In recent years, laser-induced fluorescence (LIF) coupling with capillary electrophoresis has been employed for the detection and separation of cells. Armstrong and coworkers have applied CE to separate bacterial cells [13]. The apparent separation of *M. luteus, E. aerogenes, P. fluorescens, and S. cerevisiae* was achieved in less than 10 min, using a capillary having dimensions of 100-μm i.d. and 27 cm length. According to the author, by properly using a polymer additive (*i.e.*, polyethylene oxide (PEO)) in the running buffer, the electropherogram of microbes could be transformed from broad peaks into sharp peaks that increased the separation efficiency. It was subsequently found in other works by Armstrong *et al.* that aggregation played a significant role in obtaining single sharp peaks during the CE separation of cell mixtures [45-47]. According to Armstrong *et al.* [47], the agglomeration of cells require a dilute polymer solution (*i.e.*, polyethylene oxide (PEO)) in the separation medium, electroosmotic flow, and a DC electric field. In their report [47], three possible mechanisms of the aggregation of colloidal particles were outlined, including "Field-Induced Aggregation Model", "Hairy Particle Model" and "Shape-Induced Differential Mobility Model". However, the study of the described agglomeration of microorganisms in Armstrong's report is in its infancy.

It is apparent that the aggregation of cells during the CE could result in poor repeatability of the migration time due to the random sizes of the agglomerations. Although the correlation between the peak height, or mobility and the number of cells in the cluster may be found, the identification of cells based on the electrophoretic mobility is difficult. Additionally, since the purification of cells in each fraction of the separation

was not clearly shown in Armstrong *et al.*'s reports, the separations were false separations based on our definition. The question remains: is the microchip-based identification of single cells based solely on their apparent electrophoretic mobility truly feasible?

1.3.3 Opportunities and Challenges for On-chip Separations

Microchip-based CE has been successfully used in the separation of biomolecules [48-51]. It has several advantages over conventional large-scale counterparts, which have been discussed earlier. As for biological cells, CE on microchips remains a new area for researchers. Besides these practical advantages of microchips over conventional capillaries, a couple of advantages may be available for the separation of cells on microchips. According to Pfetsch and Welsh, thermal field-flow fractionation (TFFF) type effects might be one of the causes of the poor resolutions of cell CE on capillaries [52]. TFFF itself is an elution separation technique similar to chromatography except the separation field is normal to the sample flow [53]. Due to the use of relatively large inner diameter capillaries, the thermal gradient in the direction normal to the sample flow in the capillary may be involved as the separation field of the TFFF. Using microchips, this type of effect could be effectively minimized due to a better heat dissipation of the microchannels as discussed earlier in this chapter. Uncoated capillaries were employed for the CE of cells in most capillary-based publications. The apparent mobility of cells was thus the result of both their electrophoretic mobility and the electroosmotic mobility of the bulk fluid. For instance, in the report from Armstrong *et al.* [13], negative-charged cells migrated towards –ve electrode due to a significant EOF. Since the bulk fluid flow of EOF may result in hydrodynamic effects, especially on microchips as discussed above, the suppression of EOF may improve the separation of cells. In our lab, dynamic coatings are being successfully used in DNA separations on microchips for the suppression of EOF. The application of those dynamic coatings in cell CE on microchips may unveil true differences of mobilities among various types of cells.

On the other hand, the CE of cells on microchip is challenging in some aspects. For instance, the CE of cells in earlier reports often employed very low concentration buffers [13, 36, 52], which may not be suitable for CE on microchips because the small

reservoirs on microchips have low buffering capability (*i.e.*, pH readily changed by current-induced electrolysis). This topic will be addressed in Chapter 4 and 5.

1.4 Scope of This Thesis

Focusing on the CE separation of cells on microchips, the thesis is summarized in seven chapters. Concepts and a general discussion of the thesis are introduced in this chapter. The next two chapters introduce two important techniques, the flow check and microchip rejuvenation techniques. The following chapter explores the long-term stability of electrophoresis, in terms of the change of the electric current. The observations and discussions in that chapter provide useful information on the repeatability of cell electrophoresis. In Chapter 5, separations of biological cells are demonstrated on microchips. Chapter 6 presents some preliminary work towards identification of bacteria cell based-on immuno-fluorescence binding and CE. The conclusion and future work is summarized in Chapter 7.

Table 1. 1 Viscosity Data

Liquid at 25 °C	Viscosity (cP)
Water	0.89
Methanol	0.0547
Ethylene glycol	~16
PDMA (25 kDa) [a)]	25

a) A mixture of 6.5 % PDMA, 8 M urea, 100 mM TAPS (pH 8). Viscosity was measured at 30°C [54]

1.5 References

[1] A. Manz, N. Graber, H. M. Widmer, *Sensors and Actuators B-Chemical* 1990, 1, 244-248.

[2] V. Dolnik, S. Liu, S. Jovanovich, *Electrophoresis* 2000, 21, 41-54.

[3] N. A. Lacher, K. E. Garrison, R. S. Martin, S. M. Lunte, *Electrophoresis* 2001, 22, 2526-2536.

[4] A. J. Gawron, R. S. Martin, S. M. Lunte, *European Journal of Pharmaceutical Sciences* 2001, 14, 1-12.

[5] P. C. H. Li, D. J. Harrison, *Analytical Chemistry* 1997, 69, 1564-1568.

[6] Y. Huang, E. L. Mather, J. L. Bell, M. Madou, *Analytical and Bioanalytical Chemistry* 2002, 372, 49-65.

[7] M. U. Kopp, H. J. Crabtree, A. Manz, *Current Opinion in Chemical Biology* 1997, 1, 410-419.

[8] V. Sieben, C. Backhouse, *Electrophoresis* accepted at June, 2005.

[9] H. Stone, A. Stroock, A. Ajdari, *Annual Review of Fluid Mechanics* 2004, 36, 381-411.

[10] B. Kirby, E. Hasselbrink, *Electrophoresis* 2004, 25, 187-202.

[11] A. Zhu, Y. Chen, *Journal of Chromatography* 1989, 470, 251-260.

[12] Pretoriu.V, B. J. Hopkins, J. D. Schieke, *Journal of Chromatography* 1974, 99, 23-30.

[13] D. W. Armstrong, G. Schulte, J. M. Schneiderheinze, D. J. Westenberg, *Analytical Chemistry* 1999, 71, 5465-5469.

[14] A. E. Herr, J. I. Molho, J. G. Santiago, M. G. Mungal, T. W. Kenny, M. G. Garguilo, *Analytical Chemistry* 2000, 72, 1053-1057.

[15] E. A. S. Doherty, K. D. Berglund, B. A. Buchholz, I. V. Kourkine, T. M. Przybycien, R. D. Tilton, A. E. Barron, *Electrophoresis* 2002, 23, 2766-2776.

[16] E. A. S. Doherty, R. J. Meagher, M. N. Albarghouthi, A. E. Barron, *Electrophoresis* 2003, 24, 34-54.

[17] N. J. Munro, A. F. R. Huhmer, J. P. Landers, *Analytical Chemistry* 2001, 73, 1784-1794.

[18] H. J. Tian, J. P. Landers, *Analytical Biochemistry* 2002, 309, 212-223.

[19] J. C. Sanders, M. C. Breadmore, Y. C. Kwok, K. M. Horsman, J. P. Landers, *Analytical Chemistry* 2003, 75, 986-994.

[20] J. Horvath, V. Dolnik, *Electrophoresis* 2001, 22, 644-655.

[21] E. N. Fung, E. S. Yeung, *Analytical Chemistry* 1995, 67, 1913-1919.

[22] M. Chiari, M. Cretich, J. Horvath, *Electrophoresis* 2000, 21, 1521-1526.

[23] Applied-Biosystems, *ABI PRISM® 310 Genetic Analyzer User's Manual* 2001, 1-20.

[24] M. J. Fulwyler, *Blood Cells* 1980, 6, 173-184.

[25] H. Andersson, A. van den Berg, *Sensors and Actuators B-Chemical* 2003, 92, 315-325.

[26] P. R. C. Gascoyne, J. V. Vykoukal, *Proceedings of the Ieee* 2004, 92, 22-42.

[27] F. F. Becker, X. B. Wang, Y. Huang, R. Pethig, J. Vykoukal, P. R. C. Gascoyne, *Proceedings of the National Academy of Sciences of the United States of America* 1995, 92, 860-864.

[28] Y. Huang, K. Ewalt, M. Tirado, R. Haigis, A. Forster, D. Ackley, M. Hellller, J. O'Connell, M. Krihak, *Analytical Chemistry* 2001, 73, 1549-1559.

[29] T. Heida, W. L. C. Rutten, E. Marani, *Journal of Physics D-Applied Physics* 2002, 35, 1592-1602.

[30] D. Voisard, F. Meuwly, P. A. Ruffieux, G. Baer, A. Kadouri, *Biotechnology and Bioengineering* 2003, 82, 751-765.

[31] P. Yuen, L. Kricka, P. Fortina, N. Panaro, T. Sakazume, *Genome res* 2001, 405-412.

[32] P. Wilding, J. Pfahler, *Clin Chem* 1994, 40, 43-47.

[33] P. Wilding, L. J. Kricka, J. Cheng, G. Hvichia, M. A. Shoffner, P. Fortina, *Analytical Biochemistry* 1998, 257, 95-100.

[34] A. Y. Fu, H. P. Chou, C. Spence, F. H. Arnold, S. R. Quake, *Analytical Chemistry* 2002, 74, 2451-2457.

[35] M. A. McClain, C. T. Culbertson, S. C. Jacobson, J. M. Ramsey, *Analytical Chemistry* 2001, 73, 5334-5338.

[36] R. C. Ebersole, R. M. McCormick, *Bio-Technology* 1993, 11, 1278-1282.

[37] M. E. Bayer, J. L. Sloyer, *J. Gen. Microbiol.* 1990, 136, 867-874.

[38] M. F. DeFlaun, C. W. Condee, *J. Hazard. Mater.* 1997, 55, 263-277.

[39] O. Gaal, G. A. Medgyesi, L. Vereczkey, *Electrophoresis in the separation of biological macromolecules* John Wiley & Sons, 1980.

[40] R. C. Weast, Ed., *CRC handbook of chemistry and physics* CRC Press, Boca Raton, FL, 1988.

[41] Interfacial Dynamics Corporation "Certificate of analysis for surfactant-free sulfate white polystyrene latex" (2003), Portland, OR, USA.

[42] C. B. Coulter, *J. Gen. Physiol.* 1920, 3, 309.

[43] T. G. Pretlow, T. P. Pretlow, Eds., *Cell separation methods and selected applications,* Academic Press, London, NY, 1982.

[44] D. S. Kompala, P. Todd, Eds., *Cell separation science and technology,* American Chemical Society, Washington, 1991.

[45] J. M. Schneiderheinze, D. W. Armstrong, G. Schulte, D. J. Westenberg, *Fems Microbiology Letters* 2000, 189, 39-44.

[46] L. F. He, R. J. Jepsen, L. E. Evans, D. W. Armstrong, *Analytical Chemistry* 2003, 75, 825-834.

[47] D. W. Armstrong, M. Girod, L. F. He, M. A. Rodriguez, W. Wei, J. J. Zheng, E. S. Yeung, *Analytical Chemistry* 2002, 74, 5523-5530.

[48] C. Backhouse, M. Caamano, F. Oaks, E. Nordman, A. Carrillo, B. Johnson, S. Bay, *Electrophoresis* 2000, 21, 150-156.

[49] C. Backhouse, H. J. Crabtree, D. M. Glerum, *Analyst* 2002, 127, 1169-1175.

[50] C. Backhouse, T. Footz, S. Adamia, L. M. Pilarski, paper presented at the ICMENS, Banff, AB, Canada, 2003, p. 377-382, IEEE Computer Society, Los Alamitos, California, U.S.A.

[51] C. J. Backhouse, A. Gajdal, L. M. Pilarski, H. J. Crabtree, *Electrophoresis* 2003, 24, 1777-1786.

[52] A. Pfetsch, T. Welsch, *Fresenius J. Anal. Chem.* 1997, 359, 198-201.

[53] T. L. Edwards, B. K. Gale, A. B. Frazier, *Analytical Chemistry* 2002, 74, 1211-1216.

[54] R. S. Madabhushi, *Electrophoresis* 1998, 19, 224-230.

Chapter 2

A Rapid Performance Assessment Method for Microfluidic Chips

2.1 Introduction

In this chapter, we present a method to assess microchip performance for on-chip electrophoretic separations. The assessment is realized through electrophoretic manipulation of a DNA size standard using specially designed electric voltage programs. Results achieved from the assessment could be used as an indicator of microchip "aging" in terms of lowered resolutions and fluctuations in electro-osmotic flow (EOF).

As the size shrinks, the surface modifications of the microchannel become more critical for microchip electrophoresis in terms of controlling electro-osmotic flow (EOF) and reducing reagent-wall interactions [1, 2]. We have employed dynamic coating for microchannels in our work, because it is much simpler than other approaches [2]. However, the dynamic coatings require regeneration after a number of consecutive runs [3], because "aging" of the coating can introduce artifacts in electrophoretic analyses.

It is well known that the onset of EOF is one of the key indicators of microchip "aging". In 1996, Williams *et al.* reported an EOF measurement method that is cited frequently in the literature [4]. In that method, a neutral dye is used as an EOF marker whose movement indicates the presence of EOF. The Williams method requires precisely controlled pressure for the placement of the neutral dye band. For applications on a microchip the use of an accurate pressure driven injection is far more difficult than electrical injection, but since the dye is neutral only the pressure driven injection is feasible. Munro *et al.* described a method of degradation-analysis for a coated capillary [5], and this method involved EOF measurement (also using a neutral dye) with the analysis of a DNA size standard before and after exposing the capillary to a 1×TBE/PCR mixture for extended periods of time.

The method we present in this chapter can be easily integrated into analysis procedures without the requirement of special samples. This method of microchip performance assessment (MPA) for on-chip electrophoresis provides information upon resolution and EOF. It is quantitative and can warn of performance loss. In our work on cell manipulations on-chip, those moving micro-scale particles which may often physically contact or scratch the surface of channel wall, may easily destroy the coatings of the channel. Therefore, the monitoring of chip performance is even more frequently performed.

This chapter is based on a published conference paper by Ma et al.[6].

2.2 Materials and Methods

2.2.1 Reagents

GeneScan® polymer (7%, P/N: 401885) was obtained from PE Biosystems (Foster City, CA, USA). The DNA size standard, GeneScan® 500 was obtained from Applied Biosystems (Streetsville, ON, Canada). The sieving matrix for DNA fragment separation was 5% GeneScan® polymer and 10% Glycerol ("5GS10G"). Glycerol (SigmaUltra, lot No.: 121K0121) was obtained from Sigma-Aldrich (St Louis, MO, USA). Trizma base and Boric Acid were obtained from Fisher Scientific. EDTA was obtained from Merck (KGaA, Darmstadt, Germany). Genetic Analyzer Buffer with EDTA ("GABE", part #402824) was obtained from Applied Biosystems. Depending on the application, "1TBE10G" (1×TBE and 10% glycerol) or GABE was selected as running buffer. We assess chip performance using the same buffer as in the application of interest. The formulation of sieving matrix and buffer was based on the protocol published in "GeneScan® Reference Guide – Chemistry Reference for the ABI310, Applied Biosystems, 2000" [7].

2.2.2 Microchips and Microfluidic Tool Kit

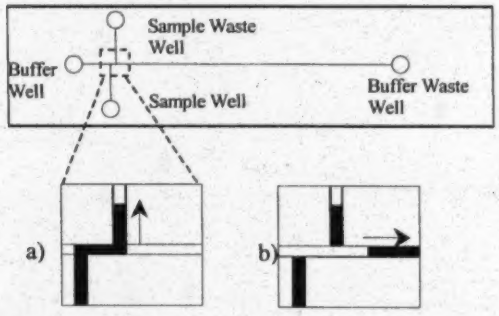

Figure 2.1 Diagram of a double cross microchip and the schematic drawing of sample manipulation: a) injection; b) separation.

Figure 2.1 shows a double cross microchip (Micralyne Inc., Edmonton, AB) consisting of 4 wells (or reservoirs) linked by two microchannels, one of which serves as a separation channel approximately 80 mm in length, the other one serves as an injection channel approximately 8 mm in length. The channels are nominally 50 μm wide and 20 μm deep. Both double cross (Figure 2.1) and single cross (two channels intersecting at right angles) microchips were used in this work. Their electrophoretic behavior was indistinguishable.

The Microfluidic Tool Kit (μTK, Micralyne) was used to manipulate reagents and DNA samples. The μTK is designed to facilitate the operation of electrophoretically based protocols upon microchips by providing the necessary high voltages and a laser induced fluorescence (LIF) excitation and detection system. In this work we used a LIF system that provides excitation at a wavelength of 532 nm and detection at 578 nm. A compiled LabVIEW® interface supplied by Micralyne was used to record the LIF signal at 200 Hz. Analysis of the fluorescence data proceeded by means of a C program programmed in our lab. The microchips and the μTK were described in more detail elsewhere [8].

2.2.3 Microchip Loading

Before loading any reagents, the microchip has to be cleaned thoroughly. All reservoirs are rinsed with water, followed by a pressure-driven rinsing of the channels using a 1 mL syringe (fitted with a 0.45 μm filter). At least 3 μl water is pumped through the channels

from the "buffer waste well". A flow of air is then maintained through the chip until dry. The channels and wells of the chip are examined under a microscope and if particles or agglomerations are seen (*e.g.* dried polymer or contaminating particles), then the rinsing and drying is repeated. After microchip cleaning, the sieving matrix ("5GS10G" solution) is forced into the channel from the "buffer waste well" using a syringe. Then each reservoir is loaded according to Table 2.1.

Table 2.1 Reagents in each well of the microchip for MPA

Reagent	Sample well	Buffer well	Sample waste well	Buffer waste well
1TBE10G	-	3 μL	3 μL	3 μL
1:10 Dilution of 1TBE10G	2.7 μL	-	-	-
GeneScan 500	0.3 μL	-	-	-

2.2.4 DNA Sample Injection and Separation

Following the loading of reagents, the chip is immediately mounted into the μTK. The LIF detection point is located 76 mm downstream from the intersection of channels to the "buffer waste well". The injection/separation voltage program of the μTK involves applying 500V/cm electric field between the "sample well" and the "sample waste well" for 60s (the 1st time injection/separation), and consequent 705 V/cm between the "buffer well" and the "buffer waste well" for 180s. As the electric potential is applied along injection channel (400V at the "sample waste well", the "sample well" ground), the negatively charged DNA fragments move toward the "sample waste well". After several seconds the sample DNA fills the injection channel. If a voltage is then applied at the "buffer waste well" (6 kV) with the "buffer well" held at ground (all other wells disconnected), the sample contained in the intersection (the sample plug) is separated into its constituents along the separation channel. The arrival time of each strand of DNA at the LIF detection point will be determined by its mobility, a function of its length.

To verify repeatability, a second injection/separation is conducted. Because the "sample well" arm of injection channel has now been filled with the sample, the second

injection can be much shorter, *i.e.* 10 s and this is the only difference between the 2nd injection/separation and the 1st.

During the process of injection/separation, all the data is recorded and then analyzed by the software programmed in our lab. The migration time, peak amplitude, FWHM (full width at half maximum) and migration velocity of the peaks are generated automatically. We first calculated a term (Rs) as in [7]:

$$Rs = |P_1 - P_2| / (0.5 \times (W_1 + W_2)),$$

Where P_1 and P_2 are the peak arrival times during separation, W_1 and W_2 are the full-widths at half maximum of the peaks. The resolution we used was the product of the difference in the fragment length between a given peak and the next peak divided by Rs. Resolutions of the peaks 200bp and 250bp were used for the resolution assessments in this work.

2.2.5 Flow Check Method

The flow check starts after the second injection/separation. The LIF detection point is relocated to 125 μm from channel intersection toward the "sample well". The electric voltage and polarity settings of the μTK for the flow check are listed in Table 2.2.

The flow check includes three stages. Each stage starts by applying a separation voltage for 5s to remove the sample plug from the channel intersection and move it towards the LIF detection point (steps 2, 5 and 9 in Table 2.2). An extra 40s injection is added before the 5 seconds separation in the 1st stage (step 1 in Table 2.2). Then the sample in the injection channel is pulled back toward the "sample well" and the "sample waste well" respectively (steps 3, 6, and 10 in Table 2.2). After that, the separation voltage is applied between the "buffer well" and the "buffer waste well" for various durations (0s, 30s and 60s for each stage respectively). After each such separation, the sample is again moved toward the intersection (step 4, 8 and 12 in Table 2.2). Each such re-injection stage tests how long it takes for the DNA sample to return to the detection point after different separation intervals (each of which may have produced an EOF-induced movement).

Table 2.2 Voltage Program for Flow Check

Step	Time	Sample waste well	Buffer waste well	Sample well	Buffer well
1	40s	0.40 kV	Float	Ground	Float
2	5s	Float	6.00 kV	Float	Ground
3	15s	0.20 kV	Float	0.20 kV	Ground
4	10s	0.40 kV	Float	Ground	Float
5	5s	Float	6.00 kV	Float	Ground
6	15s	0.20 kV	Float	0.20 kV	Ground
7	30s	Float	6.00 kV	Float	Ground
8	10s	0.40 kV	Float	Ground	Float
9	5s	Float	6.00 kV	Float	Ground
10	15s	0.20 kV	Float	0.20 kV	Ground
11	60s	Float	6.00 kV	Float	Ground
12	10s	0.40 kV	Float	Ground	Float

When present, the EOF typically flows towards the cathode in a bare microchannel. This physical movement of fluid will lead to pressure variations in the channel, resulting in movement. With the effects of any EOF during the various periods of separation (0s, 30s or 60s) the DNA should take shorter or longer times (depending on the direction of flow) to return to the detection point. Otherwise the time interval for the DNA to return to the detection point should be consistent, assuming other pressure-driven flow is negligible.

We have found that other sources of flow (*e.g.* pressure-driven flow) are generally negligible unless a microchip is loaded with greatly different levels of reagents in the various reservoirs. Such effects could be tested by adding a 4^{th} flow-test stage, in where the separation step is conducted without an applied voltage (*i.e.* no electrophoresis). This would test for pressure driven flow rather than EOF.

As one of key indicators of EOF, the sample's returning time in each flow check stage (named t_1, t_2, t_3 for each stage respectively) is determined based on data derived from electropherograms of the flow check. First, the average and standard deviation are calculated for the LIF data in the last portion of the preceding pullback step (when no DNA is present). Upon the return of the sample, the time when the signal is equal to the average plus 100 times the standard deviation is defined as the sample returning time. The difference between the 2^{nd} re-injection and the 1^{st} re-injection is defined as $d_1 = t_2 -$

t_1. The difference between the 3rd re-injection and the 1st re-injection was defined as $d_2 = t_3 - t_1$.

2.3 Results and Discussions

The microchip performance assessment (MPA) method is based on the electrophoretic separations of DNA fragments and an electro-osmotic flow (EOF) check. All such tests are done using the same load of reagents and require less than 10 minutes. The resolution of the electrophoretic separations was assessed with a DNA size standard commonly used in sequencing applications (GeneScan 500). Near-single-base-pair resolution could be achieved from a very rapid separation on a simple cross microchip [9]. The resolution is sufficient for many genetic analysis applications, including heteroduplex analysis of single nucleotide polymorphisms (SNPs) [10, 11]. In addition, Backhouse *et al.* have developed a microchip-based method of attaining the resolution characteristics of a very large separation distance through a series of electrophoretic operations in a channel that is only a few mm long [8].

Figure 2.2A shows the arrival of a broad and incompletely resolved set of peaks (near 90s) followed by a series of peaks, each representing the passage of a set of progressively longer strands of DNA at the detection point at 76 mm, near the buffer waste well. Such a set of DNA strands of varying lengths is known as a 'DNA ladder'. Figure 2.2A is this electrophoretic run with a repetition. Figure 2.2B represents the three successive electropherograms produced in the flow check phases of Table 2.2: steps 4, 8 and 12. In each of these the fluorescence signal indicates the presence of DNA returning to the intersection after a pullback step. (Similarly for Figure 2.3B, 2.4B and 2.5B) Variations in this return time are often an indicator of the presence of EOF.

Based on our MPA results, microchips could be divided into four categories: a) those with good resolution and $d_1 \approx d_2 \approx$(approx) 0.5s (Figure 2.2); b) those showing poor resolution (or no DNA peak) and $t_3 > t_2 > t_1$ (Figure 2.3); c) those showing poor resolution and $d_1 \approx d_2 \approx$(approx) 0.5s (Figure 2.4); d) those showing rising baseline and $t_3 < t_2 < t_1$ (Figure 2.5).

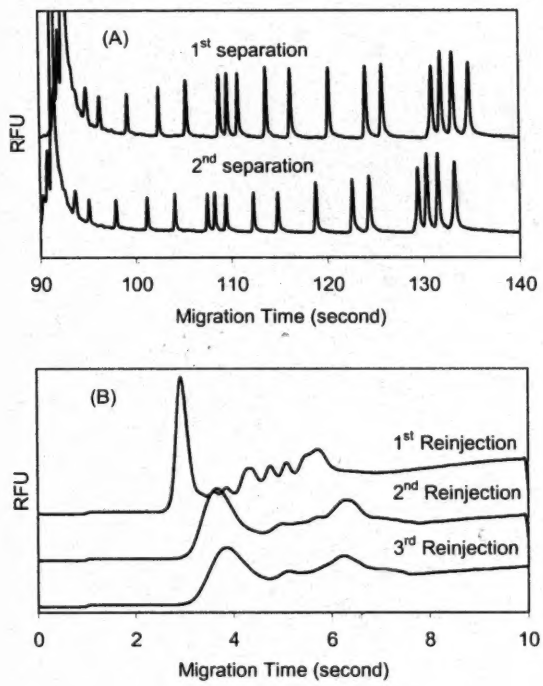

Figure 2.2 Microchips with good resolution in reproducible injection/separations (A) and consistent re-injection returning times (B): t_1=2.69s, t_2=3.04s, t_3=3.13s. Y-axis is in relative fluorescence intensity units (RFU).

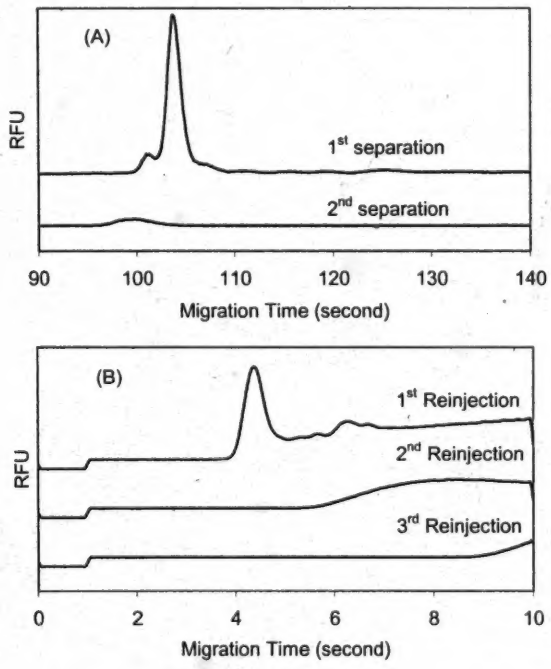

Figure 2.3 Microchips showing low signal intensity (A) and progressive increasing of re-injection returning times (B): t_1=3.94s, t_2=5.92s, t_3=9.33s

In the electropherogram of each injection/separation, microchips of type a) (Figure 2.2A) show a very strong initial peak followed by uniform DNA ladder peaks of equally strong intensity. In the electropherogram of each re-injection in the flow check (Figure 2.2B), a very low signal is present for several seconds as the DNA approaching the detection point. Upon the arrival of the returning DNA, a strong signal peak is first present, followed by minor signal variations.

Microchips of type a) have resolution of (approx.) 5 bp on average at the DNA fragment peak of 200 bp. We define good microchips as those having resolution better than 8 bp at the peak of 200 bp. Surprisingly, the resolution of brand new microchips at the peak 200 bp is, on average, 6.2 bp (based on 3 microchips), worse than the average of type a). The relatively poor resolution of brand new microchips may be related to the time needed to fully form the polymer coating of the wall - the adsorption kinetics of polymer coatings requires a certain period of time to allow polymer to reach its adsorption plateaus [1], brand new microchips may need longer time for the formation of a stable polymer layer compared with used microchips.

For microchips of type b), the intensity of peak signals is greatly reduced (Figure 2.3A). The progressive increasing of the time interval for the return of the sample plug (Figure 2.3B) indicates that the sample was significantly influenced by EOF.

Microchips of type c) show poor resolution of the DNA fragment separation (Figure 2.4A). However, the consistency of the DNA return times (Figure 2.4B) suggests that the poor resolution is not due to EOF.

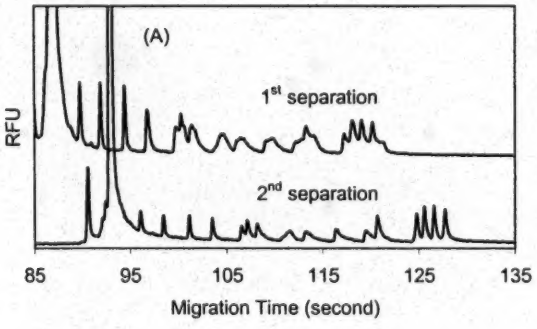

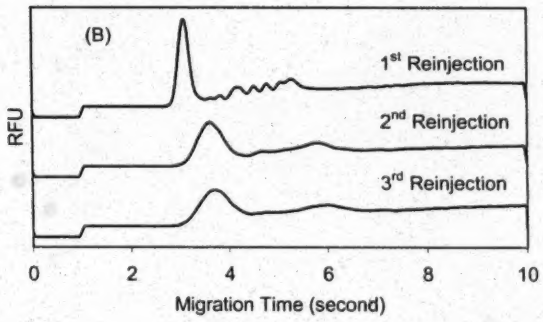

Figure 2.4 Microchips with poor resolution (A) and consistent re-injection returning times (B): t_1=2.93s, t_2=3.33s, t_3=3.42s

For microchip type d), the rising baseline (Figure 2.5A, the typical baseline of electropherogram achieved using our μTK system is less than 0.15 V.) indicates the sample "leakage" during the second injection/separation run. The progressive shortening of the time interval for the return of the sample plug (Figure 2.5B) indicates that the sample was drawn toward the intersection by the separation being performed in a neighboring channel. Longer separation times led to more movement of the sample toward the intersection. This would be consistent with movement under EOF. For eliminating the sample "leakage", applying the "pullback" voltage during separation was suggested in [8]. We prefer not to apply the pullback voltage in electrophoretic analysis because we need to be able to detect the onset of EOF as it may affect our peak arrival time.

An interesting observation is that even in good microchips there is a significant difference between t_3 and t_2 on the one hand, and t_1 on the other. This suggests that there is another mechanism at work that affects t_1 differently than t_2 and t_3 – *i.e.* that EOF is not playing a role in this difference in arrival times. Since the flow check involves multiple steps of injection and pullback in the relatively short injection channel, space charges in the channel may vary with time and so does the current. The variance of the current probably resulted in the difference between t_3 and t_2 on the one hand, and t_1 on the other. In Chapter 4, we will address the topic of space charge limited current in more detail.

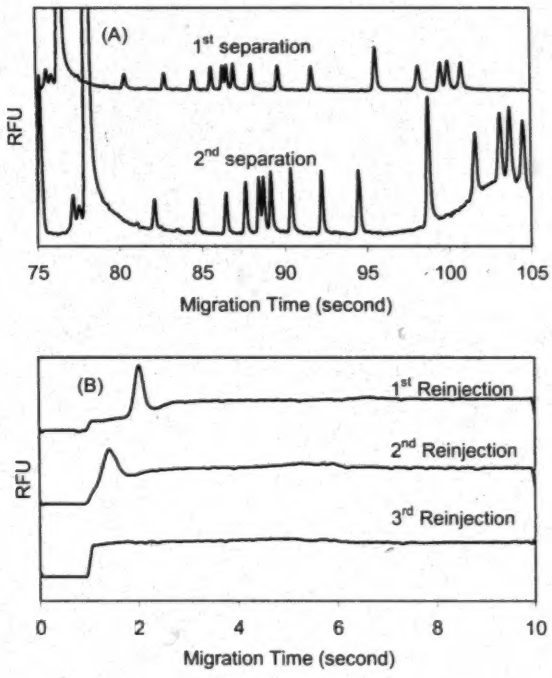

Figure 2.5 Microchips with rising baseline (A) and progressive reducing re-injection returning times (B): t_1=2.0s, t_2=1.3s, t_3=1.0s

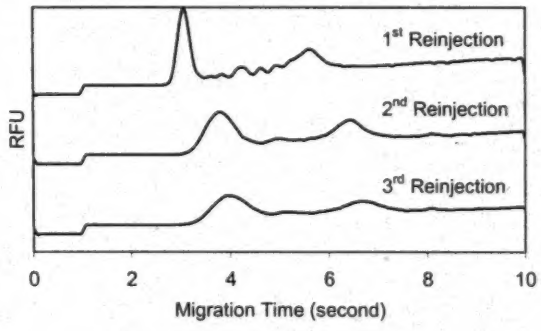

Figure 2.6 Re-injection profile (unit of Y axis is relative fluorescence unit, RFU): All wells were disconnected in steps 7 and 11 of Table 2.2. The re-injection returning times were t_1=3.14s, t_2=3.5s, t_3=3.665s, similar behavior to that when electrophoretic separations were done (*e.g.* Figure 2.4B). Since no electrophoresis actually took place during the 'separation stage' there was no EOF and the consistent shift in return time for all but the first re-injection suggests that EOF did not play a role.

In order to corroborate this, we performed a second set of measurements of a microchip with a revised program in which all four wells were disconnected for steps 7 and 11 (of the sequence shown in Table 2.2). This means that there were no separation

steps and hence there could be no production of EOF from the separation. As shown in Figure 2.6, our results were essentially identical to the result in regular EOF check. The same behavior was found in other "good microchips". This surprising result suggests that the act of injecting and separation has introduced a perturbation that "relaxes" on a time scale of 30s or so. We propose that this perturbation is an alteration of the ionic distribution within the injection arm, a perturbation that is affected by sequence and timing of the injection and pullback steps. This is consistent with our observation of sample stacking effects leading to a transient increase in the fluorescence intensity by a factor of approximately 3 in the first analysis, and 2 in the following two analyses (*e.g.* Figure 2.6). This increase is obviously associated with a localized higher concentration of (charged) fluorescently tagged DNA. Such a concentration could easily give rise to a localized high-field region that would dissipate once the applied voltages were removed. The time required for such dissipation could readily be on the time scales we have observed. This effect is analogous to the high field domain seen in the Gunn effect [12] observed in III-V semiconductors. In the present work we are using sample "stacking effects" to better inject sample, this being done by using a 0.1×TBE in the "sample well". However, we have found much the same behavior when using exactly the same buffers in the "sample well" as used in the other wells. We are studying this phenomenon further but note that it could significantly affect the performance (*e.g.* resolution) of microchip applications.

2.4 Conclusions

The microchip performance assessment method presented in this chapter is capable of monitoring the performance of microchips in a manner that does not require special equipment, requires little time, and could make use of virtually any sample (*e.g.* PCR product) for the assessment of EOF. This monitoring is quantitative and may allow the provision of warnings about imminent performance loss of the microchip.

2.5 References

[1] E. A. S. Doherty, K. D. Berglund, B. A. Buchholz, I. V. Kourkine, T. M. Przybycien, R. D. Tilton, A. E. Barron, *Electrophoresis* 2002, 23, 2766-2776.

[2] E. A. S. Doherty, R. J. Meagher, M. N. Albarghouthi, A. E. Barron, *Electrophoresis* 2003, 24, 34-54.

[3] J. Horvath, V. Dolnik, *Electrophoresis* 2001, 22, 644-655.

[4] B. A. Williams, G. Vigh, *Analytical Chemistry* 1996, 68, 1174-1180.

[5] N. J. Munro, A. F. R. Huhmer, J. P. Landers, *Analytical Chemistry* 2001, 73, 1784-1794.

[6] R. Ma, K. Kaler, C. Backhouse, paper presented at the ICMENS Proceedings, Banff, AB, Canada 2004, pp. 680-686,IEEE Computer Society, Los Alamitos, California, U.S.A.

[7] Applied-Biosystems, "GeneScan Reference Guide - Chemistry Reference for the ABI310-Applied Biosystems" (2000).

[8] C. J. Backhouse, A. Gajdal, L. M. Pilarski, H. J. Crabtree, *Electrophoresis* 2003, 24, 1777-1786.

[9] C. Backhouse, T. Footz, S. Adamia, L. M. Pilarski, paper presented at the ICMENS, Banff, AB, Canada 2003, p. 377-382, IEEE Computer Society, Los Alamitos, California, U.S.A.

[10] T. Footz, M. J. Somerville, R. Tomaszewski, K. A. Sprysak, C. J. Backhouse, *Genetic Testing* 2003, 7, 283-293.

[11] T. Footz, M. J. Somerville, R. Tomaszewski, B. Elyas, C. J. Backhouse, *Analyst* 2004, 129, 25-31.

[12] S. M. Sze, *Physics of semiconductor devices* Wiley, New York, ed. 2nd ed., 1981.

Chapter 3

Microchip Rejuvenation

3.1 Introduction

In Chapter 2, a rapid microchip assessment method was presented. In case that an "aged" microchip was found, rejuvenation of the chip had to be performed. In this chapter, we present a method to rejuvenate glass microchips that had been used for capillary electrophoresis (CE) to the extent that their performance was degraded. This degradation was due to one of two mechanisms, (1) a deterioration of the polymer coating on the inner surface of the microchannel, or (2) an aging of the glass substrate.

Since the introduction of microfluidic devices in the early 1990s [1, 2], glass has been the dominant fabrication material. This is primarily because the fabrication methods in glass have been well established by the semiconductor industry, the surface properties of glass have been well characterized by the chromatography industry among others, and that many properties of glass, such as optical transparency, chemical inertness and the lack of electrical conductivity are very suitable for use in microfluidic systems. However, glass microchips have possibly limited lifetime and relatively complex fabrication procedures, and these result in high cost. Principally due to the higher manufacturing costs of glass devices, much effort is being invested in the development of polymer-based microfluidic devices (PDMS [3, 4], PMMA[5, 6], *etc.*). However, glass has several advantages over polymers as a material for microfabrication. In particular, its rigidity and flatness facilitate alignment in multi-layer structures [4, 7]. If glass microchips can be rejuvenated and thereby be given a long lifetime, then it is feasible to explore higher levels of integration and functionality on glass microchips even in applications requiring a low cost-per-test. Although the glass chips may be costly, their benefits, coupled with their long lifetimes, will allow the manufacturing cost to be recouped. For this reason it is critically important for the glass microfabrication technology to ascertain whether it is

feasible to improve the longevity of glass microchips through surface modification and regeneration.

As aforementioned, it is unavoidable that the dynamic polymer coatings degrade during electrophoresis [8] and this deterioration of the capillary wall coating results in a loss of resolution. The degradation is due to a variety of factors such as adsorption of ionic compounds [9] and alkaline hydrolysis [10]. To extend the useful lifetime of a microchip, regenerations of the dynamic coating must be performed after a number of consecutive runs. The regeneration process typically involves chemical treatments of the capillary and refilling with polymer solution. In 1995, Fung and Yueng introduced a regeneration method for poly(ethylene oxide) (PEO) coated fused silica columns in the application of DNA sequencing [11]. This method extended the capillary lifetime for more than 30 runs through flushing with 0.1M HCl for 10~15 minutes after each run (otherwise, the capillary had to be replaced after one or two runs due to a dramatic degradation of separation resolution). HCl was also used in the dynamic coating regeneration processes demonstrated by Iki *et al.* for PEO coatings [12] and Yan *et al.* for poly(vinylpyrrolidone) (PVP) coating [13]. Sodium hydroxide (NaOH) was also reported as a common chemical for capillary regeneration (*e.g.* [14, 15]). Shihabi reported another procedure for hydroxypropylmethylcellulose (HPMC) coating regeneration: the capillary was washed between samples with 0.2 M NaOH for 0.5 min and with 0.2M HCl for 0.5 min [16]. Most of the aforementioned regeneration processes [11-13, 16] were used on fused silica capillaries and had to be performed after each run in order to restore the original performance in CE. More recently, Chiari *et al.* reported that 50 DNA separation runs were achievable with the same capillary after each regeneration of the poly(dimethylacrylamide-co-allyl glycidyl ether) coating by 10 minutes of flushing with 0.1 M NaOH [17]. Tian and Landers also reported that HCl flushing was performed on microchips as the key step of the regeneration of their hydroxyethylcellulose (HEC) coating and a slight decrease in resolution and an increase in migration time in DNA separations were observed after approximately 100 runs [18]. Often the approach taken is similar to that proposed by [19], *i.e.* that the capillary or microchip be replaced after ~100 runs.

In our lab, GeneScan® polymer (Applied Biosystems Inc., Foster City, CA, USA), a PDMA-based polymer for dynamic coating [20], is being extensively used for CE on microchips. The proposed mechanisms for the dynamic wall coating of PDMA includes hydrogen bonding of the polymer with silanol groups on the silica surface [21], and hydrophobic interactions between polymer segments and the hydrophobic siloxane groups on the silica surface [8, 22]. Madabhushi *et al.* reported a regeneration method for PDMA coating that consisted of consecutive washings with water, tetrahydrofuran, and 1M HCl [8]; Ren *et al.* reported another method involving 30 minutes of flushing with 1M HCl and 5 minutes of water rinsing. However, with either method the number of CE runs with comparable resolution decreased dramatically after regenerations.

It is common for the regeneration procedures reported in the literature to incompletely rejuvenate the microchip – the subsequent performance is limited in terms of resolution and/or the number of runs that can be performed before deterioration again sets in. Hence, it is common to discard the capillary or microchip rather than to attempt regeneration. It is unclear as to whether the incomplete rejuvenation is due to insufficient removal of degraded polymer or to an ongoing degradation of the glass itself. Therefore, the aging effects of glass substrates have to be studied and minimized in order to extend microchip lifetime and determine if a regeneration process can work "forever". The possible mechanisms of glass aging include glass corrosion [23] and ion migration [24-26]. According to Kaupp *et al.* [23], during the long-term storage of a capillary the surface corrosion is steady and continuous. However, they found that this "storage effect" could be minimized by filling the capillary with dry air of low relative humidity and sealing it afterwards. As discussed by Verzele *et al.*, chromatographic grade silica may contain a variety of metals: Na, Ca, Fe, Mg, Al, and Ti [27] that are present at significant concentrations (*e.g.* several hundred *ppm* [28]) and influence the surface properties [29]. It is also well known that alkali ions such as sodium are leached out from the glass to an aqueous solution in contact with the glass (in a process of ion exchange) [24-26]. To our knowledge, the glass aging effect due to ion migration within the glass, and ion movement from glass to buffer has yet to be investigated in microfluidic devices. Generally, investigations into adsorbates on glass or the migration of ions into glass requires complex equipment such as SIMS [30]. Moreover, many of these surface

characterization techniques do not readily lend themselves to the analysis of the interior of microfluidic channels. In this work, we introduce a simple method for investigating glass-aging effects by assessing the CE performance of microchips before and after various methods of rejuvenation (including glass annealing).

We have compared different chemical treatments on microchips and developed a rejuvenation protocol with simple processing steps that can completely rejuvenate microchips even after extensive use. Following the protocol presented here, more than 50 "aged" microchips in our lab were effectively rejuvenated and reused with performance equal to that of brand new chips and this suggests that the "aging effect" of the glass substrate is negligible. We believe that, through rejuvenation, glass microchips can be used indefinitely; we suggest that this finding makes feasible the exploration of high levels of integration and functionality on glass microchips.

This chapter is based on a recently published journal paper by Ma et al. [31].

3.2 Materials and Methods

3.2.1 Reagents and Solutions

GeneScan® polymer (7%, P/N: 401885) and GeneScan® 500 (a DNA ladder) were obtained from Applied Biosystems (Foster City, CA, USA). . A Tris-borate with EDTA buffer (TBE) was made with Tris base and boric acid from Fisher Scientific (Fair Lawn, NJ, USA) and EDTA from Merck (Darmstadt, Germany). The running buffer, referred to as "1TBE10G", was made with glycerol (SigmaUltra, lot No.: 121K0121) from Sigma-Aldrich (St Louis, MO, USA) and TBE buffer so that the final concentration of glycerol was 10% w/w, and the TBE was 1×TBE (pH: ~8.4). The sieving matrix for DNA fragment separation was 5% (w/w) GeneScan® polymer and 10% (w/w) Glycerol in 1×TBE buffer (referred to as "5GS10G"). The formulation of sieving matrix and buffer was based on the protocol published in the "GeneScan® Reference Guide – Chemistry Reference for the ABI310, Applied Biosystems, 2000" [19]. Concentrated Sulfuric Acid (H_2SO_4, *c.a.* 96%) was obtained from Anachemia (Montreal, QC, CA). 5 M sodium hydroxide (Fisher Scientific, Nepean, Ontario, Canada) was diluted to 1 M

concentrations. 1M HCl solution was diluted from *c.a.* 37% HCl, which was obtained from Anachemia (Montreal, QC, Canada).

3.2.2 Microchip and Microfluidic Tool Kit

Standard microchips were used in this work. Refer to Chapter 2 for descriptions of microchips and the μTK.

3.2.3 Microchip Treatments

The microchips were prepared with one or more of the following treatment procedures.

In the "hot H_2SO_4 process" a hot plate (Corning PC 351) was preheated to ~350 °C under a fume hood. All wells of the microchip were rinsed with distilled water followed by a pressure-driven rinsing of the channels using a 1 ml syringe (fitted with a 0.45 µm filter). At least 3 µl of distilled water was pumped through the channels from the buffer waste well. Air was subsequently pumped through the microchannel by syringe until no water droplets were found in the wells and channels (as seen under inspection by microscope). About 3 µl of concentrated sulfuric acid was added into the buffer waste well and allowed to fill the microchannels via capillary forces. All wells were then filled with 3 µl of H_2SO_4. The microchip was then placed on top of the preheated hotplate for about 1 minute until the H_2SO_4 acid boiled out. The microchip was left in the air for about 5 minutes to allow it to cool gently down to room temperature. Finally, the chip was rinsed with distilled water for about 3 minutes and dried by syringe-pumped air for 2 minutes.

Microchip flushing: The microchip flushing was performed using an in-house manufactured unit that can accommodate 3 microchips at once. A 100 μl volume of HCl or NaOH solution was forced through from the buffer waste well to the other wells by applying nitrogen at 45 psi. It took about 30 minutes for the chemical solution to pass through the channels completely. After flushing with the chemical solutions, the microchannels and reservoirs of the microchips were rinsed for 3 minutes and dried for 2 minutes (as described above).

Microchip annealing: Before annealing, the microchip was rinsed and dried (as described above in the flushing procedure). The channels and wells of the microchips

were then examined under a microscope. The rinsing and drying was repeated if particles or agglomerations (*e.g.* dried polymer or contaminating particles) were seen. The microchip was placed in a glass-annealing oven for an overnight cycle, in which the oven temperature was gradually raised to its highest point (~560 °C) and cooled slowly to allow the release of stress. After annealing, the microchip was rinsed and dried again.

3.2.4 Microchip Evaluation

The microchip evaluation employed in this work involved the separation of a DNA size standard, GeneScan® 500, in "5GS10G". The LIF detection point is located 76 mm downstream (from the intersection of channels to the buffer waste well). The injection/separation process involves applying a 500V/cm electric field between the sample well and the sample waste well for 60s, and consequently 705 V/cm between the buffer well and the buffer waste well for 180s. Data derived from the electropherogram was analyzed with a C++ computer program. As a measure of resolution, we compute the smallest difference in DNA size that could be resolved, based on the method recommended by Heller *et al.*[32].

$$Rs = \tfrac{1}{2}(w_1 + w_2) / (\Delta t_m / \Delta M) \qquad (1)$$

Where Rs is the resolution (with units of base pairs, or bp), Δt_m is the difference in migration time between the two adjacent peaks (in seconds), w_1 and w_2 are the peak half-widths (FWHM, in seconds), and ΔM is the difference in length (in base pairs) between the two fragments.

If the resolution of a rejuvenated chip was comparable with that of a brand new chip, a test for EOF was performed to assess its performance further (previously described in [33]). In brief, this method is based on the use of LIF detection to measure EOF-based movement of the sample in the injection arm during separation runs.

3.2.5 Accelerated Microchip Aging

We followed a similar approach to that described by Munro *et al.* [15], who assessed the coating longevity of covalently coated capillaries. The microchips were loaded with reagents, as in the DNA separations described above and an electrical field was applied for an extended period of time; the buffer waste well was set to 6 kV, the buffer well was

set to ground, and the other two wells were disconnected. The electric field was applied for 20 or 40 minutes, and then one set of microchip performance data was obtained. If no apparent degradation was found, new reagent was added into wells and the aging test was continued. To avoid the drying out of reagents or the requirement for frequently replenishing reagents during a long time run, sections of micropipette tips were cut and fitted into microchip wells to increase the running buffer volume from 3 μl to 9 μl in each well.

3.3 Results and Discussions

3.3.1 Establishment of the Microchip Rejuvenation Protocol

The objective of the rejuvenation protocol is to restore the surface state of the microchannels and recover the microchip performance in CE. In this work, we assessed the effectiveness of a rejuvenation protocol by comparing the performance of a "rejuvenated" microchip with that of new microchips in terms of the resolution in DNA separations. EOF values were not used as a primary evaluation tool since EOF flow was not detectable unless the chip was severely degraded. The severe degradation was more easily detected by monitoring the ongoing loss of resolution. To investigate the effect of each single chemical treatment, a microchip performance assessment was performed after each step.

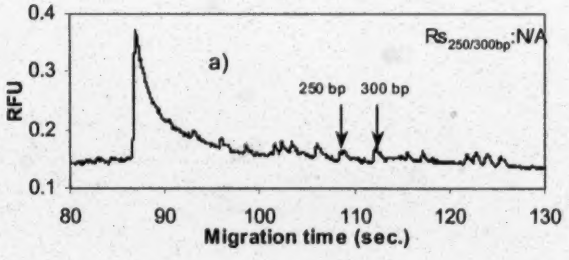

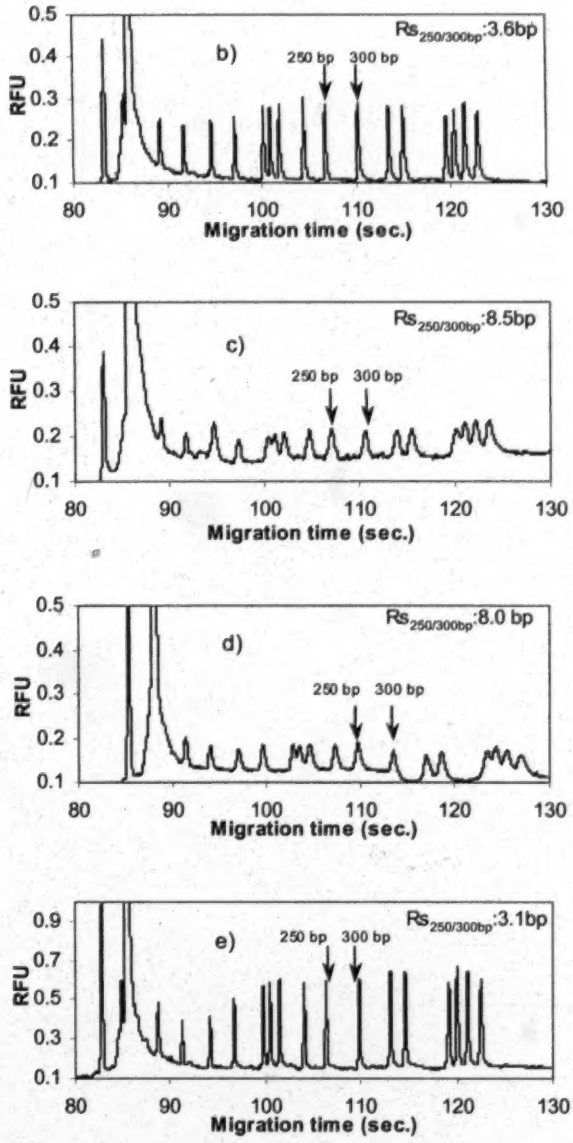

Figure 3.1 Series of electropherograms of a representative microchip showing the effectiveness of chemical treatments. (a) A typical aged chip before chemical treatments; (b) the chip was treated with the hot H_2SO_4 process, refilled with new polymer solution and evaluated; (c) the chip from (b) was rinsed with 1 M NaOH, filled with new polymerand evaluated; (d) the chip from (c) was rinsed with 1 M HCl, filled with new polymer and evaluated; (e) the chip from (d) was treated with hot H_2SO_4, 1 M HCl rinsing, filled with new polymer and evaluated.

Figure 3.1a shows the electropherogram of a typical aged microchip before treatment. This chip gave unresolved peaks due to serious peak tailing and signal loss.

After treatment with the hot H_2SO_4 process, a new solution of GeneScan® polymer ("5GS10G") was introduced into the micro-channels. DNA (GeneScan® 500) analysis was performed subsequently and, as shown in Figure 3.1b, a significant improvement in peak profile was achieved. Peak resolutions were restored to their normal levels (~3.6 bp for 250/300 bp). Statistically, the microchips treated with only the hot H_2SO_4 process achieved comparable resolution (on average) to brand new microchips that had had no chemical treatment in advance at all, and both groups had large relative standard deviations (RSDs) associated with peak resolution (Table 3.1, and discussed below). The large variation in the performance of brand new microchips may be due to factors such as the surface roughness of different fabrication batches [34-36] and to the non-optimal surface conditions resulting from the last stages of their microfabrication. We have noted that the resolution of a new microchip often improves for the first several uses and we attribute this to the gradual removal of residual contamination from the fabrication process. We occasionally found debris or particles in the channel under a 100× magnification after the microchip was treated with the hot H_2SO_4 process. (These were readily removed by subsequent HCl or NaOH rinsing.) This indicates the cleanliness of the channel varies after the hot H_2SO_4 process due to debris and particles, and this variation results in high RSD in the resolution. We also tried a number of rejuvenations with the hot plate temperature reduced from ~350 °C to ~200 °C and found that the resulting chip performance was equivalent to that with the hot plate at ~350 °C. Since much longer processing times were required to boil out the acid when the temperature was lower, we set the hotplate temperature to be ~350 °C for all the remaining tests.

Following directly its H_2SO_4 treatment for Fig 2b, the same chip was flushed with 1 M NaOH, rinsed with distilled water and dried, filled with new polymer and evaluated. The resultant electropherogram is shown in Figure 3.1c. The same chip was then flushed with 1M HCl, rinsed with distilled water and dried, filled with new polymer and evaluated. The resultant electropherogram is shown in Figure 3.1d. If the HCl or NaOH solutions were able to completely remove the polymer from the channel wall we might expect to see comparable resolution between Figure 3.1b on the one hand, and 3.1c and 3.1d on the other. Surprisingly, the microchip performance shown in Figure 3.1c and 3.1d has deteriorated dramatically. Lastly, the same chip was given the hot H_2SO_4 process,

rinsed with HCl, rinsed with distilled water and dried, filled with polymer and evaluated. The resultant electropherogram is shown in Figure 3.1e. This dramatic degradation suggests that the NaOH or HCl flushing were unable to remove the polymer, and instead degraded the performance of the coating.

Since water is a poor solvent for PDMA, the desorption of PDMA only by water has an extremely high energy of activation [8]. According to Madabhushi *et al.* [8], consecutive washings with water, tetrahydrofuran, and 1M HCl were not effective in removing all the adsorbates on the inner surface of capillary channels in DNA analysis. In order to completely remove polymer adsorbed on microchannel walls, we tried a variety of solvents including methanol [37, 38], ethanol, dioxane [39] and N,N-dimethylformamide (DMF) [39, 40]. Among those solvents, DMF worked better than others in a 6-hour-long flushing process, which generated equivalent results to the hot H_2SO_4 process. However, those treatments were time consuming and the need to avoid the dissolution of equipment (*e.g.* seals) by those organic solvents made the processing difficult and cumbersome.

Table 3.1 Chemical Treatment Comparisons

Resolution	**Group 1**		**Group 2**		**Group 3**		**Group 4**		**Group 5**	
	Ave. (bp)	RSD	Ave. (bp)	RSD	Ave. (bp)	RSD	Ave. (bp)	RSD	Ave. (bp)	RSD
250/300 bp	4.1	13.5%	3.5	14.5%	7.4	21.5%	3.3	6.0%	3.3	6.2%

Group 1 (5 microchips tested): brand new microchips without chemical treatment before performance assessment; Group 2 (9 microchips tested): treated with the hot H_2SO_4 process only; Group 3 (4 microchip tested): treated with 1M NaOH or 1M HCl alone; Group 4 (9 microchips tested): treated with the hot H_2SO_4 process, 1M NaOH flushing and 1M HCl flushing (resolution data for 2 chips in 9 were not available due to failure of assessments); Group 5 (9 microchips tested): treated with the hot H_2SO_4 process, and 1M HCl flushing.

In the literature, the proposed mechanisms for the adsorption of polymer onto a silica surface include hydrogen bonding of the polymer with silanol groups [21], and

hydrophobic interactions between polymer segments and the hydrophobic siloxane groups on the silica surface [8, 9, 22]. According to these mechanisms, the weakly bonded polymer coating can be easily removed by water rinsing and renewed by refilling. However, based on our observations, it appears that GeneScan® polymer cannot be completely removed by water rinsing, nor with mild chemicals. This indicates that covalent linkages between channel wall silanols and GeneScan® polymer may be involved in the formation of the polymer coating. If that is the case, harsh processing conditions may be needed for the cleaning of channel walls coated with GeneScan® polymer. Table 3.1 shows the statistical resolution data for 5 groups of chips: 1) brand new chips, 2) chips treated with the hot H_2SO_4 only, 3) chips treated with HCl or NaOH alone, 4) chips subjected to HCl and NaOH flushes immediately after the hot H_2SO_4 process, and 5) chips subjected to HCl flushes immediately after the hot H_2SO_4 process. Microchips treated with the hot H_2SO_4 process and 1M HCl showed the best results, in terms of average resolution and RSD data, with results even better than that of brand new chips. The experimental data in Table 3.1, Figures 3.1b and 3.1e indicate that the hot H_2SO_4 process is capable of removing the polymer coating completely.

The statistical data of Table 3.1 and Figure 3.1e also show that microchips treated with the hot H_2SO_4 process and HCl flushing have better performance than chips treated only with the hot H_2SO_4 process. This may suggest that the bare silica surface treated with HCl is favorable for the adsorption of polymer. The number of non-reactive sites [28] must have been reduced by the mild HCl flushing (conditioning), and therefore an ample fraction of the inner surface was coated by the adsorption of polymer molecules. Fung and Yeung attributed the effect of HCl to the titration of silanol groups to their original protonated state, which was ionized at pH 8.2 in buffer solutions [11] . Ren *et al.* made the assumption that hydrogen bonding was the main force driving the interactions between the polymer and the glass surface, making HCl a suitable glass surface conditioner. We think the improvement after HCl conditioning may also be explained by the leaching of metal ions from the surface of glass. It was claimed by Nawrocki [28] that trace metallic impurities are probably a source of additional adsorption sites on silica and that they increase the activity of neighboring silanols. Those additional adsorption sites make the glass surface more heterogenous and affect its coating properties. About two

thirds of these trace metals can be removed from the silica surface by HCl washing [28, 41]. NaOH is not our recommended chemical for conditioning, although the etching of the inner surface of capillaries by NaOH could reduce capillary performance variation among batches and manufacturers (according to Cifuentes [14]). It has been demonstrated [42] that the use of capillary wall conditioning methods based on flushing with NaOH, followed by HCl (or vice versa) can leave the silica surface in a state of chaos — it was found there that the silanol groups undergo a profound hysteresis loop before returning to their original ionization state two weeks later. Our experimental result was in agreement with those earlier findings: the microchip treatment with the hot H_2SO_4 process, NaOH flushing and HCl flushing often achieved comparable results to those from the method involving the hot H_2SO_4 process and HCl flushing only, however, the former method (the combination of the hot H_2SO_4 process, NaOH flushing and HCl flushing) was not always successful (2 in 9 chips failed the evaluation after treatment with electropherograms resembling Figure 3.1a, and no resolution data was available). Hence, the final established rejuvenation protocol was: the aged microchips were treated with the hot H_2SO_4 process, rinsed with distilled water for 3 minutes, dried by air for 2 minutes, and flushed for 30 minutes with 100 μl 1 M HCl (flow induced by 45 psi of nitrogen applied at the HCl reservoir). We speculate that the effectiveness of the sulfuric acid in cleaning the surface (over HCl) is due to the increased reactivity of the sulfuric acid with the polymeric wall coating and we note that sulfuric acid has been used by others as a channel cleaning procedure. A particular advantage of using concentrated sulfuric acid is that it has an elevated boiling point, allowing us to greatly increase its reactivity by heating the acid-filled channel. It is possible that the use of elevated temperatures may not be necessary for other polymers.

3.3.2 Long-term Use and Stability of Microchips

Both Table 3.1 and Figure 3.1 show only the short-term effectiveness of the rejuvenation protocol. According to Madabhushi [8], the number of successful runs that could be performed before capillary regeneration was required decreased dramatically from 100 runs initially to around 35 after successive regenerations. According to the author, this poor stability was a result of the incomplete removal of surface-bound DNA and enzymes

in the sample. In order to investigate long-term stability, we implemented continuous aging tests on rejuvenated microchips. A typical aging period was 300 minutes. After 300 minutes of aging (as one normal separation run takes about 3 minutes, this is the runtime equivalent of about 100 runs), no significant degradation in resolution was observed (Figure 3.2). This suggests that the rejuvenated microchips have very good stability. Although the rejuvenated microchips were very stable for a time comparable to the length of time taken from being a new chip to needing its first rejuvenation, the number of times rejuvenation can be implemented on the microchip remains unknown.

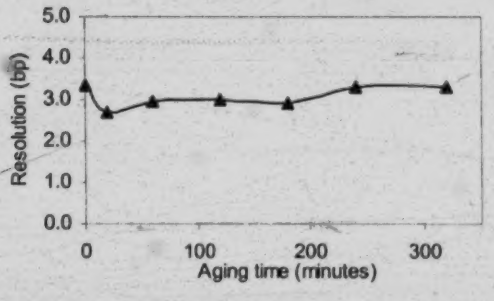

Figure 3.2 Resolution (250/300 bp) change following accelerated microchip aging.

Metal atoms in silica have been described as being either at the surface, internal or secluded [43]. Surface atoms and a proportion of the internal atoms can be removed by washing with HCl [27] or EDTA [44], but the secluded metal atoms are inaccessible. Additionally, it is well known that when a glass surface is exposed to water, alkali ions such as sodium are leached out from the glass to the aqueous solution in a process of ion exchange [24-26]. Since the annealing of glass can redistribute metal atoms and ions in the bulk silica and on its surface, any CE performance change of a microchip upon thermal treatment may indicate the existence of glass aging due to ion migration. In order to study the effect, we annealed a group of microchips in a standard glass annealing procedure, in which the temperature was slowly raised, in an overnight process, to 560 °C and then slowly lowered. The DNA separation performance of these microchips was then compared with the performance before annealing. There was no significant difference in resolution between these two groups, suggesting that the effect of ion migration in bulk glass material is negligible under the experimental and regenerative conditions used. This indicates that the effects of glass aging on microchip performance are negligible. More

than 50 microchips in our lab, used with GeneScan® polymer, POP4® and POP6® (Applied Biosystems, Foster City, CA, USA), have been reproducibly rejuvenated following the aforementioned protocol. We have been using some chips on an ongoing basis for several years without any apparent ongoing degradation. If there is any ongoing degradation (e.g. due to glass aging) the effects are not discernable on this time scale. So far, no microchip has been incapable of rejuvenation and all have been returned to a level of performance equivalent to (or better than) that of new chips. We have seen no evidence of surface non-uniformity with the method of rejuvenation and no increase in surface roughness was evident (this is not surprising since both the overnight anneal and the reagents used are components of the microchip fabrication process.

We estimate that this rejuvenation process will require about one hour of labour (with negligible reagent costs) for a set of three microchips (if processed manually). This corresponds to a small fraction (perhaps 5%) of the amount of time needed to fabricate the chips. While this may not be cost effective as compared with the cost of a new polymeric microchip (the authors note that many polymeric microchips are comparable in price to those of glass), higher levels of integration that require layer-to-layer registration are very likely to be fabricated only in glass.

3.4 Conclusions

GeneScan® polymer adsorbs rapidly onto the inner surface of micro-channel from an aqueous solution, leading to the formation of a polymer coating that is stable for hundreds of electrophoretic runs (pH ~ 8.5). To extend the lifetime of a microchip, a rejuvenation protocol has been developed in which the old coating is removed by a hot acid process and the bare microchannel surfaces are then conditioned by HCl. Similar results were achieved for microchips used with other polymer matrices such as POP4® and POP6®. We believe that these results would apply in general to electrophoretic separations based on the use of dynamic coatings. We have found that the effects of glass aging on the performance of microchips are negligible. It therefore appears to be possible to use a glass microchip "forever" through this effective rejuvenation process.

3.5 References

[1] A. Manz, N. Graber, H. M. Widmer, *Sens. Actuators B* 1990, 1, 244-248.

[2] A. Manz, D. J. Harrison, E. M. J. Verpoorte, J. C. Fettinger, H. Ludi, H. M. Widmer, *Chimia* 1991, 45, 103-105.

[3] D. S. Zhao, B. Roy, M. T. McCormick, W. G. Kuhr, S. A. Brazill, *Lab on a Chip* 2003, 3, 93-99.

[4] J. C. McDonald, G. M. Whitesides, *Acc. Chem. Res.* 2002, 35, 491-499.

[5] X. G. Du, Y. X. Guan, F. R. Wang, Z. L. Fang, *Chemical Journal of Chinese Universities-Chinese* 2003, 24, 1962-1966.

[6] Z. F. Chen, Y. H. Gao, R. G. Su, C. W. Li, J. M. Lin, *Electrophoresis* 2003, 24, 3246-3252.

[7] J. M. K. Ng, I. Gitlin, A. D. Stroock, G. M. Whitesides, *Electrophoresis* 2002, 23, 3461-3473.

[8] R. S. Madabhushi, *Electrophoresis* 1998, 19, 224-230.

[9] P. G. Righetti, C. Gelfi, B. Verzola, L. Castelletti, *Electrophoresis* 2001, 22, 603-611.

[10] M. Chiari, C. Micheletti, M. Nesi, M. Fazio, P. G. Righetti, *Electrophoresis* 1994, 15, 177-186.

[11] E. N. Fung, E. S. Yeung, *Analytical Chemistry* 1995, 67, 1913-1919.

[12] N. Iki, E. S. Yeung, *J. Chromatogr. A* 1996, 731, 273-282.

[13] X. M. Yan, W. Hang, V. Majidi, B. L. Marrone, T. M. Yoshida, *J. Chromatogr. A* 2002, 943, 275-285.

[14] A. Cifuentes, P. Canalejas, A. Ortega, J. C. Diez-Masa, *J. Chromatogr. A* 1998, 823, 561-571.

[15] N. J. Munro, A. F. R. Huhmer, J. P. Landers, *Anal. Chem.* 2001, 73, 1784-1794.

[16] Z. K. Shihabi, *J. Chromatogr. A* 1999, 853, 349-354.

[17] M. Chiari, M. Cretich, J. Horvath, *Electrophoresis* 2000, 21, 1521-1526.

[18] H. J. Tian, J. P. Landers, *Anal. Biochem.* 2002, 309, 212-223.

[19] *GeneScan Reference Guide - Chemistry Reference for the ABI310-Applied Biosystems* Applied Biosystems Inc., Foster city, California, U.S.A., 2000.

[20] R. S. Madabhushi, S. M. Menshen, J. W. Efcavitch, P. D. Grossman,"Polymers for separation of biomolecules by capillary electrophoresis",United States Patent: 5,567,292. (1994)

[21] J. C. Ren, A. Ulvik, H. Refsum, P. M. Ueland, *Anal. Biochem.* 1999, 276, 188-194.

[22] T. Tanahashi, M. Kawaguchi, T. Honda, A. Takahashi, *Macromolecules* 1994, 27, 606-607.

[23] S. Kaupp, H. Watzig, *Electrophoresis* 1999, 20, 2566-2574.

[24] R. H. Doremus, *Journal of Non-Crystalline Solids* 1975, 19, 137-144.

[25] R. H. Doremus, *Chemical durability of glass*. R. H. D. M.Tomozawa, Ed., Treatise on materials science and technology, Academic Press, New York, 1979.

[26] R. W. Douglas, J. O. Isard, *J. Soc. Glass Technol.* 1949, 33, 289-335.

[27] M. Verzele, M. DePotter, J. Ghysels, *Journal of High Resolution Chromatography & Chromatography Communications* 1979, 2, 151-153.

[28] J. Nawrocki, *Chromatographia* 1991, 31, 177-192.

[29] M. Verzele, C. Dewaele, *J. Chromatogr.* 1981, 217, 399-404.

[30] S. Kaupp, H. Watzig, *J. Chromatogr. A* 1997, 781, 55-65.

[31] R. Ma, H. J. Crabtree, C. Backhouse, *Electrophoresis* 2005, 26, 2692 - 2700.

[32] C. Heller, G. W. Slater, P. Mayer, N. Dovichi, D. Pinto, J. L. Viovy, G. Drouin, *J. Chromatogr. A* 1998, 806, 113-121.

[33] R. Ma, K. Kaler, C. Backhouse, paper presented at the ICMENS Proceedings, Banff, AB, Canada 2004, pp.

680-686,IEEE Computer Society, Los Alamitos, California, U.S.A.

[34] H. Watzig, S. Kaupp, M. Graf, *Trac-Trends in Analytical Chemistry* 2003, 22, 588-604.

[35] S. Hjerten, K. Kubo, *Electrophoresis* 1993, 14, 390-395.

[36] J. K. Towns, J. M. Bao, F. E. Regnier, *J. Chromatogr.* 1992, 599, 227-237.

[37] Y. F. Ma, M. R. Shortreed, E. S. Yeung, *Anal. Chem.* 2000, 72, 4640-4645.

[38] L. Trossarelli, M. Meirone, *Journal of Polymer Science* 1962, 57, 445-452.

[39] L. F. Wang, E. M. Pearce, T. K. Kwei, *Journal of Polymer Science Part B-Polymer Physics* 1991, 29, 619-626.

[40] J. Dai, S. H. Goh, S. Y. Lee, K. S. Siow, *Polymer* 1994, 35, 2174-2179.

[41] J. Nawrocki, B. Buszewski, *J. Chromatogr.* 1988, 449, 1-24.

[42] W. J. Lambert, D. L. Middleton, *Anal. Chem.* 1990, 62, 1585-1587.

[43] P. C. Sadek, C. J. Koester, L. D. Bowers, *J. Chromatogr. Sci.* 1987, 25, 489-493.

[44] J. Kohler, D. B. Chase, R. D. Farlee, A. J. Vega, J. J. Kirkland, *J. Chromatogr.* 1986, 352, 275-305.

Chapter 4

Stability Study of CE on Microchips

4.1 Introduction

The reagent reservoirs on microfluidic devices typically contain only a few microliters or less. Such small volumes do not have bulk solution properties and can rapidly change composition electrochemically. It is relatively easy to produce pH gradients and zeta potential changes in the microchannel [1].

During electrophoresis, several factors will play a role to affect the stability of the sample mobility. As one of those factors, it has been reported that if buffer reservoirs were not sealed, the evaporation of reagents had an impact on the sample mobility after consecutive runs of injection and separations [2]. Besides evaporation, an increasing electrolyte concentration also resulted from the electrolysis of water, which occurs at the electrodes via oxidation/reduction reactions [3]. The oxidation reaction at the anode electrode results in O_2 gas formation and an accumulation of H^+ ions. The complementary reduction in the cathode reservoir utilizes two electrons to break apart water. This results in H_2 gas evolution and an increase in OH^- ions within the reservoir. The net result is an accumulation of H+ ions in the anode reservoir and OH^- ions in the cathode reservoir. The accumulation of H+ and OH^- ions will eventually result in pH change in reservoirs. The change of the electrolyte composition in the reservoirs will eventually propagate into the microchannel, and gradually affect performance of the electrophoresis. The pH changes in electrode buffers during capillary electrophoresis (CE) has been noted experimentally as previously reported by Macka *et al.*[4], Oki *et al* [5], Bello [6] and Minerick *et al.* [1]. For instance, Minerick *et al.* reported a substantial pH gradient across the capillary (20 μm i.d.) developed from a neutral 7.4 to as high as 12 in the cathode reservoir and as low as 2 in the anode well when an electric field (~37.5 V/cm) was present for a period of 30 minutes in a PBS buffer (140 mM NaCl, 22 mM KH_2PO4, 9.1

mM K_2HPO_4) [1]. The effects of pH change on the reproducibility of CE have also been addressed in previous reports [1, 7, 8].

In particular, cell manipulations on microchips may involve multiple steps or processes such as transport [9], sorting [10], and capture [11]. These steps may take longer time than a simple CE separation. Additionally, reversing of voltage polarity may complicate the ion migration in the channels. Therefore, changes in the electrolytes (*e.g.*, pH) can greatly affect the repeatability of cell migration. On the other hand, the effective charge of the cell is greatly affected by the presence of ions in the solution, these form a layer of opposite charge around the cell [12-14]. (See Chapter 1 for the description of electric double layer and zeta potential). The electrophoretic mobility of a cell is dependent on the zeta potential. Since the ionic strength of the separation medium, which in practice is usually monitored by the conductivity, has a direct effect on the layer of ions around the cell, and therefore on the zeta potential, the change of the ion strength during CE affects the mobility of the cells. According to Shortman [13], the effect of the conductivity on the mobility of a cell can be calculated from an empirical relationship:

$$\mu_1/\mu_2 = [\sigma_2/\sigma_1]^{1/2} \qquad (1)$$

where μ_1, μ_2 are the cell mobilities before and after the change of the conductivity (ionic strength) of the medium, σ_1, σ_2 are the corresponding conductivity of the medium. According to the equation (1), the higher conductivity (or ionic strength) of the medium results in the lower cell mobility.

Studies of the stability of CE, in terms of change of electric current, are beneficial for the development of methods to minimize those unexpected effects discussed above. In this chapter, we present our observations on change of the electric current during CE. We want to determine the relative importance of electrode effects and ionic movements. Additionally, the stability of CE for microparticles, in terms of mobilities, was studied. Understanding those effects will be critical for the development of microchip protocols for cell manipulations, where small shifts in mobilities are used to identify cells.

4.2 Materials and Methods

4.2.1 Reagents

GeneScan® polymer (7%, P/N: 401885) was obtained from Applied Biosystems (Foster City, CA, USA). A Tris-borate with EDTA buffer (TBE) was made with Tris base and boric acid from Fisher Scientific (Fair Lawn, NJ, USA) and EDTA from Merck (Darmstadt, Germany). The running buffer, referred to as "1TBE10G", was made with glycerol (SigmaUltra, lot No.: 121K0121) from Sigma-Aldrich (St Louis, MO, USA) and the TBE buffer so that the final concentration of the glycerol was 10% (w/w) the TBE was 1×TBE (pH: ~8.3). The 1TBE10G and the 1×TBE were diluted 10× (unless otherwise specified) using distilled water. The separation medium was 5% (w/w) GeneScan® polymer and 10% (w/w) Glycerol in the 1×TBE buffer (referred to as "5GS10G").

Surfactant-free sulfate white polystyrene latex beads with a diameter of 9.6 μm (Product No. 1-10000) were purchased from Interfacial Dynamics Corporation (Portland, OR, USA). The latex beads are suspended in distilled de-ionized water from the manufacturer. The particle number per milliliter the suspension is 8.6×10^7. The coefficient of variance (CV) of the diameter is 7.4% (from the manufacturer). An aliquot of the stock bead suspension (*e.g.*, 10 μl) was mixed with a running buffer (*e.g.*, 10× dilution of the 1×TBE) in a 200-μl PCR tube so that the concentration of the beads was 8.6×10^5 ea. per milliliter. The separation medium for the latex beads was 5% (w/w) GeneScan® polymer in a 0.5×TBE buffer (unless otherwise specified). In order to inject beads, the sample waste well was connected to 200 V; the sample well was connected to ground, while the other two wells were electrically disconnected. The transport of cells in the separation channel was obtained by connecting the buffer waste well to 2 kV (otherwise specified) and the buffer well to ground. For transport of the beads in reverse direction, the electrical connection was reversed.

4.2.2 Microchips and Microfluidic Tool Kit

Standard microchips were used in this work. As detailed in section 2.2.2 of Chapter 2, microchip performance assessment and microchip rejuvenation were performed when a microchip was taken out of storage for experiments.

4.2.3 Voltage Programs and Positioning of the Electrodes

The microchip was loaded with 5GS10G in the channels and all wells (3 uL for each well). Refer to section 2.2.3 of Chapter 2 for the procedure of microchip loading. A typical voltage program used in this work is shown in Table 4.1. It consists of two steps. In the first step, the buffer waste well was connected to 6 kV; the buffer well was connected to ground, while the other two wells were electrically disconnected. In the second step, the electric field polarity was reversed. In this report, only the electric current measured at the ground side was analyzed due to a better accuracy of the measurement at the ground side (according to the manufacturer).

Table 4.1 Voltage Program for Current Stability Study

Step	Time (sec.)	Sample waste well	Buffer waste well	Sample well	Buffer well
1	600	Float	6.00 kV	Float	Ground
2	600	Float	Ground	Float	6.00 kV

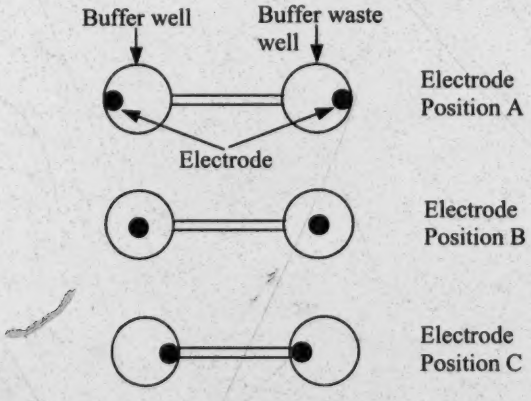

Figure 4.1 Positioning of the electrodes in wells (top view) for the study of electrode position effect on electrophoresis stability

The effect of electrode position on current stability was studied using nickel electrodes. Cylindrical nickel electrodes have diameter of ~0.5 mm. Wells on the

microchip have diameter of ~2 mm. The tip of inserted electrodes reached the bottom of each well. Various horizontal positions of electrodes were tested (shown in Figure 4.1). Experiments were performed in such a way that only the position of the electrode was changed. The microchip was loaded with fresh reagent for each test. The voltage program in Table 4.1 was used.

4.2.4 Chemical Treatments of Platinum Electrodes

In addition to the work with Ni, the chemical stability of Pt electrodes was investigated. Two chemical treatments of platinum electrodes were performed in order to find out if the electrode surface conditions (*e.g.*, surface oxidation) could affect the current stability. In treatment A, the two electrodes were first rinsed with distilled water thoroughly, followed by a 10 minute immersion in 1M nitric acid, and a 2 minute rinse with distilled water. This treatment was supposed to be able to remove all organic adsorbents on the surface of the electrode and oxidize the surface [15]. In treatment B, the electrodes were placed into a 2M ferrous sulfate solution for 30 minutes followed by a 2-minute rinsing with distilled water. Treatment B was supposed to be able to remove the oxide layer on the electrode surface [3]. Fresh reagent and buffer were used in each CE test.

4.2.5 Stability of Mobilities of Single Microparticles

Latex beads (9.6 μm) were selected for the study of electrophoresis stability, because their size and color were suitable for direct observations using the eyepiece of the μTK. It was found that the beads migrated towards the +ve electrode in the specified CE conditions. Since the EOF was negligible in 5GS10G (refer to Chapter 3), the migration direction indicated that the latex beads were negatively charged. In order to capture one bead each time in the intersection of the channels, the bead concentration in the sample well was kept low (*i.e.*, ~10^6 ea. per milliliter). Upon application of the injection voltage, beads migrated from the sample reservoir towards the sample waste reservoir. A bead was selected at the intersection of channels by turning off the injection voltage at the appropriate time. The bead was then transported 5 mm away from the intersection in the separation channel by applying a voltage along the channel. The selected bead was moved back and forth between two fixed spots (5 mm apart) in the channel by switching

voltage polarities. The voltage was turned off manually when the bead reached either of the specified spots. The migration time of the bead, in each one-way trip from one spot to another during those successive reversals, was recorded by the control software of the μTK and was read out from the screen. The average velocity of each single bead was calculated by dividing the distance (*i.e.*, 5 mm) by the migration time of each one-way trip. The voltages applied along the channel (~8.2 cm) were kept at 4 kV. The velocity of beads was used for the analysis of migration stability of the beads.

4.3 Results and Discussions

4.3.1 Typical Current Changing Patterns

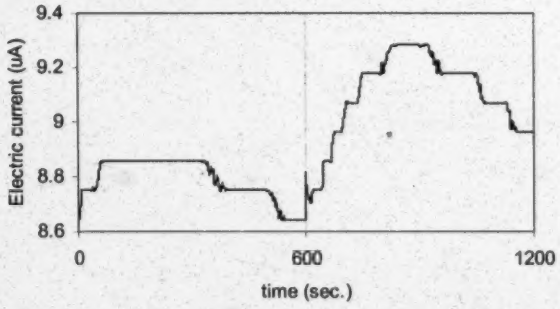

Figure 4.2 A typical pattern of electric current change with time. Platinum electrodes were used. Refer to section 4.2.2 for electrophoresis conditions. Current data acquisition frequency was 25 Hz. Data smoothing was performed using DPlot (version 2.0.1.4, HydeSoft computing, Vicksburg, MS, USA). Smoothing window was 100. The current measurement quantization was 100 nA (Quantized by resolution of ADC).

As shown in Figure 4.2, in a 600s electrophoresis, a typical current changing pattern showed a minor increase of the current (~2%) within ~50 s in the beginning of the electrophoresis run, and then became stable for a period of about 250s, followed by a stepped decrease until the end of the step. In the second step, in which the voltage polarity was reversed, the measured current initially increased upon the application of the voltage. It reached its maximum after about 250s, and kept stable for a short time (~100s), followed by a decrease until the end of the voltage program.

In order to understand the current changing pattern, further experiments were performed, as described below.

4.3.2 Start Point of Electrode Surface Conditions

It is well known that all noble metal electrodes, including platinum, are not as chemically inert as might be assumed. The oxidation of Pt to PtO, and the adsorption of organics are the reaction pathways that compete with the desired Faradaic reactions at the platinum electrode [3, 15]. First, a surface oxide layer of platinum will be formed if the electrode has been subjected to anodic potentials for sufficient times [3]. On the other hand, the oxidized platinum can be converted to a reduced platinum electrode by cathodic conditions [3]. Besides the oxidation and reduction reactions on the platinum electrodes, the adsorption of organic compounds on electrode has also been frequently reported [16-21], and is referred to as "electrode fouling" [19, 21-24].

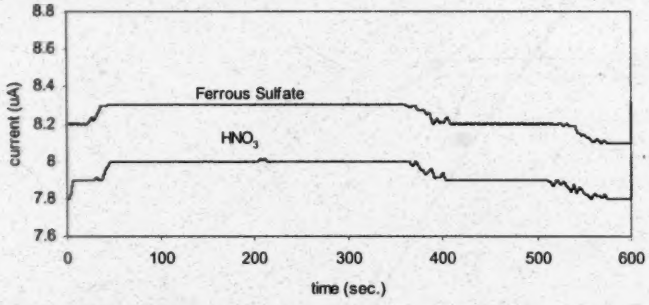

Figure 4.3 Current changing patterns after two different chemical treatments to platinum electrodes. Data smoothing was performed using DPlot (version 2.0.1.4, HydeSoft computing, Vicksburg, MS, USA). Smoothing window was 100. The current measurement was quantized by resolution of ADC (100 nA).

If the aforementioned reactions on the electrode surface were significant in changing the electrode surface, the CE runs might have started from a different starting point of the electrode conditions without any treatments of the electrodes. To find out how a different starting point affects the current pattern, we treated the electrodes chemically using various methods as described in section 4.2.4. Treatment A was first performed on two platinum electrodes. Those two electrodes were then used in a CE test using a voltage program (step one in Table 4.1). After that, the two electrodes were treated with method B, followed by the same CE test. As shown in Figure 4.3, after treatment with HNO_3 (treatment A), a relatively low current was obtained during the CE, as compared to the current obtained after the treatment with ferrous sulfate (treatment B). The low current

was probably due to the oxidation of the surface of the electrodes after the treatment with the HNO_3. In contrast, the treatment with ferrous sulfate resulted in a less oxidized surface of the electrode and therefore the electrodes had higher conductivity. However, although the current levels were different after those treatments, the current changing patterns were essentially identical. This observation suggests that the oxidation status of the electrodes may vary among the electrophoresis runs but it is not associated with the current changing patterns.

4.3.3 Effect of Electrode Positions

To study the effect of positions of electrodes in the electrophoresis, all experiments were performed in such a way that only the position of the electrodes changed. Since the analysis time of each CE test was relatively short, we assumed that the oxidation and reduction reactions on the electrodes were negligible. Therefore, the only variable of those experiments was the position of electrodes in wells.

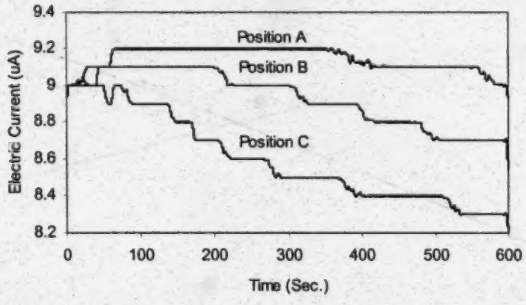

Figure 4.4 Electric current changes with electrophoresis time. The reagent was 5GS10G. The electric field was 760 V/cm. The electrode material was nickel. Data smoothing was performed using DPlot (version 2.0.1.4, HydeSoft computing, Vicksburg, MS, USA). Smoothing window was 100. The current measurement quantization was 100 nA (Quantized by resolution of ADC).

As shown in Figure 4.4, the pattern of electric current's changing with time was found to be dependent on the lateral positions of the electrodes in the wells. When the electrodes were placed near the inlet of the channels (position C in Figure 4.1), the current started to decrease almost immediately upon application of the voltage. When the electrodes were placed in position B (the middle of the wells), the electric current started to increase upon application of the voltage, then the current was stable for ~180 seconds,

followed by decreasing value. When the electrodes were placed in position A (the furthest position from the inlet), the electric current started to increase upon application of the voltage, then the current was stable for ~300 seconds, followed by decreasing value. The closer the electrodes were placed to the inlet of the channels, the earlier the current started to decrease, and the lower the final current level was. The result was repeatable and order independent.

Macka *et al.* has reported the relative positions of electrode and capillary had effects on the reproducibility of migration times and peak area in a CZE separations [4]. It was found that good reproducibility and stable baseline were obtained when the capillary end was positioned below the electrode tip and with a certain lateral distance (1 mm). Instead, when the electrode and capillary were touching and capillary end was higher than the electrode, poor reproducibility and baseline instability were evident. The poor reproducibility was explained as the result of pH change inside the capillary: the closer the electrode to the capillary inlet, the easier the access of H^+ and OH^- to the capillary. Our observation of the dependence of current stability on the electrode positions was in agreement with those earlier findings.

Since 1×TBE buffer was used in our experiments, the pH change might not be significant during the CE. We believe that the aforementioned observations of current changes during CE could be explained by space charge distributions. Due to the geometry of the channel network and wells, the electric field intensity in the channels is much higher than it is in the wells. Meanwhile, a gradient of the electric field exists in those wells (simulation of the electric field distribution will be discussed in Chapter 5 in detail). Ions in different locations experience different electric forces and therefore have different migration velocities. The redistribution of the space charges under an electric field results in a change of current with time. The minor increase at beginning of a CE run (when electrodes were at position A or B) was probably caused by the migration of ions from the wells to the channel and the resulting enrichment of space charges. The decrease of current probably resulted from the decrease of ion concentrations within the network of channels. As more and more anions migrate into the anode reservoir while cations migrate into the cathode reservoir (and each exchange their charges with electrodes), the concentration of charged ions will decrease and result in eventual decrease of the current.

The switching of the polarities results in reversed migration of ions, and reversed current changing direction. Because the electric field lines mainly distribute between those two electrodes, space charges between those two electrodes contributed most to the current, provided diffusion and convention mass-transfer are negligible [25]. Therefore, minor variation of the electrode position in the well will result in a big difference in ion numbers involved into the electromigration. The closer the electrode is to the inlet of the channel, the fewer ions in the wells are involved, and the shorter the time before the ion concentration is affected; the further the electrode is to the inlet of the channel, the more ions in the wells are involved, and the longer the time with relatively stable ion concentrations.

4.3.4 Effect of Electrode Materials

Using platinum and nickel electrodes, a total of 13 current changing curves were obtained in such a way that reagent composition, reagent volume and voltage program were identical for each run (however, the electrode position in wells was unknown). It was found that the current increasing pattern in the first step of the voltage program (Table 4.1) was associated with the decreasing pattern in the second step of the voltage program. A typical electropherogram obtained using the platinum electrodes and a typical electropherogram obtained using the nickel electrodes are shown in Figure 4.5. As shown in Figure 4.5A, we defined a triangle with area $A = 0.5 * \Delta t * \Delta i$, where Δt is the duration from the point that current starts to decrease to the end of the 1st step of the voltage program (600s), Δi is the total decrease in current in the 1st step. In the second step, the rate of increase of the current was defined as $R = h / w$, where h is the difference between the maximum current and the minimum current in the 2nd step; w is the duration of the current increasing in the second step. R was plotted against A. It was found that the R had a roughly linear correlation with A (see Figure 4.6).

The data of R and A obtained using two types of electrodes, platinum and nickel, were plotted in the same graph. As shown in Figure 4.6, data obtained using nickel electrodes were significantly different from those obtained using the platinum electrodes. The observation indicates that electrode reactions played a key role for the current stability in CE. It is believed that the mass transfer will accompany the electron exchange

between ions and electrodes [25]. For instance, positively charged ions receive electrons from the electrode and then become neutral particles. When the polarity of electric field is reversed, some neutralized particles on the surface of those electrodes become charged again and become involved in ion migration, resulting in the increase of space charge and current. The net effect of the exchange of electrons is the consumption of buffer ions. The rate of the increase of the current, after the polarity of electric field is reversed, is determined by the number of the released ions. The fewer the released ions from the electrode surface, the slower increase of the current in the second step, and vice versa. As a relatively more active metal, the releases of previously deposited ions from the surface of the nickel tend to be less significant than those on the platinum electrodes. According to the graph in Figure 4.6, for a specified value of A, the h/w value on the curve for the nickel electrodes was smaller than that on the curve for the platinum electrodes, indicating a relatively lower increase rate of current in the second step of the CE using nickel electrodes. This was in agreement with current curves in Figure 4.5.

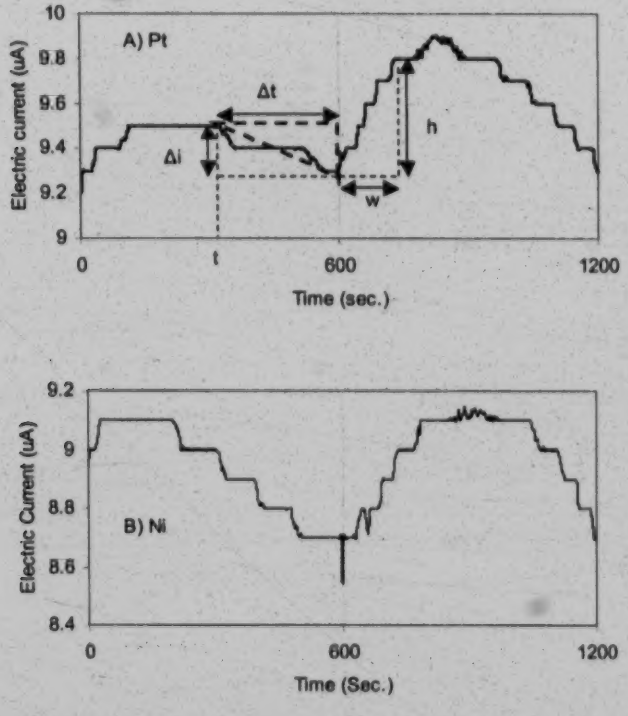

Figure 4.5 A) Electropherogram obtained using platinum electrodes and definition of the curve features; B) Electropherogram obtained using nickel electrodes. Data smoothing was performed using DPlot (version

2.0.1.4, HydeSoft computing, Vicksburg, MS, USA). Smoothing window was 100. The current measurement quantization was 100 nA (Quantized by resolution of ADC).

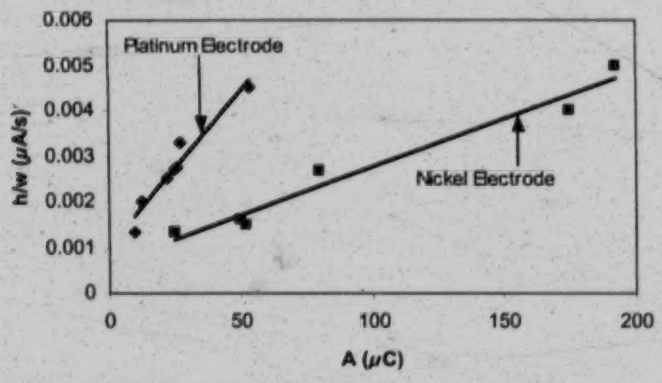

Figure 4.6 Derived data from current changing curves: electric current increasing rate (h/w) against triangle area (A)

Both the effect of the electrode positions and the effect of the electrode materials are associated with the change of space charges with time. In a summary, the electric current during CE is determined by the concentration of space charges in the channels, which change with time due to electrochemical reactions. The mechanism of those electrochemical reactions is not the focus of this work. However, the awareness of those effects and relative variables is critical to obtain repeatable CE analysis.

4.3.5 Stability of CE of Single Microparticles

Using the method described in the section 4.2.5, it was found that the migration velocity of a single bead changed with time during CE. We found that the changing pattern of the migration velocity of latex beads was associated with the concentration of the running buffer of the electrophoresis. Figure 4.7 shows the typical velocity changing patterns of single 9.6 μm beads in various buffer concentrations. In 0.5×TBE (and 5% GeneScan polymer addition), the migration velocity of one latex bead decreases progressively until roughly stable (<5% variation) after ~6 minutes. In 1×TBE (and 5% GeneScan polymer addition), the migration velocity of one latex bead increased in the first 2 minutes and then became stable. In 2×TBE (and 5% GeneScan polymer addition), the migration velocity of one latex bead increased in the first 5 minutes and then became stable. Due to

the heterogeneity of the latex bead population on electrophoretic mobility in a certain CE condition, the pattern of the velocity change of latex beads varies. However, the dependence of the velocity pattern of beads on the buffer concentration was consistent.

During our investigations of the instability of the bead velocity, it was also found that buffer replenishment could result in a sudden change of the velocity of a bead. Figure 4.8 shows a typical changing pattern of a 9.6 μm bead. The velocity was about 300 μm/s at the beginning of the test. When the velocity decreased to about 150 μm/s after about 600 seconds, the buffers in the wells were replenished. After the buffer replenishment, the velocity started to increase until roughly stable again after about 1000 seconds of elapsed time. The observation indicated that the reagents in the reservoirs changed with time and affected the migration of beads significantly.

Since the changes in the reagents are inevitable during CE, we believe that microparticle velocity changes with time during electrophoresis are unavoidable. However, this should not be a concern for cell separations, because all cells in a mixture will migrate in the same ionic environment during the separation. As long as the cell mixture is separated in identical CE conditions, the repeatability of the cell separations will not be a problem. Alternatively, a standard (*e.g.*, latex beads) that has a known electrophoretic mobility in certain electrophoresis conditions may be used for the differentiation of cells.

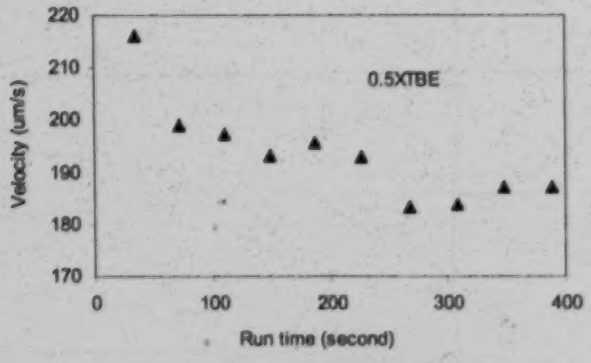

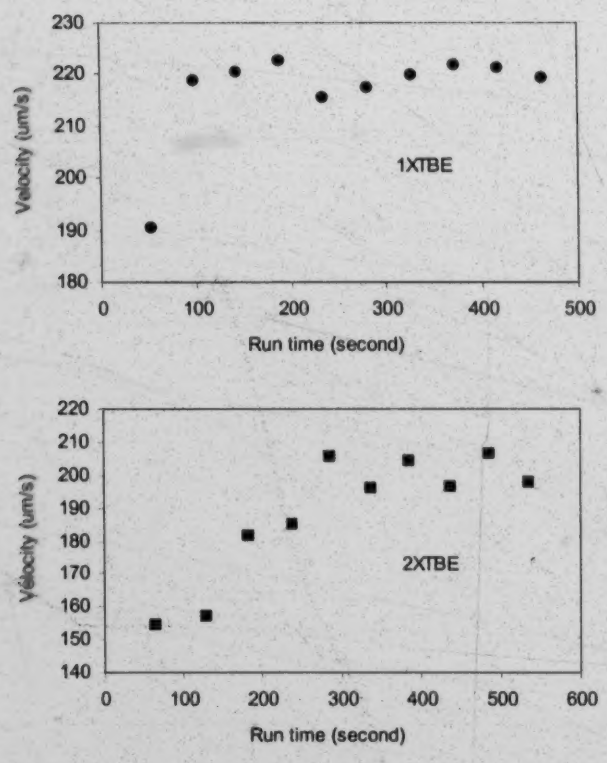

Figure 4.7 Typical patterns of the velocity changes of 9.6 μm single beads. Electric field was 470 V/cm. ▲ represents the data point of a bead in 0.5×TBE and 5% GeneScan polymer; ● a bead in 1×TBE and 5% GeneScan polymer; ■ a bead in 2×TBE and 5% GeneScan polymer. Platinum electrodes were used.

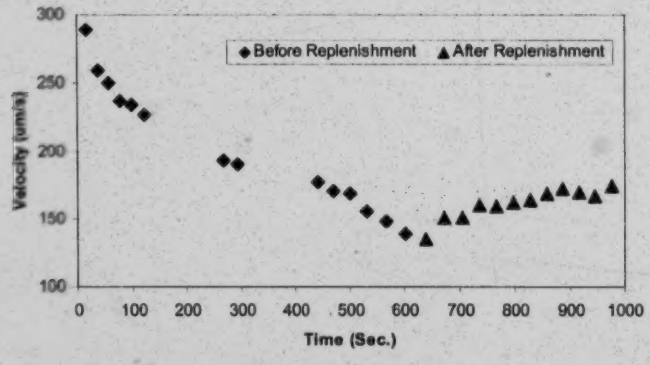

Figure 4.8 Velocity change with time of a latex bead when the buffer was replenished. Reagent in the channel was 0.5×TBE and 5% GeneScan polymer. Electric field was 470 V/cm. Platinum electrodes were used.

4.4 Conclusions

A small volumed reagents and reduced sample consumption are major advantages of the size shrinkage of microchips. However, the small volumes of reagents result in ionic limitations in the sense that relatively a small number of ions are available to prevent the change of pH, and the change of electric current.

Our observations of the effect of electrode positions and the effect of electrode materials were believed to be the results of the electrode electrochemistry and the change of space charge distribution with time. These effects will eventually affect the mobility of the sample during CE analysis. To obtain a repeatable electrophoresis, the awareness of those effects and the control of related variables are critical.

The CE stability was also evaluated using microparticles in various buffer concentrations. Our observations suggested that the microparticle mobility changes with time during the electrophoresis were unavoidable, independent on the buffer concentration. Cells in the same population have heterogeneous properties. Their responses to the change of CE medium may vary. However, as long as the mobility distributions of cell populations do not overlap in a specified time, the separation of cell mixtures by CE is still feasible.

4.5 References

[1] A. R. Minerick, A. E. Ostafin, H. C. Chang, *Electrophoresis* 2002, 23, 2165-2173.

[2] M. Albin, J. E. Wiktorowicz, B. Black, S. Moring, *American Laboratory* 1991, 23, 27-35.

[3] R. N. Adams, *Electrochemistry at solid electrodes* Marcel Dekker, New York, 1969.

[4] M. Macka, P. Andersson, P. R. Haddad, *Analytical Chemistry* 1998, 70, 743-749.

[5] A. Oki, Y. Takamura, Y. Ito, Y. Horiike, *Electrophoresis* 2002, 23, 2860-2864.

[6] M. S. Bello, *Journal of Chromatography A* 1996, 744, 81-91.

[7] M. A. Strege, A. L. Lagu, *Journal of Liquid Chromatography* 1993, 16, 51-68.

[8] A. V. Stoyanov, J. Pawliszyn, *Analyst* 2004, 129, 979-982.

[9] P. C. H. Li, D. J. Harrison, *Analytical Chemistry* 1997, 69, 1564-1568.

[10] A. Y. Fu, C. Spence, A. Scherer, F. H. Arnold, S. R. Quake, *Nat. Biotechnol.* 1999, 17, 1109-1111.

[11] M. S. Yang, C. W. Li, J. Yang, *Analytical Chemistry* 2002, 74, 3991-4001.

[12] O. Gaal, G. A. Medgyesi, L. Vereczkey, *Electrophoresis in the separation of biological macromolecules*, John Wiley & Sons, 1980.

[13] K. Shortman, *Annu. Rev. Biophys. Bioeng.* 1972, 1, 93-130.

[14] B. Kirby, E. Hasselbrink, *Electrophoresis* 2004, 25, 187-202.

[15] S. W. Feldberg, C. G. Enke, C. E. Bricker, *Journal of the Electrochemical Society* 1963, 110, 826-834.

[16] V. A. Bogdanovskaya, A. Y. Safronov, M. R. Tarasevich, A. S. Chernyak, *Journal of Electroanalytical Chemistry* 1986, 202, 147-167.

[17] S. Hughes, D. C. Johnson, *Anal. Chim. Acta* 1981, 132, 11.

[18] S. Hughes, P. L. Meschi, D. C. Johnson, *Anal. Chim. Acta* 1981, 132, 1.

[19] D. P. Manica, Y. Mitsumori, A. G. Ewing, *Analytical Chemistry* 2003, 75, 4572-4577.

[20] A. J. Gawron, R. S. Martin, S. M. Lunte, *Electrophoresis* 2001, 22, 242-248.

[21] S. S. Lord, L. B. Rogers, *Analytical Chemistry* 1954, 26, 284-295.

[22] W. Lu, G. G. Wallace, M. D. Imisides, *Electroanalysis* 2002, 14, 325-332.

[23] J. Wang, G. Chen, A. Muck, D. C. Shin, A. Fujishima, *Journal of Chromatography A* 2004, 1022, 207-212.

[24] A. J. Saterlay, R. G. Compton, *Fresenius Journal of Analytical Chemistry* 2000, 367, 308-313.

[25] J. O. M. Bockris, A. K. N. Reddy, *Modern electrochemistry* Plenum Press, New York, 1970.

Chapter 5

Electrophoretic Separation of Biological Cells on Microfluidic Chips

5.1 Introduction

The feasibility of handling biological cells in microfluidic devices using various physical forces has already been demonstrated in the literature [1-4]. For example, Li and Harrison used electroosmotic pumping to transport biological cells within a network of channels on glass microchips [1]. Other methods for manipulating cells on microfluidic devices have included using off-chip pumps for cell transport [5], using optical or dielectrophoretic traps for cell sorting [6], and using specially-designed microstructures for cell docking [7]. Besides the techniques for cell manipulation, the integration of multi-step cellular analysis has also been demonstrated in recent reports [2, 3]. For instance, according to Waters *et al.*[2], cell lysis, PCR amplification, and electrophoretic analysis of the genetic amplicons were performed successfully on a monolithic microchip. However, in all those reported Micro Total Analysis Systems (μTAS), the separations of particular cells of interest from mixed populations were performed off-chip to reduce the complexity of the design. For achieving effective levels of integration of μTAS, on-chip separation or sorting of cells is of vital importance. Besides the demand for the integration of the μTAS, chip-based techniques for bacterial cell separation and detection are also required for applications in many other fields, such as food and environmental water monitoring, to replace the conventional methods that are extremely costly and labor extensive.

As summarized in Chapter 1, biological cells can be separated by various techniques on micron scale devices. Among those techniques, dielectrophoresis (DEP) is one of the most popular approaches for on-microchip cell sorting [6, 8]. DEP separation is based on the principle that dielectric particles placed in an AC electric field are polarized and

experience a variable translation force, which depends on the applied frequency and the properties of the medium. Thus, by manipulation of the medium conductivity and applied frequency one can separate biological cells based on their dielectric properties. However, this approach has its limitations (see Chapter 1).

Capillary electrophoresis (CE) has been successfully used to separate a wide variety of biomolecules such as proteins [9-11] and DNAs [12-14], whose sizes are usually expressed in terms of angstroms. As for cells, which typically have sizes of microns and possess a broad distribution of the electrophoretic properties (so-called electrophoretic heterogeneity [15]), the separation of cells by CE is challenging. Ebersole and McCormick were among the first to demonstrate the feasibility of preparative separations of biological cells by conventional CE [16]. According to their report, artificial mixtures of two types of bacterial cells, *S. pyogenes and S. pneumoniae,* were separated in 0.05 ×TBE (pH 9.5) using 250 cm long, 100 μm *i.d.* capillaries over periods longer than one hour (in an electric field of ~120 V/cm). Analysis of the fractions of the separation indicated that the cells were quantitatively resolved and could be recovered at purities greater than 98%. Microscopic examination showed that the peaks were composed of single cells (each of a single type for each peak), indicating that those separations were true separations. Pfetsch and Welsch reported the separation of four different types of bacterial cells by CE under similar conditions (using 250 μm *i.d.*, 250 cm long capillaries; in a TBE buffer with ion strength of 0.0015 mol/L (pH 9.6)*; in an electric field of 120 V/cm) in a period of about 40 minutes [17]. Besides the CE analysis of bacterial cells, many publications on CE separations were focused on mammalian cells, especially red blood cells (RBC). Tsuda *et al.* reported the separation of RBCs at the single cell level by CE in saline containing 1% bovine serum albumin [18]. It was found that the intensities of the scattered light signals of single RBCs in the electropherograms corresponded to the distribution of their electrophoretic mobilities. Zhu and Chen analyzed the electrophoretic mobilities of a variety of RBCs (human, chicken, pig and rabbit) using fluorinated ethylene-propylene (FEP) capillaries (0.45 mm *i.d.*) [19].

* According to the authors, the ion strength of the TBE buffer was calculated by assuming the presence of the following ions: $Tris^+$, OH^-, $EDTA^{4-}$, $5Na^+$, $B(OH)_4^-$.

Significant differences in the electrophoretic mobilities among different types of cells were observed (discussed in detail later in this section).

The aforementioned separations were always accomplished in a relatively long time (*e.g.*, longer than one hour for the separation of two types of bacterial cells, *S. pyogenes and S. pneumoniae* in [16]) and long distance (*e.g.*, ~ 1m in [16]). Additionally, using any of the aforementioned techniques, the broad distributions of cell mobilities always resulted in broad peaks in the electropherograms (*e.g.*, the FWHM of bacterial peaks was at the level of minutes according to [16]).

In recent years, a few groups have reported the separation of bacterial cells at the population level with relative short analysis times and sharp peaks. According to Armstrong *et al.* [20], the separations of *M. luteus, E. aerogenes, P. fluorescens, and S.cerevisiae* were achieved in less than 10 minutes, using 100-μm *i.d.* and 27 cm long capillaries. Those high efficiency separations were attributed to the use of a polymer additive (0.025% (w/w) polyethyleneoxide) in a running buffer (0.5 mM TRIS, 0.5 mM boric acid, and 0.011 mM EDTA, pH 8.4 [20]). The exact mechanism for the resulting separations was not completely understood in their early reports [21-23]. It was subsequently shown in other works by Armstrong *et al.* that aggregation of cells played a significant role in obtaining the single sharp peaks during the CE separations of the cell mixtures [24-26]. It remains unknown whether a small number of cells (*e.g.*, less than 10 ea) will aggregate together using the technique described in [21-23]. Moreover, since the number of cells in the agglomerate cannot be determined beforehand in a real world application (unless counting the cell numbers in each fraction afterwards [21]), and cell agglomerates with various sizes have different mobilities, the repeatable migrations of each cell subpopulation are not achievable. In other words, the identification of cells based solely on their mobilities is not feasible if aggregation takes place in the CE. Therefore, the separations in the reports of Armstrong *et al.* [21-23] were false separations. In another report by Shintani *et al.*[27], single sharp peaks of cell populations were obtained in the separation of *Salmonella enteritidis* and *Salmonella typhimurium* by adding 0.01% sodium alginate in the CE running buffer of TBE. However, the purity of cells (or contamination rate) in each fraction and the mechanism of the sharp-peak

separations in their publication were not clarified, and therefore the separations could be false separations.

As described above, some work has been done towards the separation of biological cells by CE. Unfortunately, many of those results were controversial. Additionally, the CE separations of different cell populations are possible only when sufficiently large differences exist in their electrophoretic mobilities (μ_{EP}). The question remains: is the identification of single cells based solely on their apparent electrophoretic mobility truly feasible [25, 26]?

Electrophoretic mobility values of some cells have already been obtained using conventional CE. For instance, according to Zhu and Chen [19], under identical CE conditions, the average retention time (the migration time from the injection point to the detector [19]) of human RBCs was 14 minutes, while the average retention time of rabbit RBCs was 26.6 minutes (see Table 5.1). Since the mobility difference from the human RBC to the rabbit RBC is far larger than the variation of cell mobilities in each population (*e.g.*, 9.2% for the human RBC), it suggests that the CE has the ability to separate those two cell populations. Silvinsky *et al.* collected the electrophoretic mobility of eukaryotic cells from the literature published worldwide during the past about 40 years [28]. The mobility differences among some of those cells were significant (see Table 5.1 for some examples). Although those electrophoretic mobility values were obtained by different people under different CE conditions, the information unveiled from those data was apparent: mobility differences exist among a wide variety of cells, and CE has the ability to separate cells in many applications. As discussed in Chapter 1, CE on microchips offers many advantages over its conventional counterpart. It may also provide opportunities for improving the efficiency and accuracy of cell separations.

Table 5.1 Electrophoretic Mobilities of Various Cells

Cell type	μ (μm.cm.v^{-1}.s^{-1})	Electric field or voltage	Additives or ions in medium	Ref.
Rabbit RBC	1.64	~243 V/cm	0.1% HPMC, pH 7.18	[19]
Human RBC	3.55			
Human T-cells, CD4+	1.18	5~15 V/cm	145 mM NaCl	[29]
Human B-cells	0.78	5~15 V/cm	145 mM NaCl	[29]
Human nasopharyngeal cells, CNE 2L2	1.37	20 V	145 mM NaCl	[28]

* HPMC is the abbreviation of hydroxypropylmethylcellulose

The goal of the work presented herein was to investigate the feasibility of the electrophoretic separations of biological cells on microfluidic devices. Based on the characterization of the electrokinetic transport properties of cells in microchannels, we developed protocols for the on-chip injection and separation of cells. On-chip separations of mixtures of cells were also demonstrated. It has been proved that the selection of particular cells of interest on a microchip, based solely on their electrophoretic mobility, is feasible and promising.

5.2 Materials and Methods

5.2.1 Reagents

GeneScan® polymer (7%, P/N: 401885) was obtained from Applied Biosystems (Foster City, CA, USA). A Tris-borate with EDTA buffer was made with Tris base and boric acid from Fisher Scientific (Fair Lawn, NJ, USA) and EDTA from Merck (Darmstadt, Germany) (10×TBE, 890 mM Tris, 890 mM boric acid, and 20 mM EDTA, pH: ~8.3). The running buffer, referred to as "1TBE10G", was made with glycerol (SigmaUltra, lot No. 121K0121) from Sigma-Aldrich (St Louis, MO, USA) and the TBE buffer so that the final concentration of the glycerol was 10% (w/w), and the TBE was 1×TBE. The separation medium was 5% (w/w) GeneScan® polymer and 10% (w/w) Glycerol in 1×TBE buffer (referred to as "5GS10G"). MilliQ water was made by filtering distilled water through a Millipore Ultra-Pure Water System, and it was kindly supplied by Dr. Glerum, Department of Medical Genetics, University of Alberta. In some experiments in this work, glycerol was not used in the separation medium. GeneScan polymer was added into the TBE buffer so that the final concentration of the polymer was 5% (w/w), and the TBE concentration was 1×TBE (referred to as 5GS1TBE). Except a reduced viscosity, we found the performance of the 5GS1TBE in the separation experiments was identical to the 5GS10G.

To-Pro-3 iodide solution in DMSO, a monomeric cyanine nucleic acid stain, was obtained from Molecular Probes (Eugene, OR, USA).

A modified Alsever's solution was obtained from Canadian Blood Services (CBS, 1800 Alta Vista, Ottawa, ON). The solution was used as a red blood cell preservation

solution. According to the CBS [30], this reagent is a solution of trisodium citrate, sodium chloride, inosine, glucose, citric acid, neomycin sulphate, chloramphenicol, adenine and sodium hydroxide.

5.2.2 Latex Beads and Cells

Latex beads were used in some experiments in this work due to their similarity to cells in terms of size and shape, and their ease of use. White sulfate beads with diameter of 4 μm (Product No. 1-4000) were purchased from Interfacial Dynamics Corporation (Portland, OR, USA). The latex beads are suspended in distilled de-ionized water from the manufacturer. The particle number per milliliter of the 4μm latex is 1.2×10^9. The coefficient of variance of the diameter is 5.1%. An aliquot of the stock bead suspension (*e.g.*, 10 μl) was mixed with a running buffer in a 200-μl PCR tube so that the concentration of the beads was 1.2×10^8 ea. per milliliter, followed by centrifugation (Eppendorf centrifuge Model 5415D) at 3600 rpm (~1200 g) for 2 minutes to form a pellet of the beads. The supernatant was carefully removed using a micropipette. The pellet of the beads was then resuspended into the running buffer and the concentration of the beads was maintained to the original level (*i.e.*, 1.2×10^8 ea. per milliliter). After a 30 second vortex step, this process (including the centrifugation and resuspension) was repeated two times.

Saccharomyces cerevisiae (baker's yeast), purchased as dry powder, was a product of Fleischmann's (Lasalle, QC, Canada). Before the CE experiments, the yeast powder was suspended in a running buffer to obtain a final concentration of 20 mg/ml (w/v) (otherwise specified). The yeast cell suspension was washed twice following the same procedure as the latex described earlier in the section.

Reagent red blood cells (Panoscreen®) were obtained from Immucor Gamma (Norcross, GA, USA). The cells were spun down by centrifuging at 4000 rpm (~1333 g, Eppendorf 5415D) for 10 minutes and resuspended in a modified Alsever's solution. Before CE, an aliquot of the RBC suspension (*e.g.*, 50μl) was transferred into 1TBE10G to obtain a final concentration of 2% RBC in the suspension (packed cell volume: buffer volume = 2: 100). The RBC suspension in 1TBE10G was washed 2 times following a

similar procedure to the latex beads except using different centrifuge parameters (4000 rpm, 2 minutes) and using hand-shaking instead of vortexing to disperse cells.

Bio-safety precautions were as follows: all the cell suspensions were transferred into a 10% bleach solution (less than 8 hours old) using a micropipette. The bleach solution was disposed of down the drain after 12 hours. The work area was wiped using TechniCloth® wipe and 70% ethanol. All solid waste, such as used pipette tips and contaminated TechniCloth, was put into a small plastic bag and disposed into a biohazard waste container.

5.2.3 Staining of Cells

In order to detect cells using laser induced fluorescence (LIF) or fluorescence microscopy, some cells and beads were incubated with To-Pro-3 (excitation 642 nm, emission 661 nm, Molecular Probes) before CE in some experiments. Cells were first suspended into a running buffer following the procedures described in section 5.2.2. An aliquot of the stock To-Pro-3 solution was added into the cell suspension to obtain a final concentration of the To-Pro-3 of 10 μM (otherwise specified). The dye was mixed with the cell suspension immediately by shaking the container by hand. Vortexing was avoided for RBCs to prevent possible damage of the intact cells. The mixture of cells and the dye was incubated at room temperature in the dark (*e.g.*, container was covered by an aluminum foil) for 10 minutes. After the incubation, two cycles of the washing process were performed in order to remove the free dye from the cell suspension.

According to Sakamoto *et al.* [31], the To-Pro-3 was used for the staining of fixed *E. coli* O157:H7, and bright fluorescence from the cells was detected under an epifluorescence microscope. In our work, the cell staining method was modified from the one reported by Sakamoto *et al.* in [31]. The staining and the fluorescence detection of cells will be discussed in section 5.3 in detail.

5.2.4 Microchip and Microfluidic Tool Kits (μTK)

Figure 5.1 shows a single cross microchip (Micralyne Inc., Edmonton, AB) consisting of 4 wells (or reservoirs) linked by two microchannels, one of which serves as a separation channel approximately 92 mm in length, the other one serves as an injection channel

approximately 10 mm in length. The channels are nominally 140 μm wide and 60 μm deep. This type of chips (referred to as Type A) was used for the separation of RBCs and yeast cells. Standard double cross microchips (refereed to as Type B in this chapter, refer to the section 2.2 of Chapter 2 for the description in detail) were also used in some experiments, especially for the separations of yeast and latex beads. Microchips were rejuvenated (following the procedure described in Chapter 3) before each run of cell electrophoresis.

Please refer to the section 2.2 of Chapter 2 for the description of the Microfluidic Tool Kits (μTK). In this work, we used a LIF system that provides excitation at a wavelength of 630 nm and detection at 670 nm. The excitation laser was focused at the center of the channel on microchips. The position of the detection point varied according to the purpose of the experiment.

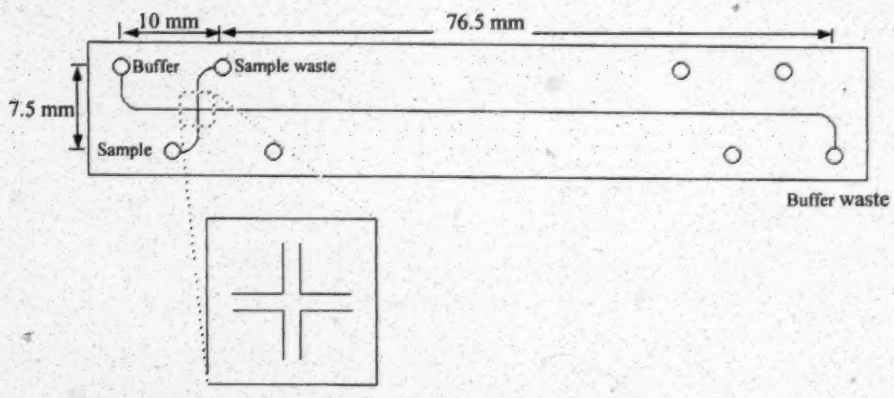

Figure 5. 1 Diagram of a single cross microchip (Type A)

5.2.5 Injection and Separation of Cells on Microchips

Prior to loading, the microchip was rejuvenated following the protocol described in Chapter 3. The reagents in wells and channels used in different experiments were listed in Table 5.2. The separation medium was first forced into the channels from the buffer waste well using a syringe. The buffer waste well, the sample waste well, and the buffer well were loaded with 3 μl running buffer respectively. Finally the sample well was loaded with a 3-μl cell suspension. In the experiments of the separations of latex beads and yeast cells, a 1.5 μl latex bead suspension mixed with a 1.5 μl yeast cell suspension was added into the sample well, followed by stirring using the tip of the micropipette to

mix the cells. In the experiments involving the separations of RBC and yeast cells, 1.5 μl RBC suspension and 1.5 μl yeast cell suspension were added into the sample well, followed by stirring using the tip of the micropipette to mix the cells.

Table 5.2 Reagents in wells and channels for experiments

Experiments	Microchip	Channels	Sample well	Sample waste well	Buffer well	Buffer waste well
RBC involved experiments	Type A	5GS10G	3 μl cell suspension in 1TBE10G	3 μl 1TBE10G	3 μl 1TBE10G	3 μl 1TBE10G
Others	Type B	5GS1TBE	3 μl cell suspension in 1TBE	3 μl 1TBE	3 μl 1TBE	3 μl 1TBE

Table 5.3 A Typical Voltage Program for Cell Separation

Step	Time	Sample waste well	Buffer waste well	Sample well	Buffer well	Function
1	60s	0.20 kV	Float	Ground	Float	Injection
2	0.5s	Float	2 kV	Ground	Float	Plug formation
3	30s	0.4 kV	2 kV	0.4 kV	Ground	Separation

Table 5.3 shows a typical voltage program for the injection and separation of cells. Upon application of the injection voltage, a stream of cells migrated from the sample well towards the sample waste well. Upon arrival of the main stream of cells to the intersection, a brief injection of the cells into the separation channel was performed by the application of an electric field between the sample well and the buffer waste well. This brief injection was designed to achieve a larger sample plug for the subsequent separation. Pullback voltages (as discussed in section 5.3.2) were applied during separations to prevent possible leakage of cells (unless otherwise specified).

5.2.6 Fluorescence Microscopy

Fluorescence Microscopy was performed using a Zeiss AxioVert 200 inverted microscope (Carl Zeiss) equipped with a fluorescence filter set (Chroma 41008) and a camera (Hamamatsu EM-CCD C9100) for image acquisition. A custom-made microchip holder was used in order to acquire images or videos during the application of μTK voltage program.

Some images of cells were acquired using a digital camera (Nikon Coolpix 995) mounted on a microscope (Fisher Micromaster, magnification 100×).

5.3 Results and Discussions

As an additive to the separation medium, GeneScan polymer was used in our CE work on-chips. Using this polymer had 3 advantages. 1) The EOF was effectively suppressed because the polymer served as a dynamic coating of the channel wall [32]. Since the EOF was negligible, we considered that the cells were transported solely by electrophoretic forces. 2) The polymer coating also eliminated the adhesion of cells, which have tendency to adhere to native glass surfaces [33]. 3) The increased viscosity due to the polymer additive minimized the pressure-driven flow in the channel, which resulted from factors such as minor difference of liquid level in reservoirs.

Under the specified CE conditions described in section 5.2, all types of cells studied in this work migrated towards the +ve electrode under a DC electric field (*i.e.*, they were negatively charged in the aqueous solution).

5.3.1 Injection of Cells

In the literature, cell injections were often realized by using pressures [20, 27, 34]. In our work, an electrokinetic approach was employed for the injection of cells. Using voltage programs, the injection and separations could be performed automatically. In order to monitor the movements of cells under an electric field during injections, direct observations through the eyepiece of the μTK were performed. Initially, the migration behavior of cells during injections was studied using latex beads. Information obtained in experiments of cell injection and separations suggested that the migration behavior of other cells during injections was similar to the latex beads.

Upon application of an injection voltage, cells in the sample well moved slowly as they approached the inlet of the injection channel. Once cells moved into the channel, their migration speed showed a sudden increase. This increase of velocity was observed when the buffer concentration and reagent viscosity in the sample well were the same as that in the channel. The geometry of the sample well results in relatively lower electric field intensity in the well, and therefore smaller electrophoretic forces on cells. If the

concentration of buffer in the sample well was lower than that in the channel (*e.g.* 0.1×TBE in the sample well, but 1×TBE in the channel), the difference of the velocity of a cell at different locations between the sample well and the channel was minimized. That allowed movement of more cells into the channel in a given time, and therefore the cell concentration in the channel was increased. However, the low concentration of the buffer in the sample well could result in other problems such as flow anomalies. For instance, we found that RBC cells in a diluted suspension* first migrated electrophoretically towards the sample waste well (+ve electrode), but headed in the other direction after a brief period (*e.g.*, ~30s) under an electric field of ~250 V/cm. Increasing the electric field made the situation worse. This was probably caused by the low buffering capacity of the diluted buffer and the resulting pH gradient. A similar observation was also reported by Minerick *et al.*[35], who attributed the flow reversal of red blood cells (RBC) to the formation of a pH gradient that resulted from an electrolysis reaction at the electrodes. We also observed that cells tend to aggregate around the inlet of the injection channel after a period (*e.g.*, ~30s) when the buffer concentration in the sample well was low (*e.g.*, 0.1×TBE). At the beginning of the electrokinetic injection, cells moved into the channel rapidly. As time passed, cells around the inlet slowed down and halted around the corners. Cells coming later started to aggregate at those locations. Eventually, those cells aggregated into clumps and plugged the inlet of the injection channel. The phenomenon was probably in part a result of pH change due to the consumption of buffers. According to Minerick *et al.*[35], a similar phenomenon was also observed around the entrance of capillaries when no buffer was used.

Based on a FEMLAB simulation of the electric field around the inlet of the injection channel (see Figure 5.2), the electric field intensity in the channel is much higher than that in the sample well. There is also a gradient of electric field intensity in the well. Additionally, the field singularities are shown around the corners of the channel inlet. The experimental observations of the electrophoretic mobility of cells at different locations were in agreement with the simulation. According to Minerick *et al.*, the

---

* The phenomenon was observed when cells were suspended in 10× dilution of a 1× PBS buffer, while the channels were filled with the 1× PBS and 5% GeneScan polymer. No test was performed in diluted TBE buffer because it was found that most RBC cells were damaged in a short time in 10× dilution of the 1× TBE buffer.

corners of the channel tend to have large zeta potentials due to the field singularities, which can also be derived from the electrostatic Laplace equation [35]. Cells having the opposite zeta potentials are likely to be attracted to those corners. On the other hand, the pH of the electrolyte in the cathode reservoir (the sample well) tends to increase due to the generation of OH^- ions [36]. The pH change will also alter the surface properties of both the glass and the cells, and therefore, the migration behavior of the cells in the sample reservoir will change accordingly. Those observations of the injection of cells suggest that the geometrical design of microchips is critical for cell injections.

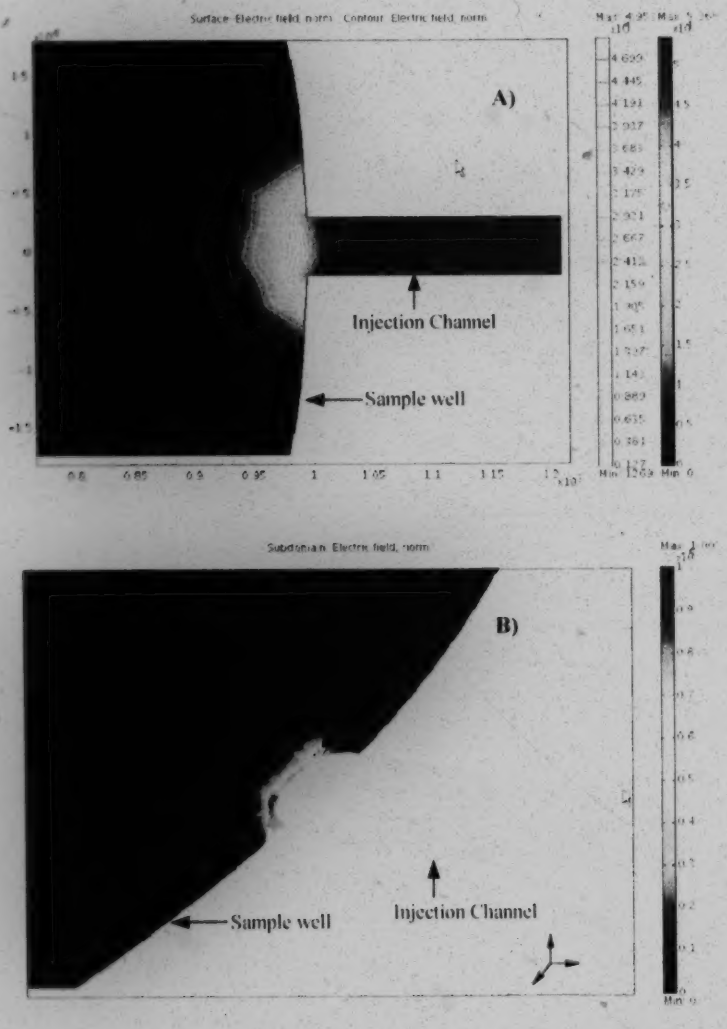

Figure 5.2 FEMLAB simulation of the electric field in the sample well and around inlet of the injection channel. The sample well was connected to ground; the sample waste well was connected to 0.4 kV. The

conductivity of the fluid in the channel and well was assumed to be 0.1 S; its relative permittivity was assumed to be 80. A) 2D simulation, B) 3D simulation.

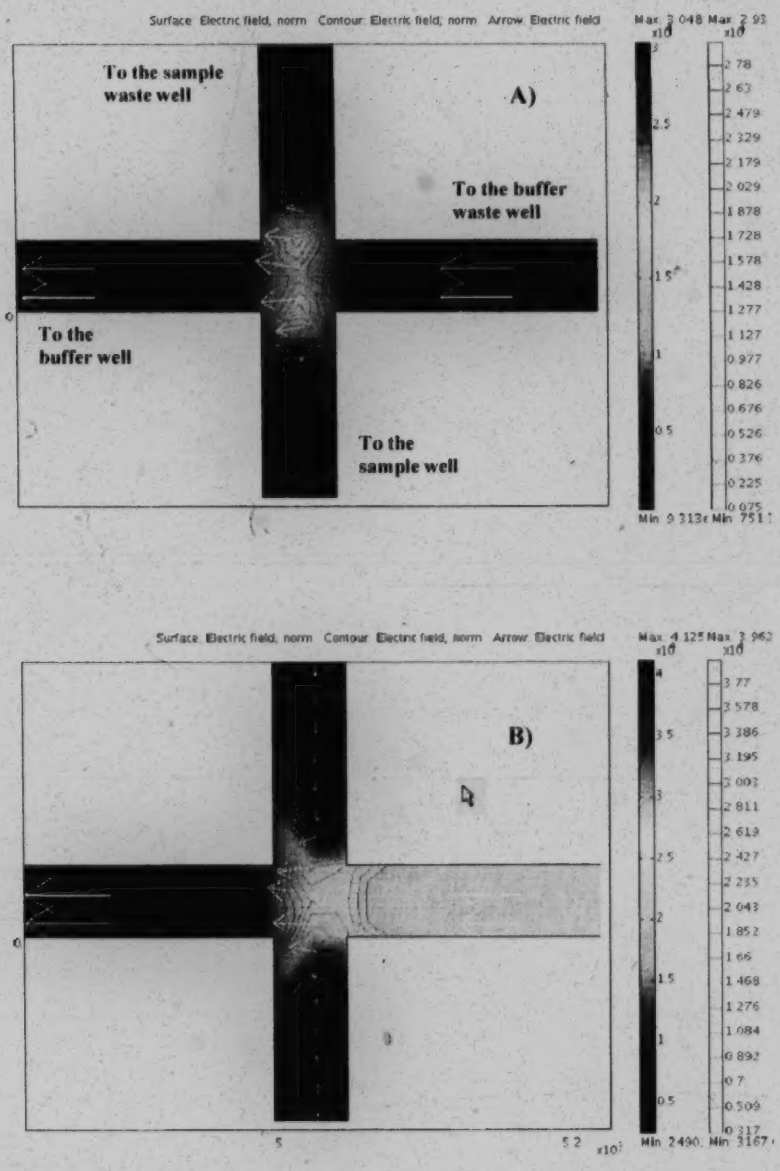

Figure 5.3 FEMLAB simulation of the electric field at the intersection of the channels. Arrows show the current direction, which is opposite to the direction of the cell migration. The buffer well was connected to ground; the buffer waste well was connected to 2.5 kV. A) the sample well and the sample waste well were floating; B) the sample well and the sample waste well were connected to 220 V. The conductivity of the buffer in the channel was assumed to be 0.1 S, the relative permittivity 80.

5.3.2 Forming of Sample Plugs

It is apparent that the concentration of the injected cells has to be high enough to ensure that there are a sufficient number of cells in the intersection of channels to form a sample plug. By lowering the buffer concentration and reagent viscosity in the sample well (*e.g.*, 0.05×TBE in the sample well and 5GS1TBE in the channel), and therefore increasing the velocity of cells in the well, we were able to increase the concentration of injected latex beads in the injection channel. However, as discussed earlier, lower concentration of the buffer may lead to change of pH. Additionally, it is not feasible for a biological cell (*e.g.*, RBC) because the low buffer concentration in the sample well caused cells to lyse (*i.e.*, burst).

One solution to form a large plug is to redesign the layout of the chip to obtain a large Twin-T intersection [37] (also refer to Figure 2.1). However, the dimension of the Twin-T intersection must be altered for different cell types that may have different concentrations and sizes. Another method to obtain a large sample plug was employed in our experiments. The method was based on the modification of voltage programs. Upon the arrival of the main stream of injected cells at the intersection of the channels, a brief injection (*e.g.*, 0.5 s) from the sample well to the buffer waste well of a single-cross chip was performed to transport some cells into the separation channel. The separation voltage was applied between the buffer well and the buffer waste well subsequently. The advantage of this approach was that the brief injection time could be easily modified in order to form a sample plug with a suitable size.

A simulation by FEMLAB showed that the electric field in the separation channel is uniform and has a high intensity (Figure 5.3A). The geometry determines a distorted distribution of the electric field around the intersection of channels. Under the electric field, some cells around the intersection will move latterly into the separation channel under a relatively weak electric field long after the sample plug has left. Those later cells will result in the broadening of the cell bands. Furthermore, a minor flow of the fluid in the injection channel may result in a constant leakage of the cells from the injection arm to the separation channel and degrade the separation.

There are several possible causes of leakage flow of the fluid. a) Due to factors such as the unbalanced pressure of the reagents in wells or capillary action, a pressure-driven

flow may be generated in the injection arms. b) Experiments in the literature have shown that the EOF through the separation channel could induce a leakage flow from the side injection channels to the separation channel, even without an electric field within the side channels [38, 39]. c) The leakage may arise from the Venturi effect [40], which is used commonly in water aspirators to create a vacuum in a side channels [41]. The leakage of cells was suppressed in our experiments by applying bias voltages to all reservoirs during the separation step to pull cells in the side channels back towards the sample well and the sample waste well simultaneously. By treating each segment of the channel as a resistor, the electric potential at the intersection can be easily estimated for the determination of the bias voltages (pullback voltages). As shown in Figure 5.3B, a FEMLAB simulation of the electric field can show the expected migration direction of cells when the pullback voltages are applied. In the simulation, the buffer well was grounded; the buffer waste well was connected to 2.5 kV; the sample well and the sample waste well all were connected to 220 V. Cells in the separation channel migrated towards the buffer waste well, while cells in the injection arms migrated towards the sample well and the sample waste well with a smaller velocity.

The experimental injection of cells was demonstrated in Figure 5.4. Cells (RBCs) migrated from the sample well towards the sample waste well when the injection voltage (100 V) was applied. Injected cells passed through the intersection and dispersed slightly around the intersection due to the field distribution (Figure 5.4A). When an electric field (~298 V/cm) was applied between the sample well and the buffer waste well, cells in the lower injection arm moved to the separation channel for a specified period (one second in this case, Figure 5.4B). After the brief injection, an electric field (~272 V/cm) was applied between the buffer well and the buffer waste well, while the sample well and the sample waste well were electrically disconnected. Cells in the separation channel migrated towards the buffer waste well (Figure 5.4C and 5.4D). Since cells were migrating quite quickly, only some traces of cells were captured in the separation channel by the camera. Figure 5.4D shows a worst-case scenario — a few cells were leaking into the separation channel, which resulted from a physical flow of the fluid in the injection channel.

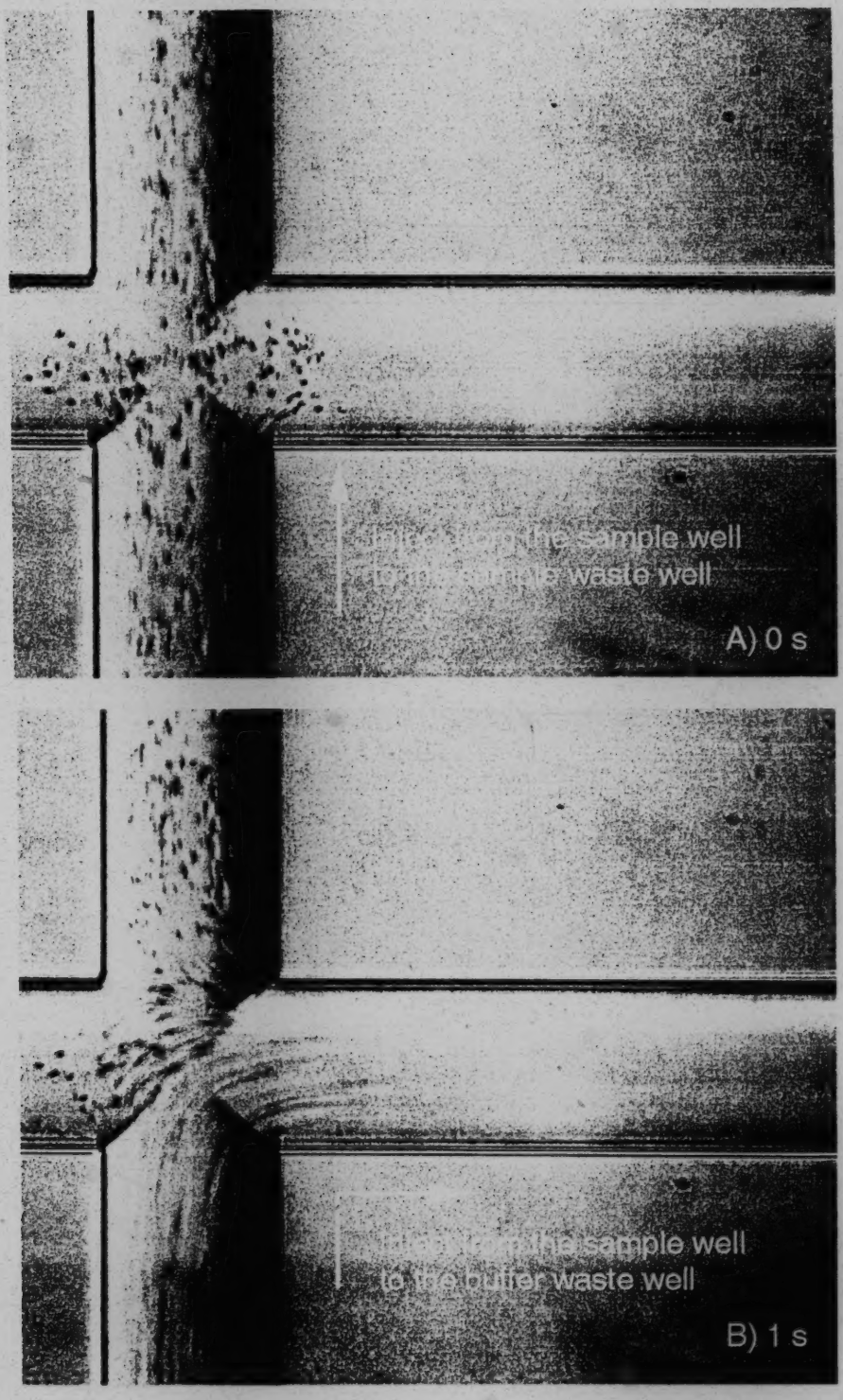
to the sample waste well
A) 0 s
to the buffer waste well
B) 1 s

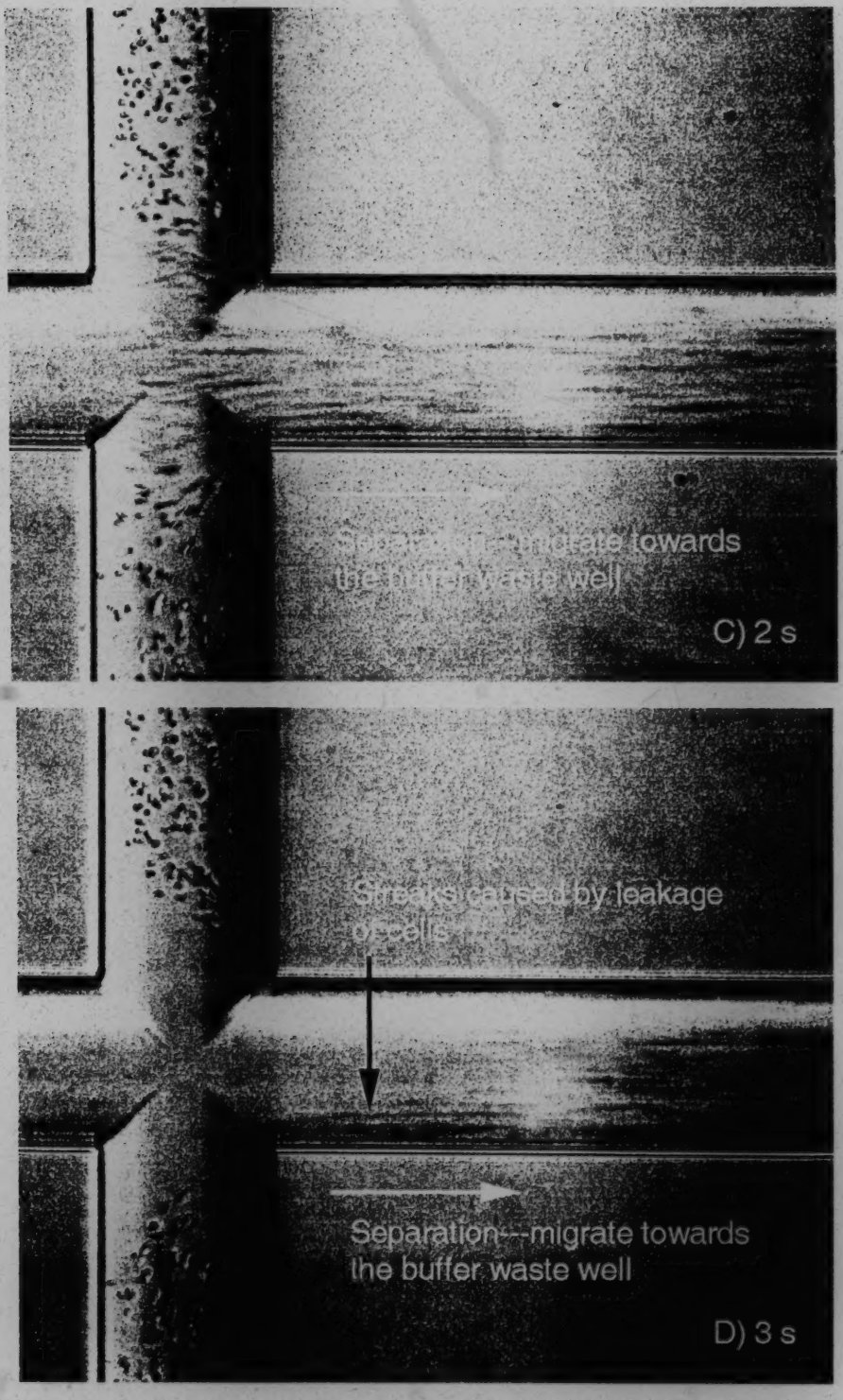

Figure 5.4 Images of cells during the injection and separation. A) Cells were injected from the sample well to the sample waste well under an electric field of 100 V/cm. B) One second later, cells were moved from

the sample well to the buffer waste well to form a sample plug under an electric field of 298 V/cm. C) Another second later, a plug of cells migrated from the buffer well towards the buffer waste well under an electric field of 272 V/cm. D) Cells in the channels after one more second of the separation. No pullback voltage applied. Microscope objective magnification: 20×; halogen lamp voltage: 1.5 V.

In Figure 5.4D, the leakage was found from only one side-channel, indicating that the Venturi effect was not significant (because the Venturi effect should be symmetric on two side-channels). The leakage shown in Figure 5.4D was probably due to unbalanced pressure in wells.

5.3.3 LIF Detections of Cells

According to the operating manual of the μTK, reflected light cannot be filtered out completely by the optical system. In some of our experiments, the reflected light was utilized for the detection of non-stained cells. Figure 5.5 shows the electropherograms of the RBCs in three CE separations, in which the x-axis is the separation time, and the y-axis is the reflected light signal intensities collected by the LIF system of the μTK. In each of those CE separations of the RBCs alone, a group of spikes was detected at the detection point in the separation channel (5 mm downstream from the intersection). As shown in Figure 5.5, the mobilities of those spikes showed excellent repeatabilities. It was confirmed by direct observations using a microscope that those spikes represented the passage of RBCs through the detection point. Figure 5.6 shows a picture of the RBC band in the separation channel after a 50-second separation, which was taken by the Nikon camera attached to a microscope (magnification: 100×). It was found that the band of RBC in Figure 5.6 was composed of only single cells. According to Tsuda *et al.* [18], the distribution of spikes in the electropherogram corresponded to the distribution of the electrophoretic mobilities of the RBCs. Our observation was in agreement with their report.

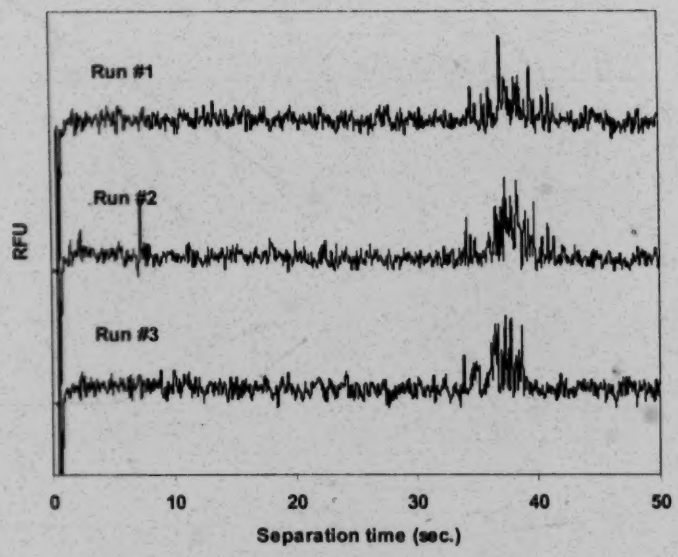

Figure 5.5 Electropherograms of RBCs in 3 separation runs. The reflected light signal of RBCs (near 37 s) was detected by the optical system of the μTK. Separation electric field was 217 V/cm, with pullback voltages of 0.4 kV. Detected at 5 mm from the intersection. PMT gain was 0.8 V.

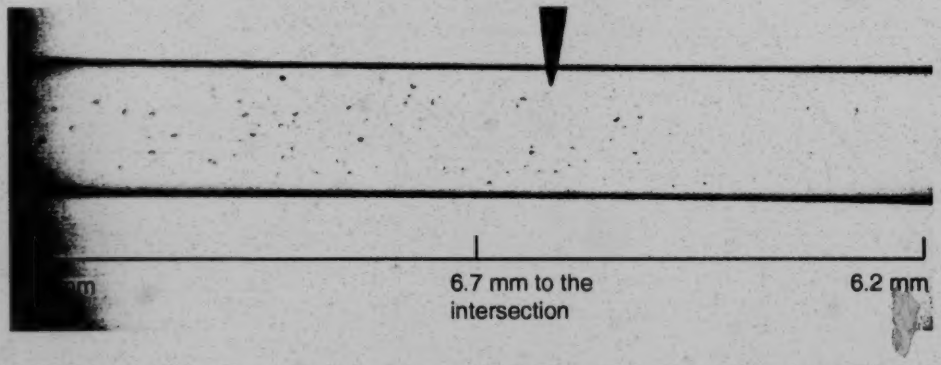

Figure 5.6 RBC band after a 50s separation of the run #3 in Figure 5.5. The estimated mobilities of the RBCs were 6.2+/-0.5 $\times 10^{-5}$ $cm^2.v^{-1}.s^{-1}$. Picture was taken by a Nikon Coolpix 995 camera. Microscope magnification was 100×.

Although the reflected light signal for RBCs was detectable, as shown in Figure 5.5, the signal to noise ratio was low. We found that the reflected light signals for yeast cells were even weaker. In order to demonstrate the separation of cells by the LIF detection, cells were incubated with a nucleic acid stain, To-Pro-3, for a short time (see section 5.2.3 for detail). It was found that much stronger signal intensities were obtained after the staining. Figure 5.7 shows the detected peaks of RBCs, which were incubated with 10

μM To-Pro-3 for 10 minutes prior to the CE. It was known that the relatively high signal intensities were not caused from a true fluorescence staining of the RBCs because the To-Pro-3 was a nucleic acid stain and the RBCs were devoid of nuclei. A hypothesis for the mechanism behind the observation was that because the To-Pro-3 molecules were positively charged [42] and the RBCs were negatively charged in 1TBE10G, To-Pro-3 molecules might attach on the surface of the RBCs due to electrostatic attraction. Probably the emission of the To-Pro-3 on the surface of the RBCs due to the "pseudo staining" resulted in the high intensities of the detected RBC spikes. Comparison between Figure 5.5 and 5.7 showed that the mobility of the RBCs after incubation with the To-Pro-3 decreased a negligible amount.

In the same manner of the RBCs, the staining of yeast cells and latex beads was performed. It was found that the stained yeast cells showed much higher peaks in the electropherograms than the latex beads and the RBCs (Figure 5.8). The mechanism of the "staining" was not completely understood. As for the demonstration of cell separations, we assumed that the effect of the "staining" on cell mobilities were negligible.

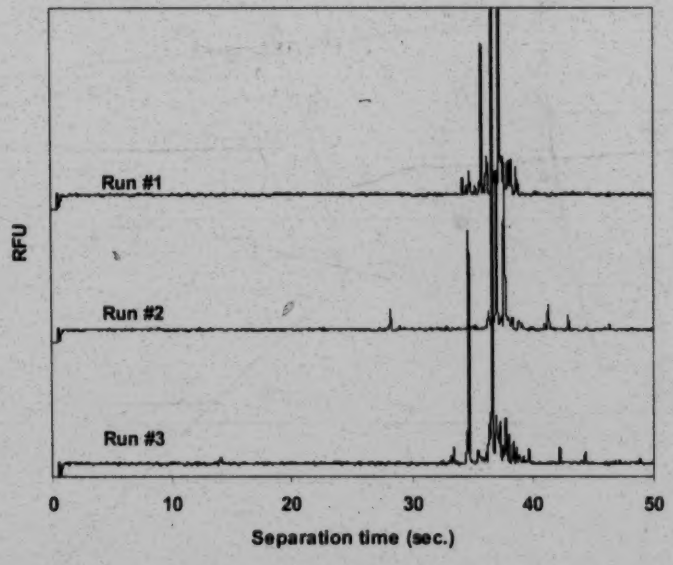

Figure 5.7 Electropherograms of RBCs in 3 separation runs. RBCs were incubated with To-Pro-3 prior to CE. Separation electric field was 217 V/cm, with pullback voltages of 0.4 kV. Detected at 5 mm from the intersection. PMT gain was 0.8 V.

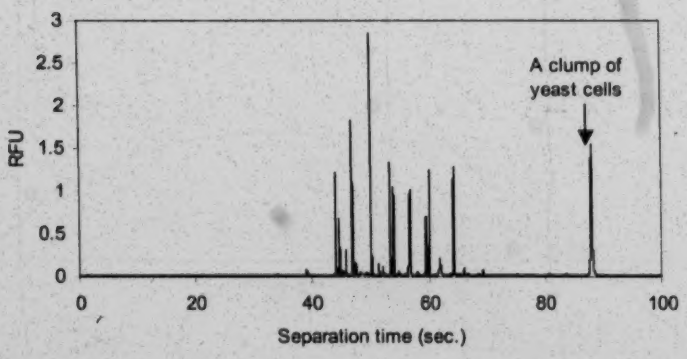

Figure 5.8 Electropherograms of yeast cells. Cells were stained by 5 μM To-Pro-3 iodide prior to CE. Separation electric field was 235 V/cm (with pullback voltage of 0.2 kV). PMT gain was 0.6 V. Detected at 5 mm from the intersection.

According to the operating manual of the μTK, the diameter of the red laser beam is ~10 μm, and the confocal ellipsoid is ~ 40 μm × 20 μm (height ×width). Since the cross-sectional dimension of the separation channel is much larger than the diameter of the laser beam, many cells were missed by the detection. This was roughly confirmed by the observation that the number of the cells in the channel in Figure 5.6 was much larger than the numbers of spikes in the electropherogram in Figure 5.5. As shown in Figure 5.7, a group of peaks for the RBC population was detected, indicating that the cells were dispersed when they passed through the laser beam. In recent publications [20, 22], single peaks of cell populations were obtained in the separations of mixed bacterial cells using conventional CE. As discussed in section 5.1, the authors later reported that those single peaks of cell subpopulations in the electropherograms were the result of cell aggregations (*i.e.,* false separations). Single peaks of the cell populations may be achieved by redesigning the optical system, and/or minimizing the electrophoretic heterogeneity of the cells. Using the described optical system, we were still able to demonstrate the separation of cells.

5.3.4 Separation of Cells

It has already been known that the large variation of the electrophoretic behavior of cells in the same population will give rise to a broad distribution of cells [43]. However, as long as the two (or more) groups of fluorescence peaks of the two (or more) cell

populations do not overlap, the differentiation or separation is still feasible. In our work, the feasibility of cell separations was demonstrated using various cell mixtures, as described below.

5.3.4.1 Separation of Latex Beads and Yeast Cells

Latex beads and yeast cells were similar in size. However, their apparent CE mobilities were very different according to our observations. Figure 5.9 shows a separation of a few cells on a Twin-T chip (Type B). Under an electric field of ~250 V/cm, the mixture of beads and yeast cells (non-stained) arrived at the intersection after ~40 seconds. Two yeast cells and eight beads were in the geometrical plug of the chip when the separation step was started. Those particles started to move towards the buffer waste well upon application of the separation voltage. The separation was paused after every second to allow the images of the particles in the channel to be captured by a camera mounted on a microscope. As shown in Figure 5.9, 2 yeast cells were separated from 8 latex beads within a couple of seconds in 5GS1TBE under a separation electric field of ~235 V/cm. As the separation time was increased, the distance between those two groups of cells was increased progressively. Meanwhile, the space among individual cells within the same subpopulations was increased also. However, this increase was almost negligible compared to the space between those two groups after a 5-second separation, indicating that the difference of the electrophoretic mobilities between those two populations of cells were significant. For instance, based on the image of the particles after the "3 s separation", the mobility of one yeast cell was ~4.5 $\times 10^{-5}$ $cm^2.v^{-1}.s^{-1}$, the mobility of the other yeast cell was ~5.0 $\times 10^{-5}$ $cm^2.v^{-1}.s^{-1}$, the mobility of the slowest beads was ~6.9 $\times 10^{-5}$ $cm^2.v^{-1}.s^{-1}$, and the mobility of the fastest beads was ~10.3 $\times 10^{-5}$ $cm^2.v^{-1}.s^{-1}$.

The separation of the mixture of yeast cells and latex beads was also demonstrated by the LIF detection of the μTK. As shown in Figure 5.10, the band of latex beads arrived at the detection point much earlier than the yeast cells. Clumps of the yeast cells moved even slower than single yeast cells. The identification of each band of cells was confirmed through a direct observation under a microscope (100× magnification) based on the color difference of the cells.

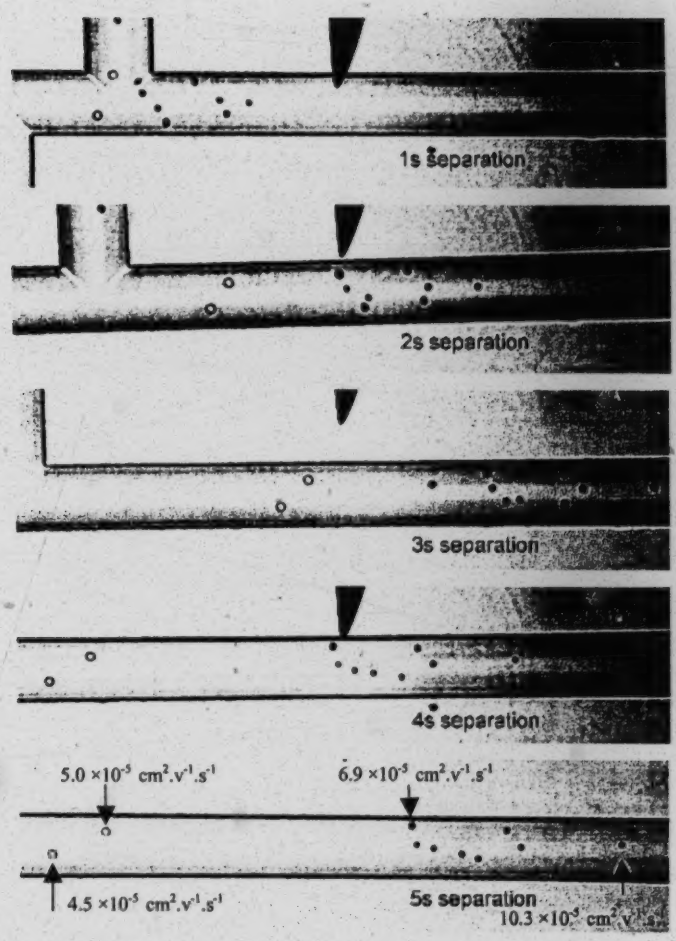

Figure 5.9 Image of yeast cells (non-stained) and 4 μm latex beads (non-stained) during a 5s electrophoretic separation. The 8 dark dots in the channel are 4 μm latex beads; the 2 bright dots in the channel are yeast cells. The separation medium was 5GS1TBE; the separation electric field was 117 V/cm, with pullback of 120 V. Yeast concentration in the sample well was 10 mg/ml initially; latex beads concentration in the sample well was 6×10^7 ea per milliliter. Pictures were taken by a Nikon Coolpix 995 camera mounted on a microscope (magnification, 100×).

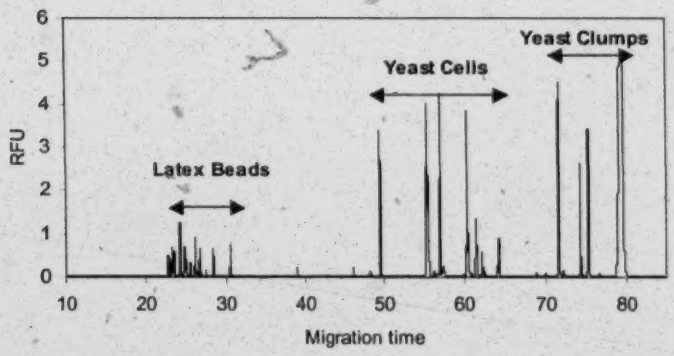

Figure 5.10 Electropherograms of yeast cells and 4 μm beads. Cells and beads were incubated with 5 μM To-Pro-3 iodide for 10 minutes; the separation medium was 5GS1TBE; the separation voltage was 2 kV (with pullback 0.2 kV); PMT gain was 0.6 V; detected at 5 mm from the intersection.

5.3.4.2 Separation of RBCs and Yeast Cells

Figure 5.11 shows the microscope observations of a mixture of the RBCs and yeast cells under a bright field during a separation. A brief injection (0.5 s) of the mixture from the injection arm to the separation channel is partially shown in Figure 5.11A. Another 3 pictures were taken each following second (Figure 5.11B, 5.11C and 5.11D), which show the separation of the mixture with time. Judging from the image captured in Figure 5.11D, a complete separation of the RBCs and the yeast cells was achieved within 3 seconds after the application of an electric field (*i.e.*, 217 V/cm) in the separation channel. Figure 5.12A shows two bands of the cells in the separation channel under a bright field after a 25-second separation. Figure 5.12B shows the corresponding fluorescence images of the cells. Only cells in the band near the intersection showed bright images. As discussed in section 5.3.3, the yeast cells showed much higher fluorescence intensity than RBCs after the incubation with To-Pro-3. It is reasonable to believe that the band of cells showing bright fluorescence is of yeast cells. This was in agreement with those earlier observations that the yeast cells moved slower than RBCs. The clumps of RBC (in Figure 5.11D) were found only at beginning of the separation. These clumps were dispersed several seconds later (*e.g.*, ~5s) and had no effect on the repeatability of the mobility of the RBC band.

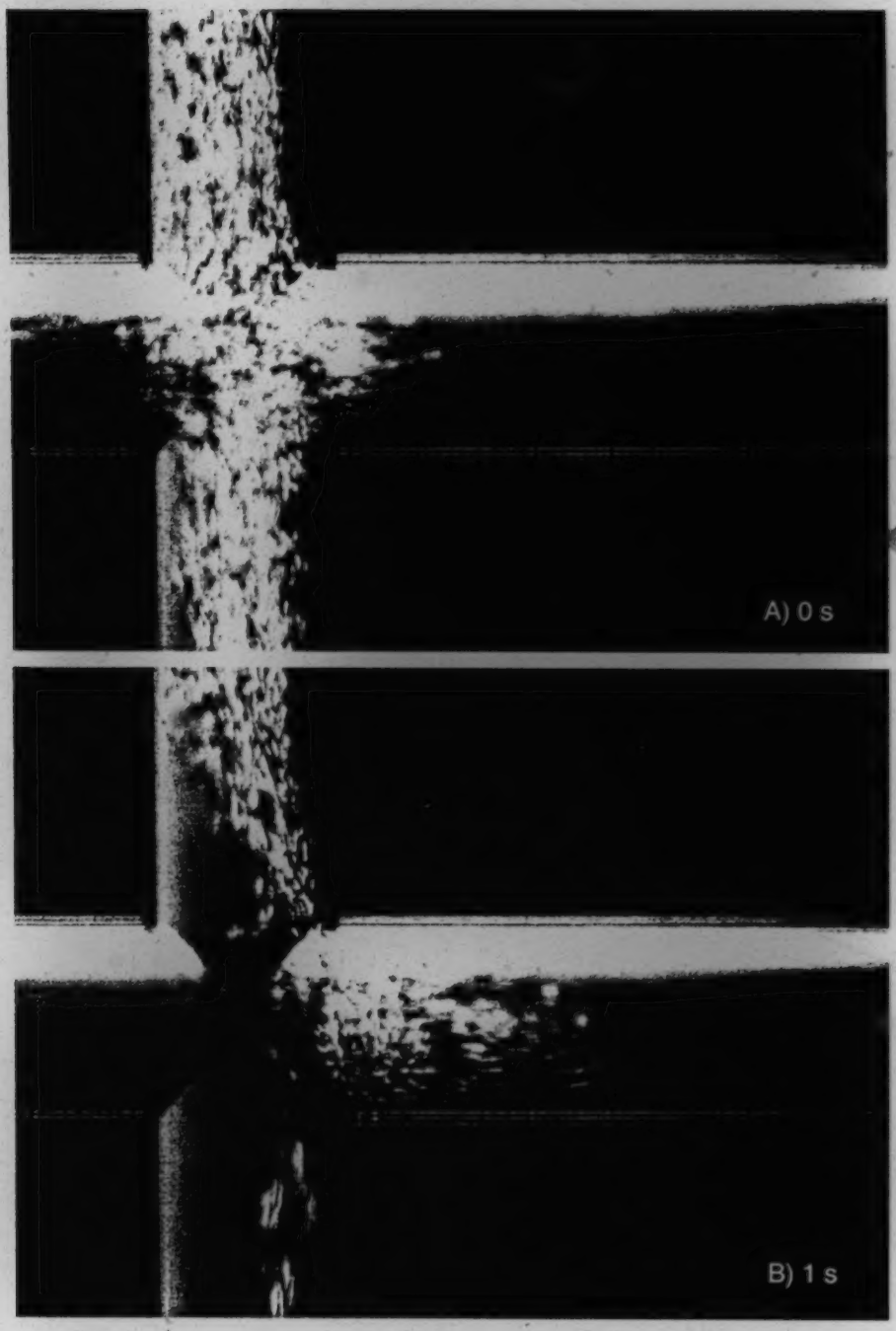
A) 0 s
B) 1 s

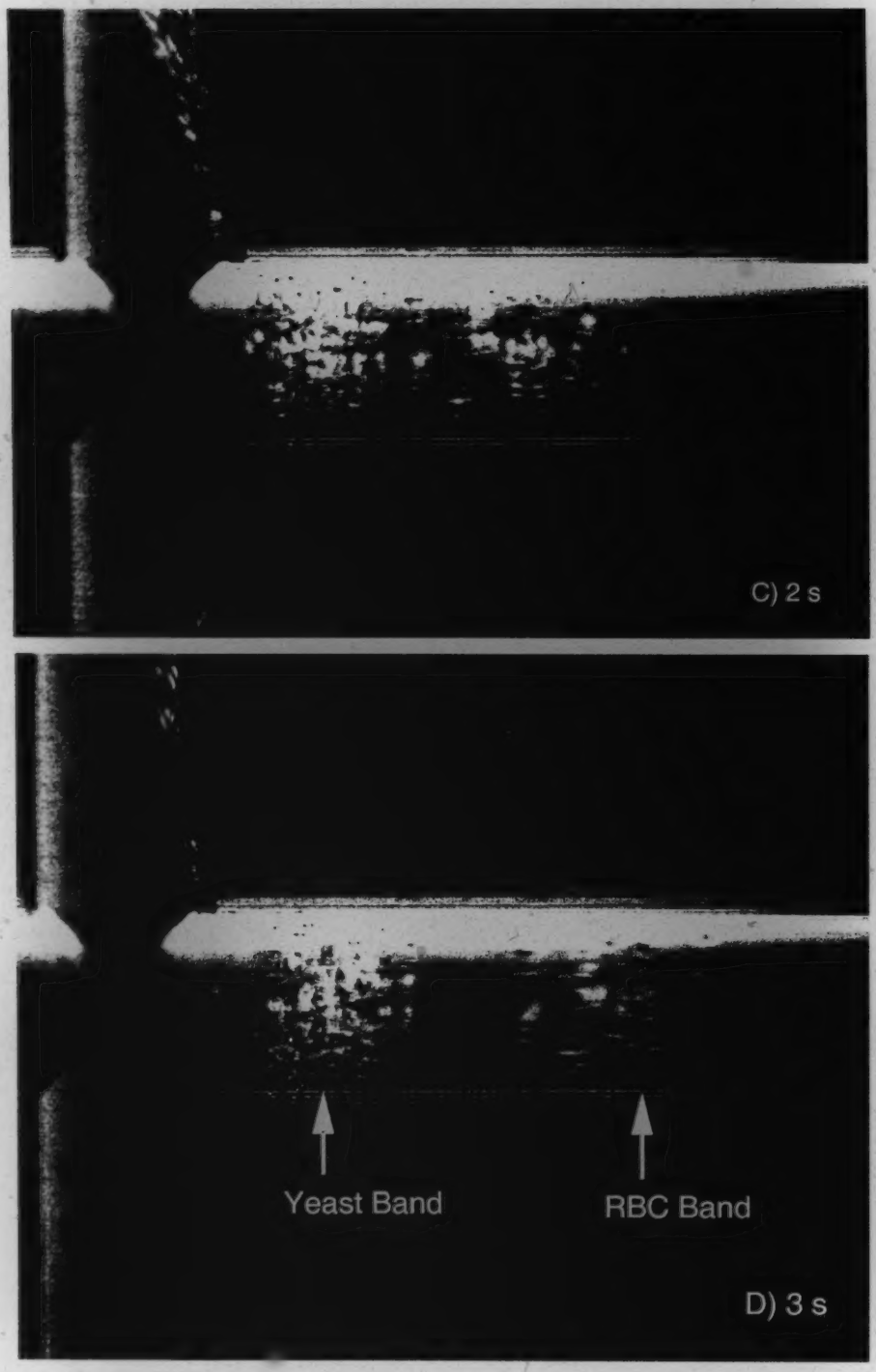

Figure 5.11 Images of RBCs and yeast cells during a separation run. Separation electric field was 217 V/cm with pull back voltage of 0.8 kV. Microscope objective magnification: 20×; halogen lamp voltage: ~1.5 V.

A)
Yeast cell band
IBC band
B)
Yeast cell band

Figure 5.12 RBCs and yeast cells in the separation channel after a 25-second separation under an electric field of 217 V/cm. A) Images of the cells under a bright field; B) fluorescent images of the cells. Microscope objective magnification: 20×; reflector for the fluorescent image: Cy5, TOPRO3; exposure time for the fluorescent image: 1 s.

Some yeast cells clumped in the 1TBE10G (or 1×TBE alone) suspension (prior to the CE) and were injected into the channel from the sample well. Some of the clumps in the channel were dispersed due to the interactions between cells (*e.g.*, bombardment). As shown in Figure 5.12A, the clumps in the band of the yeast cells had relatively smaller mobilities. In order to narrow the band of the yeast cells, the clumping of the cells must be avoided in future work. In contrast, the RBCs migrated at single cell level. As shown in Figure 5.12A, the RBC band was narrower than the yeast cell band.

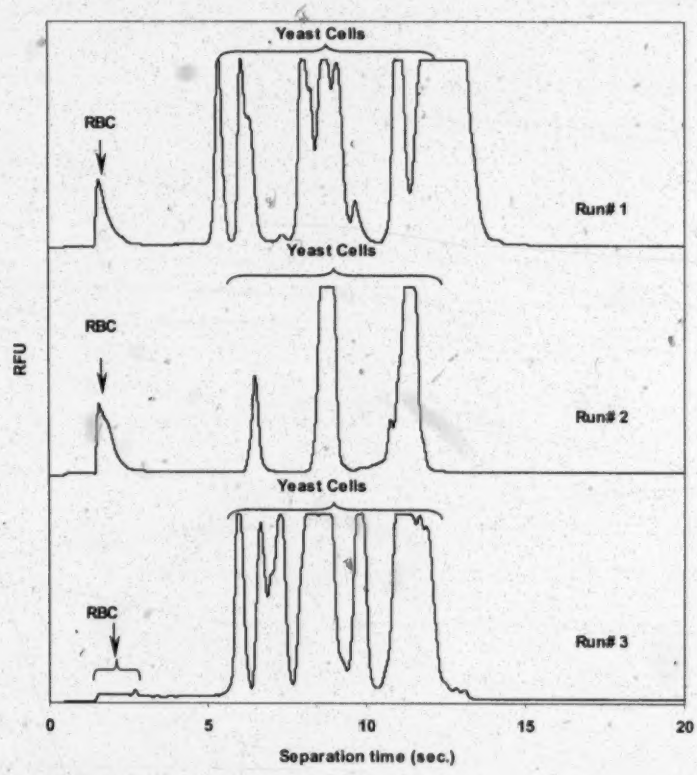

Figure 5.13 Electropherograms of the separations of RBCs and yeast cells. Yeast cells and RBCs were incubated with 10 μM To-Pro-3 iodide for 10 minutes before the CE. The separation medium was 5GS10G; the separation voltage was 2 kV; PMT gain was 0.8 V; detected at ~300 μm from the intersection.

The separation of the mixture of yeast cells and RBC was also demonstrated by the LIF detection of the μTK. Based on the observations in Figure 5.11, the mixture of cells could be completely separated within 3 seconds in a very short length of the separation channel (<500 μm). Therefore, the detected point was placed at ~300 μm from the intersection. After a migration of 300 μm from the intersection, the band of the RBCs was still compact. It showed single peaks in 2 of the 3 electropherograms in Figure 5.13. The separation run # 3 was performed after two injections and pullbacks on the same chip. The traveling of the RBCs in the injection channel may have resulted in the loss of To-Pro-3 molecules from the surface of the RBCs due to weak binding (based on the hypothesis discussed in section 5.3.3), therefore, the peak(s) of the RBC became very low. In contrast, the fluorescence from the yeast cells showed very high intensities including in the run #3, likely due to the nucleic acid staining by the To-Pro-3. The electropherograms in Figure 5.13 showed multiple peaks for the yeast cells, indicating that some yeast cells were dispersed but some were still clumps after a migration of ~300 μm. Because we knew that the fluorescence signal intensity of the yeast cells was higher than that of the RBCs, we could recognize the peaks of different cell types on the electropherogram. The identification of the cell types was also verified by direct observations in extra control runs. In one control run, a 2-second separation of the RBCs alone showed a narrow band at around 300 μm from the intersection; in another control run, a 10-second separation of the yeast cells alone showed a dispersed band of the cells at around 300 μm from the intersection. Those direct observations were in agreement with the electropherograms.

The separations of the mixture of RBCs and yeast cells were performed on microchips with large channels (~60 μm deep, ~140 μm wide). A physical flow of the fluid from the sample well to the sample waste well was often found during our experiments (despite the exist of GeneScan polymer). Since the average density of the reagent in the sample well (cell suspension in 1TBE10G) was higher than that (1TBE10G) in the sample waste well, the physical flow was probably due to a resulting pressure difference between those two wells. Pullback voltages (up to ~500 V) were applied in those separation experiments. The cell leakage during the injection and separation was suppressed. However, a minor cell flow was still found moving from the

sample well towards the sample waste well (but not in the separation channel) after the voltage program was stopped.

Table 5.4 Cell mobilities comparison

Cell Type	Separation Medium	Mobility ($\times 10^{-5}$ $cm^2.v^{-1}.s^{-1}$)
Latex Beads	5GS1TBE	~8.4+/-1.8
Yeast Cells	5GS1TBE	~3.7+/-0.7
Yeast Cells	5GS10G	~2.2+/-0.3
RBC	5GS10G	~6.2+/-0.6

*All cells were incubated with 10 μM To-Pro-3 for 10 minutes before CE

In summary, the mobilities of latex beads, RBCs, and yeast cells in some specified CE conditions were listed in Table 5.4. Those mobility data were calculated based on the method described in Chapter 1. Compared to the RBCs, the mobilities of yeast cells and the latex beads have relatively broad distributions. However, their average mobilities were very different. The band of the RBCs and the yeast cells, the latex beads and the yeast cells do not overlap. This was in agreement with what we observed under the microscope.

5.3.4.3 CE Buffer Selection for Human Blood Cell Separation

The buffer chosen for CE of human cells should preserve cell viability, have a high buffering capacity at physiological pH, and should suppress cell aggregation effects. In the literature, isotonic PBS buffers at the physiological pH level were often used for the CE of the blood cells in order to maintain the integrity and viability of the cells [1, 35, 44]. In our experiments with human RBCs, because the CE analysis was completed in a short time (*e.g.*, less than several hours including the storage time), any effects of the 1×TBE buffers (or 1TBE10G) on cell properties was not noticed. However, when human white blood cells were suspended in the TBE buffer, it was found many cells were damaged in a short time (*e.g.*, less than a couple of hours). Debris and damaged cells aggregated together during the CE. Using a 1×PBS buffer with a pH level of 7.4, the white blood cells could be maintained intact for one or two days. However, there were two problems when the PBS was used as the CE buffer. First, since the size of the white

blood cells is relatively large (*e.g.*, monocyte ~15 μm), microchips with large channels (*e.g.*, ~60 μm × ~140 μm cross section) have to be employed for the CE analysis. As the conductivity of the PBS buffer was much higher than the TBE buffer (according to our experimental data, the estimated conductivity of the 1×PBS buffer was about 1.5 S, the estimated conductivity of the 1×TBE buffer was about 0.1 S), the electric field had to be very low (*e.g.*, 85 V/cm) to avoid the current overshooting its upper limit of the μTK. Second, the relatively high ionic strength (or conductivity) of the 1×PBS buffer resulted in low mobility of the white blood cells (discussed in Chapter 4). Using a PBS buffered separation medium (5% GenScan polymer in 1×PBS), we observed that no white blood cells were injected into the channel from the sample well under an electric field of 85 V/cm within ~20 seconds. Vincent Sieben from our laboratory was able to inject a few white blood cells in PBS into a funnel-shape channel and transport the cell in 5GS10G within the channels. An electric field of 400 V/cm was applied to transport the cells in the channel. However, it was not clear how the cell population was affected, in term of integrity and mobility. According to Silvinsky *et al.* [28], 145 mM NaCl was often used in the CE separation of human cells in the literature (see Table 5.1). Unfortunately, the optimization of the buffered medium is beyond the scope and time period of this work.

5.4 Conclusions

In this work, we developed techniques of cell manipulation on microchips. The employment of a dynamic coating polymer effectively suppressed the EOF and eliminated possible adhesion of cells to the channel walls. Cells were electrophoretically transported in a network of channels on microchips. Using the planar glass microchips and automatic voltage programs, the sample plug formation and separation were realized accurately in a simple way.

Because separation is possible only when the mobility distribution of one cell population does not overlap with the others, it is critical to find out the electrophoretic mobilities of cells of interest under identical CE conditions. Unfortunately, little electrophoretic mobility data of cells on microchip is available in the literature. Silvinsky *et al.* made a summary of the cellular electrophoretic mobility data [28] that was obtained by different people who employed a variety of conventional techniques. From the limited

data collection by Silvinsky *et al.*, a wide range from 0.75 to 1.37 $\mu m.cm.v^{-1}.s^{-1}$ of human cell mobilities was still observed. According to our experiment, the mobility of human RBC had variations (due to cell variability) of about 10%. Since the difference of average mobility between two type of cells may be far larger than this variation, this suggests that CE has the ability to separate cells in many applications.

Although some cells of interest may have similar mobilities to others under one series of CE conditions, resulting in mobility distributions that overlap, it is still possible to change the distribution of their mobilities by altering the CE conditions (*e.g.*, pH)[16, 17, 20].

We are among the first to demonstrate the separation of mixtures of different cell populations (*e.g.*, human RBCs and yeast cells) on microchips. Our microscopy observations showed that the "true" separation of biological cells on-chips based solely on the difference of their electrophoretic mobilities was feasible. The LIF detection of the CE separation of cells was also performed, and it showed results consistent with the microscopy observations. During the writing of the thesis, Shintani *et al.* reported the separation of pure cultures of lactic acid bacteria and *saccharomyces cerevisiae* on microchips [37]. However, the apparent mobility of cells was the result of both electrophoretic force and the EOF. Additionally, it was not clear whether or not cell aggregation existed during the separation. According to our definition in Chapter 1, those separations in [37] could be false separations.

We believe that the CE separation technique on microchips we demonstrated in this chapter could be further developed towards the selective introduction of cells of interest for further cellular analysis (*e.g.*, genetic analysis of cancer cells), and will provide a powerful tool for applications in the fields of life sciences and environmental monitoring.

5.5 References

[1] P. C. H. Li, D. J. Harrison, *Analytical Chemistry* 1997, 69, 1564-1568.

[2] L. C. Waters, S. C. Jacobson, N. Kroutchinina, J. Khandurina, R. S. Foote, J. M. Ramsey, *Analytical Chemistry* 1998, 70, 158-162.

[3] M. A. McClain, C. T. Culbertson, S. C. Jacobson, N. L. Allbritton, C. E. Sims, J. M. Ramsey, *Analytical Chemistry* 2003, 75, 5646-5655.

[4] H. Andersson, A. van den Berg, *Sensors and Actuators B-Chemical* 2003, 92, 315-325.

[5] E. A. Schilling, A. E. Kamholz, P. Yager, *Analytical Chemistry* 2002, 74, 1798-1804.

[6] Y. Huang, K. Ewalt, M. Tirado, R. Haigis, A. Forster, D. Ackley, M. Helller, J. O'Connell, M. Krihak, *Analytical Chemistry* 2001, 73, 1549-1559.

[7] M. S. Yang, C. W. Li, J. Yang, *Analytical Chemistry* 2002, 74, 3991-4001.

[8] F. Becker, X. Wang, Y. Huang, R. Pethig, *Pro. Natl. Acad. Sci.* 1995, 92, 860-864.

[9] E. Olvecka, D. Kaniansky, B. Pollak, B. Stanislawski, *Electrophoresis* 2004, 25, 3865-3874.

[10] H. Nagata, M. Tabuchi, K. Hirano, Y. Baba, *Electrophoresis* 2005, 26, 2247-2253.

[11] J. A. Fruetel, R. F. Renzi, V. A. VanderNoot, J. Stamps, B. A. Horn, J. A. A. West, S. Ferko, R. Crocker, C. G. Bailey, D. Arnold, B. Wiedenman, W. Y. Choi, D. Yee, I. Shokair, E. Hasselbrink, P. Paul, D. Rakestraw, D. Padgen, *Electrophoresis* 2005, 26, 1144-1154.

[12] C. Backhouse, M. Caamano, F. Oaks, E. Nordman, A. Carrillo, B. Johnson, S. Bay, *Electrophoresis* 2000, 21, 150-156.

[13] V. M. Ugaz, R. D. Elms, R. C. Lo, F. A. Shaikh, M. A. Burns, *Philos. Trans. R. Soc. Lond. Ser. A-Math. Phys. Eng. Sci.* 2004, 362, 1105-1129.

[14] S. R. Liu, A. Guttman, *Trac-Trends in Analytical Chemistry* 2004, 23, 422-431.

[15] M. A. Rodriguez, D. W. Armstrong, *Journal of Chromatography B-Analytical Technologies in the Biomedical and Life Sciences* 2004, 800, 7-25.

[16] R. C. Ebersole, R. M. McCormick, *Bio-Technology* 1993, 11, 1278-1282.

[17] A. Pfetsch, T. Welsch, *Fresenius J. Anal. Chem.* 1997, 359, 198-201.

[18] T. Tsuda, N. Yamauchi, S. Kitagawa, *Anal. Sci.* 2000, 16, 847-850.

[19] A. Zhu, Y. Chen, *Journal of Chromatography* 1989, 470, 251-260.

[20] D. W. Armstrong, G. Schulte, J. M. Schneiderheinze, D. J. Westenberg, *Analytical Chemistry* 1999, 71, 5465-5469.

[21] D. W. Armstrong, L. F. He, *Analytical Chemistry* 2001, 73, 4551-4557.

[22] D. W. Armstrong, J. M. Schneiderheinze, *Analytical Chemistry* 2000, 72, 4474-4476.

[23] D. W. Armstrong, J. M. Schneiderheinze, J. P. Kullman, L. F. He, *Fems Microbiology Letters* 2001, 194, 33-37.

[24] J. M. Schneiderheinze, D. W. Armstrong, G. Schulte, D. J. Westenberg, *Fems Microbiology Letters* 2000, 189, 39-44.

[25] L. F. He, R. J. Jepsen, L. E. Evans, D. W. Armstrong, *Analytical Chemistry* 2003, 75, 825-834.

[26] D. W. Armstrong, M. Girod, L. F. He, M. A. Rodriguez, W. Wei, J. J. Zheng, E. S. Yeung, *Analytical Chemistry* 2002, 74, 5523-5530.

[27] T. Shintani, K. Yamada, M. Torimura, *Fems Microbiology Letters* 2002, 210, 245-249.

[28] G. G. Slivinsky, W. C. Hymer, J. Bauer, D. R. Morrison, *Electrophoresis* 1997, 18, 1109-1119.

[29] J. Rychly, E. Knippel, U. Thomanech, W. Schutt, D. Sabolovic, O. Babusikova, G. Eggers, O. Anders, H. Klinkmann, paper presented at the Electrophoresis'86, VCH, Verlagsgesellschaf Weinheim, Germany 1986, pp. 56~60,

[30] C. B. S. Serology Laboratory, "Product insert for modified Alsever's solution" (1998), 1800 Alta Vista, Ottawa, ON, Canada.

[31] C. Sakamoto, N. Yamaguchi, M. Nasu, *Appl. Environ. Microbiol.* 2005, 71, 1117-1121.

[32] R. S. Madabhushi, *Electrophoresis* 1998, 19, 224-230.

[33] M. A. McClain, C. T. Culbertson, S. C. Jacobson, J. M. Ramsey, *Analytical Chemistry* 2001, 73, 5334-5338.

[34] I. V. Kourkine, M. Ristic-Petrovic, E. Davis, C. G. Ruffolo, A. Kapsalis, A. E. Barron, *Electrophoresis* 2003, 24, 655-661.

[35] A. R. Minerick, A. E. Ostafin, H. C. Chang, *Electrophoresis* 2002, 23, 2165-2173.

[36] M. S. Bello, *Journal of Chromatography A* 1996, 744, 81-91.

[37] T. Shintani, M. Torimura, H. Sato, H. Tao, T. Manabe, *Anal. Sci.* 2005, 21, 57-60.

[38] D. J. Harrison, K. Fluri, K. Seiler, Z. H. Fan, C. S. Effenhauser, A. Manz, *Science* 1993, 261, 895-897.

[39] Z. H. Fan, D. J. Harrison, *Analytical Chemistry* 1994, 66, 177-184.

[40] J. M. Coulson, J. F. Richardson, *Chemical Engineering* Pergamon Press, New York, 1977.

[41] L. L. Shultz-Lockyear, C. L. Colyer, Z. H. Fan, K. I. Roy, D. J. Harrison, *Electrophoresis* 1999, 20, 529-538.

[42] V. Sieben, C. Backhouse, *Electrophoresis,* accepted at June, 2005.

[43] H. C. van der Mei, H. J. Busscher, *Applied and Environmental Microbiology* 2001, 67, 491-494.

[44] W. H. Lu, W. H. Deng, S. T. Liu, T. B. Chen, P. F. Rao, *Analytical Biochemistry* 2003, 314, 194-198.

Chapter 6

Preliminary Work Towards Selective Identification of Bacterial Cells on Microfluidic Chips

6.1 Introduction

A growing number of bacteria have been identified as important food- and waterborne pathogens [1]. Today, the possibility of bioterrorist attacks with pathogenic bacteria is also a major concern of public safety agencies [2]. Among those pathogens, *Escherichia coli* O157:H7 is considered to be one of the most dangerous food-borne pathogens, one that can easily contaminate ground beef, raw milk and chicken [3]. Recently, distribution of this pathogen in the freshwater environment has also been reported [4, 5]. Outbreaks of *E. coli* O157:H7 have led to death, especially in cases involving children and the elderly [6, 7]. Detection and monitoring of the pathogens is not only critical to prevent outbreaks of related diseases but also important to determine the physiological activities of the pathogenic bacteria in the natural environment [5]. Researchers are continuously searching for tools that are fast, accurate, and sensitive for detecting pathogenic microorganisms.

Traditionally, a culturing methodology is the gold standard for food-borne pathogens, but it is time consuming and less accurate for certain types of pathogens (*e.g.*, *E. coli* O157:H7) [8]. Along with the culturing method, antibody-based methods are often used for the identification of specific microorganisms. The basic principle of the antibody-based detection (immunoassay) is the binding of antibodies to a target antigen, followed by the detection of the antigen-antibody complexes. The most important characteristic of an antibody is the ability to recognize only the target antigen in the presence of other microorganisms. This is critical for the selective identification of

specific bacterial cells because there are many situations where a small number of pathogenic cells coexist with large numbers of non-pathogenic microorganisms in a complex biological environment. Of antibody-based methods, the enzyme-linked immunosorbent assay (ELISA) is one popular tool that based on amplification of fluorescent product by an enzymatic reaction between a substrate and an enzyme-labeled antibody conjugate [9-11]. However, this technique often involves lengthy fluid handling steps [12].

Towards the selective identification of cells, another technique, Fluorescence-Activated Cell Sorting (FACS) has been developed and is frequently used when appropriate fluorescently labeled antibodies (FAbs) exist [13-16]. In this technique, FAbs are introduced as a reagent for the immuno-conjugation with cells. The high specificity of the FAbs ideally ensures that only the target cells are fluorescently labeled. Coupling to the LIF detection, the cells of interest can be identified and sorted by a sorting device (*e.g.*, flow cytometer). In recent years, microchip-based FACS techniques for the analysis of cells have been developed [17]. For instance, according to McClain *et al.* [18], the flow cytometry of *E. coli* cells labeled with nucleic acid stains or fluorescein-labeled antibody was performed on microfluidic devices. The labeled cells were counted at rate from 30 to 85 Hz using that microfabricated flow cytometer. According to Fu *et al.*[14, 19], disposable cell sorters were microfabricated using the soft lithography technique [20]. A throughput of 20 cell/s was obtained using the microfabricated flow cytometry, which was considerably slower than conventional FACS. Both conventional FACS and microfabricated FACS are single-cell techniques, which means those techniques rely on spatially isolating single target cells from mixed population and therefore tend to be time-consuming.

As discussed in Chapter 5, capillary electrophoresis equipped with UV detection [21, 22] or LIF detection [23-25] has been utilized in recent years for bacterial cell separations at the population level. However, the CE separations of different bacterial populations are possible only when sufficiently large differences exist in their electrophoretic mobilities (μ_{EP}). Since cells typically exhibit a wide distribution of charge, size, and shape, all of which can vary with experimental conditions and time, a broad and irregular peak shape is often obtained for a single sample. Some reports in the recent literature demonstrated

sharp-peak separations of bacterial cells by CE [23-25]. As discussed in Chapter 5, however, they were false separations. Additionally, in real food, environmental water or clinical samples, various kinds of bacteria cells co-exist. Using the CE-based cell separation techniques, an excessive number of peaks of interfering bacteria, residual fats, proteins, and carbohydrates may be observed in the same run [8]. In such cases, the selective identification of target cells will be difficult because of possible overlapping of peaks.

Another technique that couples the immunoassay to the CE separation for the identification and quantification of certain types of cells has been reported. Based upon a combination of immunofluorescent staining and capillary electrophoresis, Kourkine *et al.* reported two approaches for the detection of *E. coli* O157:H7 by CE [8]. The CE was performed in fused silica capillaries (75 μm ID; total length, 27 cm; effective length, 22 cm) filled with 0.1% (w/v) solution of poly-Duramide in a 10 mM TBE buffer. The electric field for separation was 370 V/cm. In the direct approach, a peak of *E. coli* O157:H7 labeled with fluorescein-tagged specific antibodies were detected on the electropherogram of the CE, while in the indirect approach fluorescein-tagged specific antibodies were first captured by *E. coli* O157:H7 bacteria and then released and detected by CE, indicating the existence of the bacterial cells in the original samples. According to Shintani *et al.* [26], the selective identification of *Salmonella enteritidis* was demonstrated using a fluorescence-tagged antibody by a CE-LIF system. The CE was performed in fused-silica capillaries (75 μm ID; total length, 31 cm; effective length, 21 cm) filled with a TBE buffer (100 mM Tris, 100 mM boric acid, and 2 mM EDTA, pH 8.4) containing 0.01% sodium alginate and 0.2% NaCl. The electric field for the separation was 320 V/cm. On the electropherogram of the reaction mixture of the antibody (Anti-*Sal-CSA*-1) and *Salmonella enteritidis,* two peaks were detected within 10 minutes of the electrophoresis, representing the free antibody and the labeled bacterial cells respectively.

The aforementioned technique that couples immunofluorescent staining to CE has showed promise for selective cell identifications at population level. However, we have not seen any reports of this technique for the identification of cells on microchips in the literature. In the previous chapter, we demonstrated the separation of biological cells on

microchips solely based on the difference of their electrophoretic mobilities. Coupling CE to immunofluorescent staining on microchips may offer better selectivity and accuracy for the identifications of cells of interest. Since the microchip-based system may enable us to accurately detect a small quantity of bacterial cells on a compact device within a short time, it could be a powerful tool for clinical, environmental and industrial microbiology. In this chapter, we will present preliminary work towards rapid and simple bacterial cell identification based on immunofluorescent labeling and CE separation on microchips.

6.2 Materials and Methods

6.2.1 Reagents

GeneScan® polymer (7%, P/N: 401885) was obtained from Applied Biosystems (Foster City, CA, USA). A Tris-borate with EDTA buffer (TBE) was made with Tris base and boric acid from Fisher Scientific (Fair Lawn, NJ, USA) and EDTA from Merck (Darmstadt, Germany). The running buffer, referred to as "1TBE10G", was made with the glycerol from Sigma-Aldrich (St Louis, MO, USA) and the TBE buffer so that the final concentration of glycerol was 10% (w/w), and the TBE was 1×TBE (pH: ~8.3). A 10× dilution of the 1TBE10G was made by adding MilliQ water into the 1TBE10G. The separation medium was 5% (w/w) GeneScan® polymer and 10% (w/w) Glycerol in 1×TBE buffer (referred to as "5GS10G").

6.2.2 Bacteria Washing and Labeling

Escherichia coli O157:H7 (heat-killed, 10^6 ea/μl, suspended in 1×PBS) and Cy5-tagged anti-*E. coli* monoclonal antibody (FAb*, 0.125 μg/μl, suspended in 1×PBS) were kindly supplied by Dr. M. Suresh (Pharmacy and Pharmaceutical Science, University of Alberta). Upon receipt, aliquots were made of the *E. coli* O157 sample and the FAb sample into autoclaved 0.2-ml PCR tubes using a micropipette mounted with top-line filtered (aerosol resistant) tips. After the aliquoting, the *E. coli* sample was stored in the

* In this chapter, the abbreviation of fluorescence-tagged antibody is "FAb"; "Fab" is a fragment of antibody described in page 104.

refrigerator (~ 4 °C) for biohazard materials. The antibody tubes were covered with foil and stored in a freezer (~ -20 °C). Once a tube of the frozen FAb sample was thawed to the room temperature, it was discarded after being used for the day.

Dilutions of the FAb suspension were made by adding suitable volume MilliQ water into the stock FAb suspension. An aliquot of *E. coli* was centrifuged at 7600 rpm (Eppendorf Centrifuge, Model 5415D) for 5 minutes. The supernatant was carefully removed using a micropipette, and the pellet of cells was resuspended in 1×TBE, followed by a 30 second vortex step. This washing process for non-labeled cells was then repeated 2 times. After the washing, the suspension of *E. coli* (10^6 ea/μl) was then added into a volume of the stock FAb suspension (0.125 μg/μl) to obtain a final ratio of 0.25 μg of the antibody per 10^6 cells (otherwise unless specified). The resulting mixture was incubated in the dark at room temperature for 2 hours. Prior to CE, the mixture was centrifuged at 7600 rpm for 5 minutes. The supernatant was removed and discarded into a biohazard liquid waste. The pellet of cells was resuspended in 1 ×TBE. This washing process (including centrifugation and resuspension) for labeled cells was repeated 2 times.

After experiments, all the used suspensions of cells and FAbs were transferred into a 10% bleach solution (less than 8 hours old) using a micropipette. The bleach solution was disposed of down the drain after 12 hours or more. Microchips exposed to the cell or FAb suspensions were stored in 70% ethanol in plastic tubes overnight. Before the next use, the chip was rinsed with distilled water.

6.2.3 Microchips and Microfluidic Tool Kit

Standard microchips were used in this work. Refer to section 2.2.2 of Chapter 2 for the descriptions of the standard microchips and the Microfluidic Tool Kit. Microchip performance assessment (Chapter 2) was performed after 3~5 CE runs of the samples containing FAbs (otherwise specified). Microchip rejuvenation was performed once performance degradation found (Chapter 3).

6.2.4 Microchip Loading

Refer to section 2.2.3 of Chapter 2 for the microchip loading procedure. The reagent in the sample waste well, the buffer well and the buffer waste well were loaded with 1TBE10G (3 μl). The sample well was loaded with 10× dilutions of the 1TBE10G (2.7 μl) and a FAb suspension (0.3 μl) in experiments for the FAbs separations. The sample well was loaded with labeled cell suspension (3 μl) in experiments of labeled cell separations.

6.2.5 Fluorescence Microscopy

Fluorescence Microscopy was performed using a Zeiss AxioVert 200 inverted microscope (Carl Zeiss) equipped with a fluorescence filter set (Chroma 41008) and a camera (Hamamatsu EM-CCD C9100) for image acquisition.

6.3 Results and Discussions

6.3.1 Separation of FAbs

As aforementioned in Chapter 2 and 3, the microchannel was dynamically coated with GeneScan polymer and the EOF was negligible (refer to discussions in Chapter 2 and 3). Therefore, the apparent migration direction of the FAbs during the electrophoresis was determined by their surface charges only. In a preliminary injection experiment, the detection point was placed at the intersection of the channels. The sample waste well was connected to 200 V and the sample well was connected to ground, while the other two wells were electrically disconnected. Upon application of the electric field in the injection channel, the fluorescence signal was detected after ~20 seconds, indicating the arrival of the front of the FAb stream. The observation suggested that FAbs were negatively charged under the specified CE conditions. Since the injection of the sample was in itself a type of separation [27], the constituent having highest mobility in the FAb sample reached the intersection first; the constituents having relatively lower mobilities reached the intersection later. In order to ensure that all constituents of the sample reach the intersection and participate the consequent separation, the injection time was set to 60 seconds under an electric field of 250 V/cm.

In the subsequent separation step, the buffer waste well was connected to 6 kV, and the buffer well was connected to ground, while the other two wells were electrically disconnected. Upon application of the electric field (706 V/cm) in the separation channel, FAbs confined in the intersection during the injection started to migrate towards the buffer waste well. As shown in Figure 6.1, the electropherogram of the FAb separation showed multiple peaks with various intensities (the relative fluorescence unit (RFU) of the highest was ~3 V when the concentration of the FAb was 0.125 μg/ml and PMT gain was 0.8 V). The first peak arrived at the detection point (4 cm downstream from the intersection) after ~50 seconds under an electric field of ~706 V/cm. It took the last peak ~150 seconds to reach the detection point (see Figure 6.1).

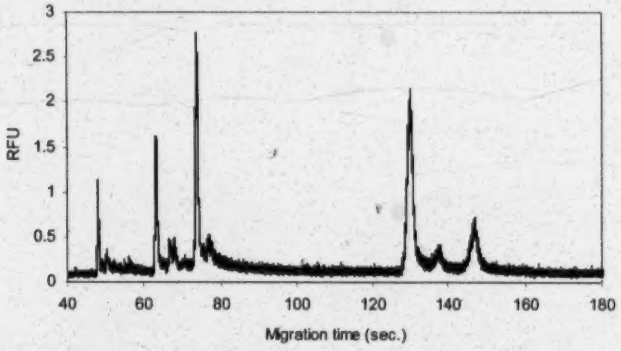

Figure 6.1 Electropherogram of the FAbs separations on a microchip. The concentration of the FAbs was 0.125 μg/ml (1000x dilution of the stock suspension). PMT gain was 0.8 V. Separation DC field was 706 V/cm. Detection point was 4 cm from the intersection.

A series of injections and separations of the FAbs with various concentrations (including 10×, 100×, and 1000× dilution of the stock FAbs) was performed on microchips. The peak profiles obtained were almost identical (except the signal intensities due to the change of concentration of the FAbs). It was found that if the sample concentration was higher than 12.5 μg/ml the peaks after 120s in Figure 6.1 could not be resolved completely. Additionally, the microchip had to be rejuvenated (following the procedure described in Chapter 3) after each CE run in order to achieve repeatable peak profiles. Figure 6.2 shows the electropherograms of 3 consecutive runs on the same chip without change of the separation medium. Progressively raised baselines and shifted migration times of the peaks were observed in those electropherograms. (For instance, the

signal intensity at 40s in the electropherogram of the 1st run was ~0.1 V; it was ~0.4 V in the 2nd run; it became ~1 V in the 3rd run.) The last 2 peaks in each run also showed significant tailing. Those anomalies (including rising baseline, tailing and shift of migration velocities) probably resulted from the adsorption of the FAbs on the inner wall of the microchannel. Using the rejuvenation protocol described in chapter 3, the chip performance was fully recovered and repeatable FAb profiles were obtained (for lower concentrations of FAb, see Figure 6.3).

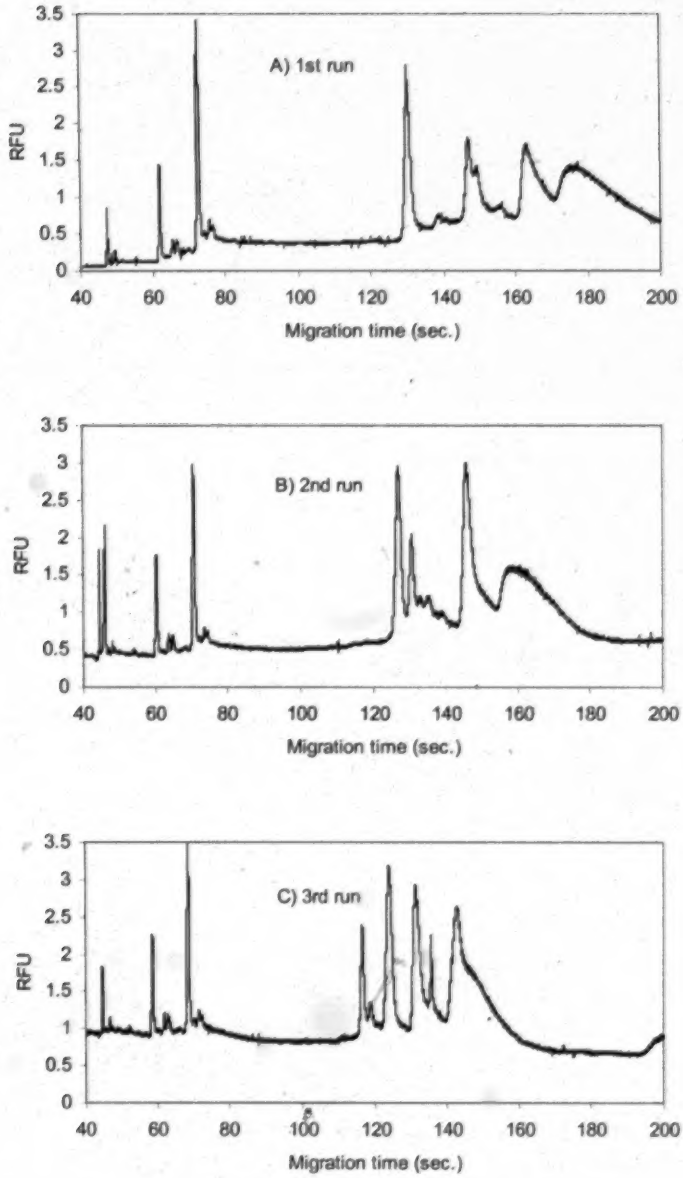

Figure 6.2 Electropherograms of the separation of the FAbs in 3 consecutive runs. A) The 1st run; B) the 2nd run; C) the 3rd run. The concentration of the FAbs was 12.5 μg/ml. PMT gain was 0.6 V. Separation DC field was 706 V/cm. Detection point was 4 cm from the intersection.

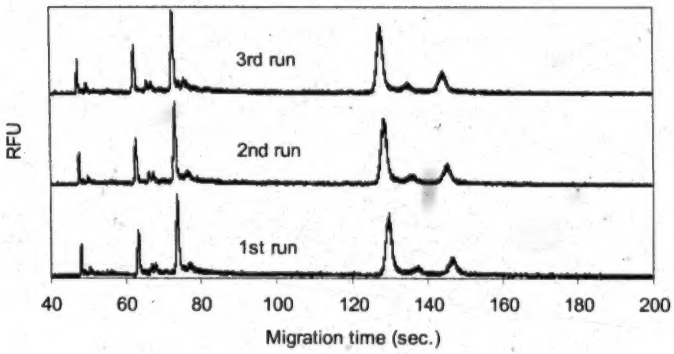

Figure 6.3 Electropherograms of the separation of the FAbs in 3 consecutive runs. A) The 1st run; B) the 2nd run; C) the 3rd run. The concentration of the FAbs was 0.125 μg/ml. PMT gain was 0.8 V. Separation DC field was 706 V/cm. Detection point was 4 cm from the intersection. The chip was not rejuvenated after the runs.

The peak profiles of the FAbs under various intensities of the electric fields were also studied. In a number of CE runs of the FAbs, the separation voltage connected to the buffer waste well was set to 6 kV, 4.5 kV, and 3 kV respectively. As shown in Figure 6.4, the velocities of the peaks in each run decreased with the separation voltage. However, the number and shape of the peaks among those runs were almost identical, indicating the multiple-peak separations were not associated with the application of high voltages causing disassociations of the FAbs.

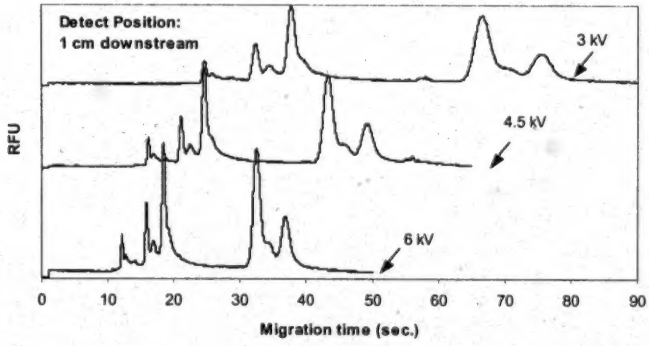

Figure 6.4 Electropherograms of the FAbs under various DC field intensities. The concentration of the antibody was 0.125 μg/ml. PMT gain was 0.8 V. Detection point was 1 cm from the intersection. Separation DC fields were 706, 529 and 353 V/cm.

As shown in Figure 6.1, the apparent migration time (and so the velocity) of those peaks in the electropherogram varied widely from ~50 s to ~150s. In order to prove that all those peaks represent active FAbs, the FAbs were incubated with *E. coli* cells (~1.25 × 10^{-9} μg FAb per cell) for more than 3 hours in an experiment. After the incubation, the mixture was centrifuged at 7600 rpm for 5 minutes to spin down the cells. An aliquot of the supernatant was then analyzed by CE under identical conditions to the FAbs before incubation. It was found that the intensity of all peaks decreased ~ 40% after the FAbs were incubated with the *E. coli* cells (data not shown), suggesting that all the peaks were involved in the immuno-reactions with the *E. coli* cells.

According to Yeung *et al.* [28], each antibody molecule usually contains more than one site that can be labeled with a fluorescence probe. Different antibody molecules may be bonded with various number of the probes [28]. The fluorescence-labeled FAb molecules may have different charges and therefore different mobilities in CE. Due to the heterogeneity of antibodies, even highly purified monoclonal antibodies would yield a broad or multiple peaks representing labeled antibody molecules [29-32]. For instance, Hunt and Nashabeh utilized the CE to separate recombinant humanized monoclonal antibodies (rMAbs) that were labeled with 5-TAMRA under an electric field of ~625 V/cm in capillaries (50 μm ID × 19.4 cm) filled with a sodium dodecyl sulfate sieving medium [30]. Multiple peaks were observed in the electropherograms of the CE. Our observations in CE of the FAbs were in agreement to those previous reports. Attiya *et al.* developed an affinity protection chromatography (APC) procedure and demonstrated the CE of Cy5 labeled monoclonal anti-ovalbumin antibody on microchips [33]. In the APC procedure, the binding sites of antibody were protected by binding to ovalbumin-coupled sepharose beads before labeling. A single peak of the FAb was obtained using the microchip CE.

Since the multiple peaks of the heterogeneous FAbs may interfere with the peak(s) of the target cells and therefore make identification difficult, homogeneous FAbs are required. To eliminate the heterogeneity of antibodies, Fab and Fab' fragment of monoclonal antibodies have been used for capillary electrophoresis-based immunoassays [34, 35]. The antibody molecule in monomeric form is a glycoprotein with a molecular weight of approximately 150 kDa that is shaped like a Y [28]. As shown in Figure 6.5,

basic structure of the monomer consists of two identical halves connected by two disulfide bonds. Each half is made up of a heavy chain of approximately 50 kDa and a light chain of approximately 25 kDa, joined together by a disulfide bond. The heavy chain is divided into an Fc portion and a Fab portion. The Fc fragment of the antibody molecule is composed only of heavy chains. The Fab fragment and Fab' fragment of the antibody molecule contains both heavy and light chains joined together by a single disulfide bond. Antibody fragments, Fab and Fab' can be generated by papain and pepsin digestion of the intact antibody respectively (Figure 6.5) [28]. It was reported that those fragments of monoclonal antibodies produced superior results as compared to those obtained using whole antibodies [34, 35].

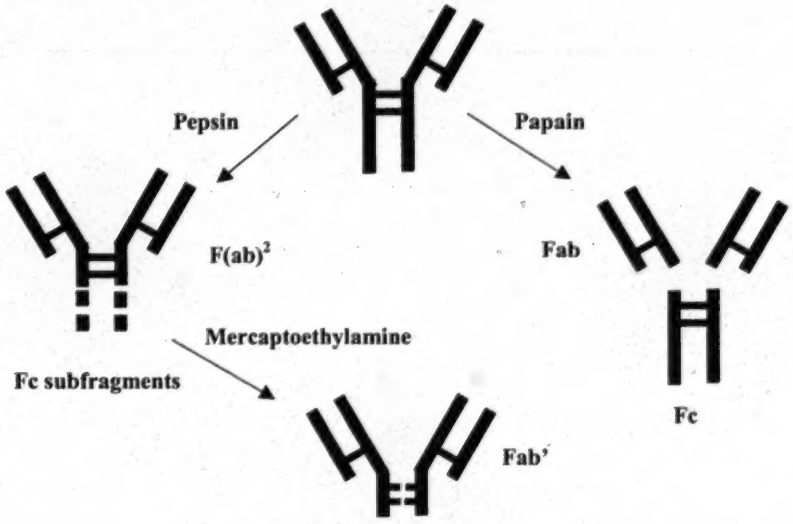

Figure 6.5 Schematic diagram of preparation of antibody fragments, redrawn from [28].

In the Suresh lab, the purity of the fluorescence-tagged antibody was verified using SDS-PAGE (Sodium Dodecyl Sulphate - Polyacrylamide Gel Electrophoresis) analysis. In the SDS-PAGE system, a large pore polyacrylamide gel, called a stacking gel, is layered on top of a separating polyacrylamide gel called a resolving gel. Each gel is made with a different buffer, and the tank buffers are different from the gel buffers (this system is called discontinuous buffer system). The discontinuous buffer system is able to concentrate the protein sample and therefore increases the resolution of the SDS-PAGE [36]. The protocol of the SDS-PAGE involves denaturing the protein sample by heating it in the presence of SDS and a reducing agent. SDS will bind to the protein causing it to

unfold, whereas the reducing agent will reduce the intramolecular and intermolecular disulfide bonds [36]. The separation of the denatured proteins is a separation of individual polypeptide subunit (*i.e.,* heavy chain and light chain) of the proteins. Figure 6.6 shows electropherograms of the SDS-PAGE that were performed in the Suresh lab. In Figure 6.6, the left lane is the markers of known molecular weight. Lane 2 shows the bands of denatured proteins. Two major bands were seen at ~50 kD and ~25 kD (one more band at ~25 kD, it may due to artifacts during the analysis according to the Suresh lab) in the electropherogram, indicating that the heavy chain and the light chain of the monomer were cleaved by the reducing agent and separated based on their size. Lane 1 shows the band of non-denatured proteins in the same electrophoresis system. Since the proteins (*i.e.*, anti-*E. coli* O157, 150 kD) were not dissociated, they could not penetrate the resolving gel, and no complete band was seen in the lane 1. Previous SDS-PAGE analysis of the same antibody (non-fluorescence-tagged) in the Suresh lab showed similar electropherograms (not shown). Those electropherograms suggested that the fluorescence-tagged antibody was pure. In denaturing SDS-PAGE separations, protein migration is determined by molecular weight only [36]. In our CE separation of the antibodies on microchips, the proteins were not denatured. Since the non-denatured proteins migrated through the sieving matrix according to their molecular mass, structural conformation and net charge, the migration behavior of the proteins in the CE on microchips should be more heterogeneous. That probably was the reason why the multiple peaks were detected using the microchip CE for the fluorescence-tagged antibody. Based on this point, the microchip CE may have great potential for high-sensitivity analysis of antibodies.

To fully understand the migration behavior of the fluorescence-tagged antibodies on microchips, more experiments need to be performed in future. For instance, the fluorescence-tagged antibody was suspended in a PBS buffer originally, but the microchip CE of the antibody was performed in 1×TBE. Since the impact from the change of buffer upon the electrophoretic behavior of the antibody is unknown, the microchip CE of the antibody in a PBS buffer needs to be performed in future work.

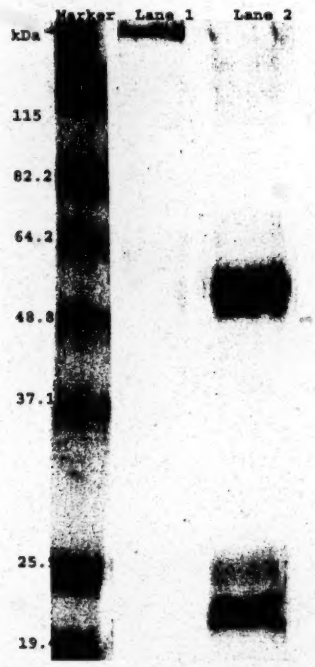

Figure 6.6 SDS-PAGE analysis of purified monoclonal antibody (anti- *E.coli*). Lane 1, non-denatured protein sample; lane 2, denatured protein sample (the reducing agent was 100 mM dithiothreitol). The resolving gel contains 12% (v/v) acrylamide, 0.39 M Tris (pH 8.8), 0.1% (v/v) SDS, 0.1% (v/v) ammonium persulfate, and 0.04% (v/v) TEMED (N,N,N',N'-tetramethylethylenediamine). The stacking gel contains 5% (v/v) acrylamide, 0.13 M Tris, 0.1% (v/v) SDS, 0.1% (v/v) ammonium persulfate, and 0.1% (v/v) TEMED. The electrophoresis buffer contains 0.025 M Tris, 0.25 M glycine (pH 8.3), and 0.1% (v/v) SDS. (Picture courtesy of the Suresh lab)

6.3.2 Detection of *E. coli*-FAb Conjugates

The electrokinetic injection of the labeled E. *coli* cells (E. *coli*-FAb conjugates) was first attempted following a similar procedure to the FAb injections described in section 6.3.1. The detection point was placed at ~150 μm from the sample well in the middle of the injection channel in order to shorten the test time (see Figure 6.7A). The sample waste well was connected to 200 V, and the sample well was connected to ground, while the other two wells were electrically disconnected. As shown in Figure 6.7B, the baseline of the electropherogram rose from ~0.5 V to ~2.5V within a couple of seconds upon application of the electric field along the injection channel. The rising baseline was believed to result from free FAbs in the suspension, which had not bound the cells. (In

the separation step, which will be discussed in the rest of this section, those free FAbs showed separated peaks.) Riding on top of the raised baseline, a series of small peaks were also detected after several seconds. Those small peaks were believed to be the E. *coli*-FAb conjugates. This was supported by microscopic images obtained after the run. After a 20 second injection, the microchip was placed under the fluorescence microscope. The microscope was first focused on a part of the injection channel under a bright field. After the fluorescence excitation light was switched on, the exposure time was adjusted to ~1 second. As shown in Figure 6.7C, bright particles were detected in the injection channel using the fluorescence microscope, indicating that labeled cells had been injected into the channel. The diversity of the intensities in Figure 6.7C indicated that cell clumps might be injected into the channel also, which had a large size and bright fluorescence in the image. The existence of cell clumps was not confirmed by direct observations due to the limited magnification of the microscope and small size of the cells (~0.5 μm).

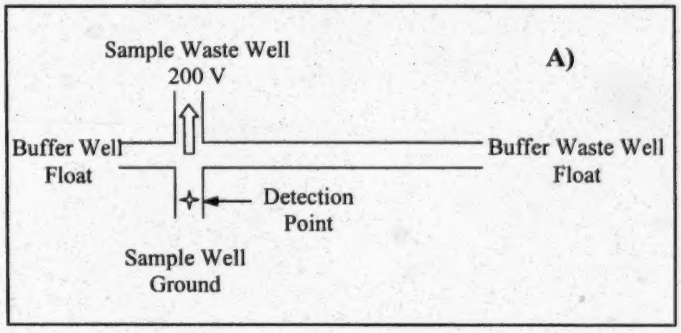

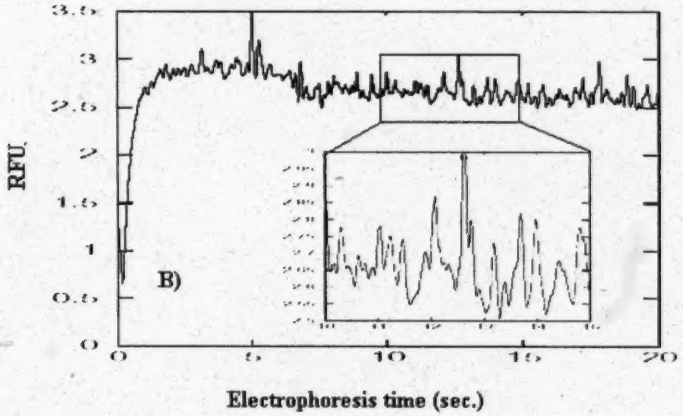

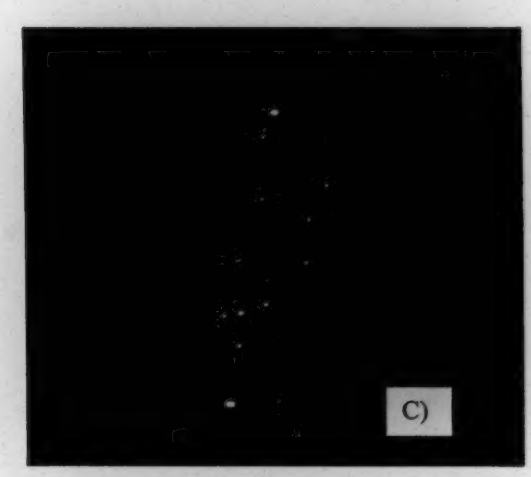

Figure 6.7 A) Schematic description of the microchip during injection of the labeled cells. Arrow in the channel indicates the cell migration direction. B) Electropherogram of the injection. PMT gain was 0.8 V. Detection point was at 150 μm from the sample well. C) Fluorescence images of the labeled cells in the injection channel under the fluorescence microscope. Microscope objective magnification: 40×; reflector for the fluorescent image: Cy5, TOPRO3; exposure time for the fluorescent image: 1 s.

Since the labeled *E. coli* cells were observed migrating towards +ve electrode, they were believed to be negatively charged under the specified CE conditions. In the experiments of labeled cell separations, the detection point was placed at 5 mm from the intersection in the middle of the separation channel. During the separation, the buffer waste well was connected to 2 kV, the buffer well was connected to ground, while the sample well and the sample waste well were connected to 220 V (see Figure 6.8A). As shown on the electropherogram in Figure 6.8B, two bumps were detected at ~22s and ~35s on the electropherogram. By comparing to the electropherogram of the FAb alone in another CE run under the same electrophoresis conditions (data not shown), these two bumps were confirmed to be the free FAb in the sample. It was noticed that the peak profile of the FAb in this experiment was different from that described in section 6.3.1. That probably indicates that the separation length in this experiment (5 mm) was too short to allow the FAbs to separate effectively into more peaks as the separations described in section 6.3.1 (which were detected at 4 cm from the intersection). We found that the signal intensity of the free FAbs in the electropherogram was strong. According to Kourkine *et al.* [8], the free FAb was still detectable even after 7 washes, and more washes resulted in the loss of signal intensities of the labeled cells. They attributed the

incomplete removal of the free FAbs from the bacterial sample to the breakage of some cells during vortexing and the release of a small amount of FAbs [8].

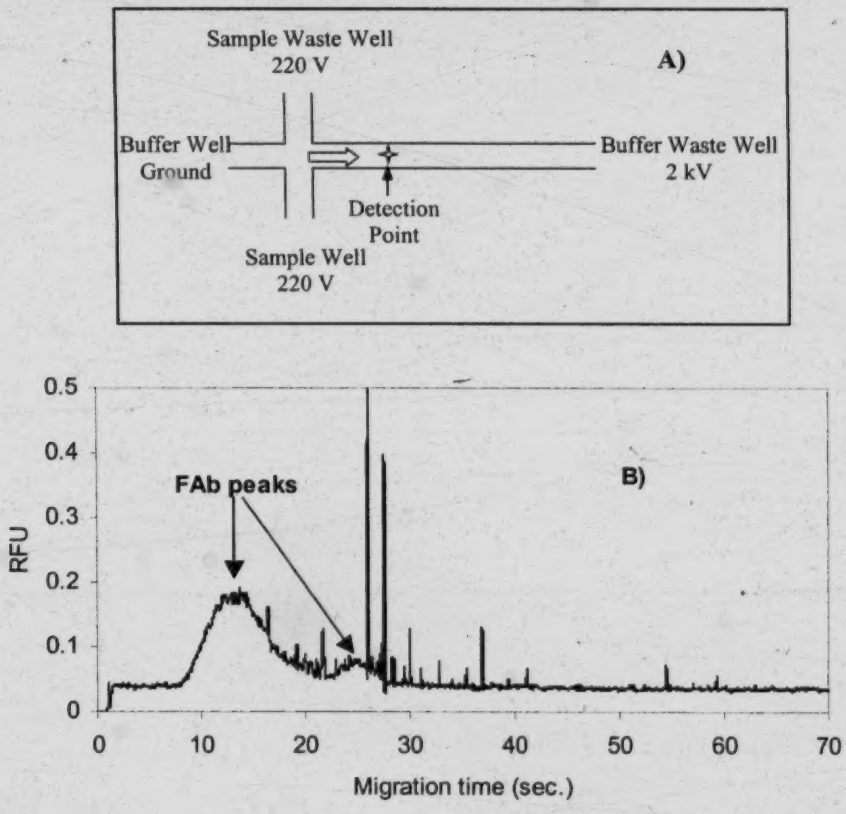

Figure 6.8 A) Schematic description of the microchip during the separation of the FAb labeled *E. coli*. The arrow indicates the direction of the cell migration. B) Electropherogram of the separation of the labeled *E. coli*. Separation medium was 5GS1TBE; the separation DC field was 235 V/cm, with pullback voltages of 220V; PMT gain was 0.8 V; detection point was 5 mm from the intersection.

On the same electropherogram of Figure 6.8B, some small peaks with various intensities were also detected after ~25s. Those small peaks were believed to be the *E. coli*-FAb conjugates. This was confirmed by the images of the conjugates in the separation channel subsequently obtained using a fluorescence microscope. After a 30s separation under an electric field of 235 V/cm, the microchip was placed under the fluorescence microscope. A band of bright particles in the separation channel was detected using the fluorescence microscope (data not shown). Both the fluorescent images and the peaks of labeled cells in the electropherogram showed wide distributions.

In another experiment, *E. coli* cells were incubated with 10 μM To-Pro-3 for 5-minute followed by washings (as described in section 6.2.2). The To-Pro-3 stained *E. coli* cells were separated in 5GS1TBE by CE. After a 10 second separation under an electric field of 235 V/cm, the microchip was placed under the fluorescence microscope. As shown in Figure 6.8, a wide distribution of bright fluorescent particles in the separation channel after the 10-second separation was detected under the microscope. We had no quantified comparisón of the mobilities between the FAb labeled and To-Pro-3 labeled cells, but both of them showed a broad distribution, indicating the broad distribution of the *E. coli* cells was associated not with the labeling method but with the intrinsic heterogeneity in cell mobility.

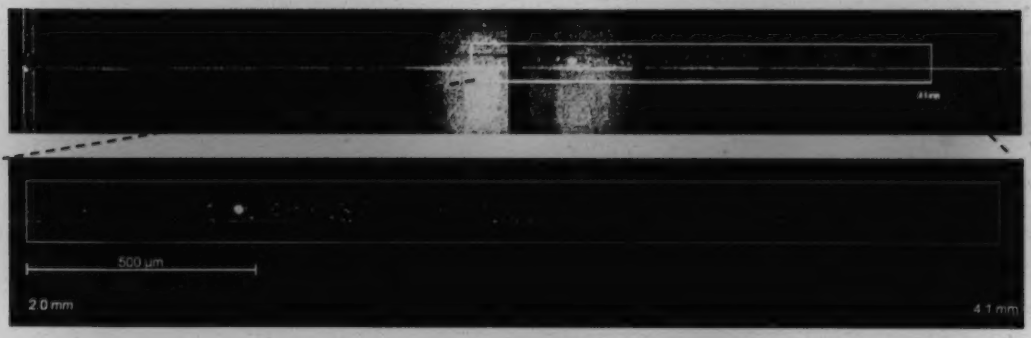

Figure 6.9 Images of To-Pro-3 stained *E. coli* cells in the separation channel after a 10-second separation. Separation medium was 5GS1TBE. Separation voltage was 2.5 kV with pullback 250 V. *E. coli* cells were incubated with 10 μM To-Pro-3 for 5 minutes. Microscope objective magnification: 40×; reflector for the fluorescent image: Cy5, TOPRO3; exposure time for the fluorescent image: 1 s.

According to Pfetsch *et al.* [21], the mobility variation of bacteria is influenced by the ionic strength of the separation medium of the CE. They obtained the narrowest bands of bacterial cells at low ionic strength. They also found that with increasing ionic strength, more and more cells were destroyed giving widened bands with small peaks riding on the main peak. Similar discussions on this topic were also given in [21, 37, 38].

Since the cells had been stored for a long time (> 3 months at ~ 4 °C), the wide distribution of the cell band in the CE was probably due to the existence of cell fragment and debris. Unfortunately, we were not able to confirm the integrity of the cells under the microscope due to the limited microscope magnification.

6.3.3 Specificity of the FAbs

The bright images of the *E. coli*-FAb conjugates (in Figure 6.7C) indicated that the FAbs had high affinity for the *E. coli* cells. (They were not FAb clumps because the FAb bands were narrow as shown in Figure 6.1.) This high affinity will provide a highly sensitive detection of the target cells and eliminate possible false-negative results. However, unless specific enough, the antibodies may bind to other cells well enough to create false-positive results. Therefore, the specificity of the FAbs has to be evaluated.

Yeast cells were used as the control sample in our experiments to evaluate the specificity of the FAbs. 1 mg baker's yeast was dispersed into 1 ml 1×TBE. About 30 minutes later, an aliquot of the yeast suspension (5 μl) was added into 5 μl of the stock FAb suspension. After a one-hour incubation in the dark at room temperature, the mixture was centrifuged at 3600 rpm for 2 minutes. The pellets of the yeast cells were resuspended in 10 μl 1×TBE. The washing process was repeated 2 times before an aliquot (~3 μl) of the yeast cells was transferred onto a microscope slide using a micropipette. The yeast cells were then inspected under a fluorescence microscope. A picture of the yeast cells in the droplet under a bright field was taken (Figure 6.10B). The fluorescence image of the cells in the same location was then taken (Figure 6.10A). As shown in Figure 6.10A, bright fluorescence was detected from the yeast cells, indicating that the FAbs had bound to the cells.

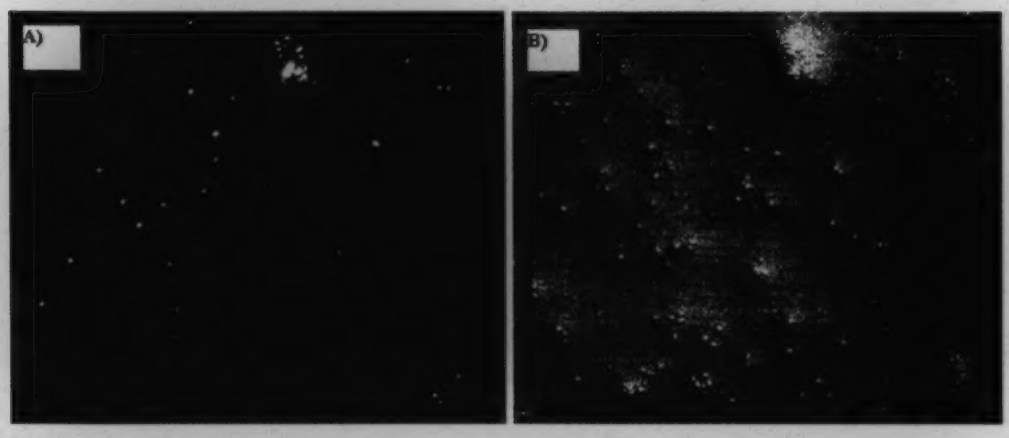

Figure 6.10 Figure 6.10 A) Fluorescence of yeast cells after incubation with the stock FAbs. B) Image of the yeast cells in a bright field. Microscope objective magnification: 20×; reflector for fluorescent image:

Cy5, TOPRO3; exposure time for fluorescent image: 1 s; halogen lamp voltage for bright field image: 1.5 V.

In Chapter 5, we mentioned that positive-charged dye molecules might be attracted to the surface of the negative-charged cells and therefore a weak fluorescence was detected from the cells (*e.g.*, RBC). In this experiment, yeast cells were negatively charged in the 1×TBE (as discussed in Chapter 5). As aforementioned in the section 6.2.1, the FAbs were negatively charged also. Therefore, the fluorescence detected from the yeast cells did not result from an electrostatic association of the FAbs in this case. According to the Suresh lab, this non-specific binding is common unless prevented by the use of a procedure that absorbs any weakly binding antibody on a sacrificial substrate such as milk or BSA. A procedure suggested by the Suresh lab is:

1) Suspend 1 mg dry yeast in 1 ml 2% milk, or in a solution of 1% BSA and 1×TBE.
2) Add 5 μg antibody sample into the yeast suspension and then vortex the mixture for 30 seconds.
3) Cover the container with an aluminum foil and incubate the mixture 3 hours at room temperature.
4) Wash the yeast cells 2 times with distilled water following the procedure described in section 5.2.2 in Chapter 5.
5) Suspend the yeast cells in water
6) Inspect the cells on a microscope slide under a fluorescence microscope. The detection of fluorescence on the yeast cells could indicate the specificity of the antibody.

Due to limited time, the proposed test was not performed.

6.4 Conclusions

The injections and separations of the FAbs were demonstrated on microchips. An excellent repeatability was achieved. Peak profiles showed clearly the electrophoretic heterogeneity of the FAbs. To make the identification of target cells easier, FAbs that are more homogeneous are desirable. Besides the homogeneity of the FAb, the binding specificity was also evaluated. Unfortunately, we found that FAbs binding was non-

specific, which was probably due to degradation of FAb performance by prolonged storage.

Preliminary injection and separation protocols have been established for the manipulations and labeling of cells. The FAb-labeled E. *coli* cells were detected by both the CE-LIF system and the fluorescence microscopy, and these showed a wide distribution of cell mobilities. Since the integrity of the cells was not clearly verified due to the limitations of instrument, and debris and damaged cells may exist in our cell samples, experiments with conformed intact cells and fresh FAb samples need to be conducted in future work to confirm our results.

The technique that couples the immunofluorescent staining to CE is a novel technique for the cell identification. Further development of this technique from the conventional capillaries to microchips will make it a powerful tool for clinical, environmental and industrial microbiology.

6.5 References

[1] A. M. McNamara, *Journal of Urban Health-Bulletin of the New York Academy of Medicine* 1998, 75, 503-505.

[2] D. Ivnitski, I. Abdel-Hamid, P. Atanasov, E. Wilkins, *Biosensors & Bioelectronics* 1999, 14, 599-624.

[3] R. L. Buchanan, M. P. Doyle, *Food Technology* 1997, 51, 69-76.

[4] G. B. J. Dubelaar, P. L. Gerritzen, A. E. R. Beeker, R. R. Jonker, K. Tangen, *Cytometry* 1999, 37, 247-254.

[5] Y. Tanaka, N. Yamaguchi, M. Nasu, *J. Appl. Microbiol.* 2000, 88, 228-236.

[6] J. K. Varma, K. D. Greene, M. E. Reller, S. M. DeLong, J. Trottier, S. F. Nowicki, M. DiOrio, E. M. Koch, T. L. Bannerman, S. T. York, M. A. Lambert-Fair, J. G. Wells, P. S. Mead, *Jama-Journal of the American Medical Association* 2003, 290, 2709-2712.

[7] M. G. Bruce, M. B. Curtis, M. M. Payne, R. K. Gautom, E. C. Thompson, A. L. Bennett, J. I. Kobayashi, *Archives of Pediatrics & Adolescent Medicine* 2003, 157, 1016-1021.

[8] I. V. Kourkine, M. Ristic-Petrovic, E. Davis, C. G. Ruffolo, A. Kapsalis, A. E. Barron, *Electrophoresis* 2003, 24, 655-661.

[9] T. Vo-Dinh, M. J. Sepaniak, G. D. Griffin, J. P. Alarie, *ImmunoMethods* 1993, 3, 85-92.

[10] P. R. Selvaganapathy, E. T. Carlen, C. H. Mastrangelo, *Proc. IEEE* 2003, 91, 954-975.

[11] A. Benkert, F. Scheller, W. Schossler, C. Hentschel, B. Micheel, O. Behrsing, G. Scharte, W. Stocklein, A. Warsinke, *Analytical Chemistry* 2000, 72, 916-921.

[12] A. K. Deisingh, M. Thompson, *J. Appl. Microbiol.* 2004, 96, 419-429.

[13] B. Yao, G. A. Luo, X. Feng, W. Wang, L. X. Chen, Y. M. Wang, *Lab on a Chip* 2004, 4, 603-607.

[14] A. Y. Fu, H. P. Chou, C. Spence, F. H. Arnold, S. R. Quake, *Analytical Chemistry* 2002, 74, 2451-2457.

[15] L. M. Fu, R. J. Yang, C. H. Lin, Y. J. Pan, G. B. Lee, *Analytica Chimica Acta* 2004, 507, 163-169.

[16] P. S. Dittrich, P. Schwille, *Analytical Chemistry* 2003, 75, 5767-5774.

[17] D. Huh, W. Gu, Y. Kamotani, J. B. Grotberg, S. Takayama, *Physiol. Meas.* 2005, 26, R73-R98.

[18] M. A. McClain, C. T. Culbertson, S. C. Jacobson, J. M. Ramsey, *Analytical Chemistry* 2001, 73, 5334-5338.

[19] A. Y. Fu, C. Spence, A. Scherer, F. H. Arnold, S. R. Quake, *Nat. Biotechnol.* 1999, 17, 1109-1111.

[20] Y. N. Xia, G. M. Whitesides, *Annual Review of Materials Science* 1998, 28, 153-184.

[21] A. Pfetsch, T. Welsch, *Fresenius Journal of Analytical Chemistry* 1997, 359, 198-201.

[22] R. C. Ebersole, R. M. McCormick, *Bio-Technology* 1993, 11, 1278-1282.

[23] D. W. Armstrong, M. Girod, L. F. He, M. A. Rodriguez, W. Wei, J. J. Zheng, E. S. Yeung, *Analytical Chemistry* 2002, 74, 5523-5530.

[24] D. W. Armstrong, J. M. Schneiderheinze, *Analytical Chemistry* 2000, 72, 4474-4476.

[25] D. W. Armstrong, J. M. Schneiderheinze, J. P. Kullman, L. F. He, *Fems Microbiology Letters* 2001, 194, 33-37.

[26] T. Shintani, K. Yamada, M. Torimura, *Fems Microbiology Letters* 2002, 210, 245-249.

[27] C. Backhouse, H. J. Crabtree, D. M. Glerum, *Analyst* 2002, 127, 1169-1175.

[28] W. S. B. Yeung, G. A. Luo, Q. G. Wang, J. P. Ou, *Journal of Chromatography B-Analytical Technologies in the Biomedical and Life Sciences* 2003, 797, 217-228.

[29] T. S. Raju, J. B. Briggs, S. M. Borge, A. J. S. Jones, *Glycobiology* 2000, 10, 477-486.

[30] G. Hunt, W. Nashabeh, *Analytical Chemistry* 1999, 71, 2390-2397.

[31] J. S. Patrick, A. L. Lagu, *Electrophoresis* 2001, 22, 4179-4196.

[32] N. H. H. Heegaard, S. Nilsson, N. A. Guzman, *J. Chromatogr. B* 1998, 715, 29-54.

[33] S. Attiya, T. Dickinson-Laing, J. Cesarz, R. D. Giese, W. E. Lee, D. Mah, D. J. Harrison, *Electrophoresis* 2002, 23, 750-758.

[34] F. T. A. Chen, *Journal of Chromatography A* 1994, 680, 419-423.

[35] K. Shimura, B. L. Karger, *Analytical Chemistry* 1994, 66, 9-15.

[36] J. Sambrook, D. W. Russell, *Molecular cloning: a laboratory manual,* p13, Cold Spring Harbor Laboratory Press, Cold Spring Harbor, N.Y., 2001.

[37] B. Palenzuela, B. M. Simonett, R. M. Garcia, A. Rios, M. Valcarcel, *Analytical Chemistry* 2004, 76, 3012-3017.

[38] M. Girod, D. W. Armstrong, *Electrophoresis* 2002, 23, 2048-2056.

Summary

The research projects undertaken as part of this thesis have resulted in the development of several techniques that focused on the reliable separation and identification of biological cells on microchips. Those techniques and achievements are briefly summarized below.

A novel technique for microchip performance assessment was developed (Chapter 2). This technique is capable of monitoring the performance of microchips in a manner that does not require special equipment, requires little time, and could make use of virtually any sample for the assessment of electroosmosis flow.

We also developed a method for microchip rejuvenation (Chapter 3). It was found that the effects of glass aging on the performance of microchips were negligible. Since glass microchips can be rejuvenated and thereby be given a long lifetime, it is feasible to explore higher levels of integration and functionality on glass microchips even in applications requiring a low cost-per-test.

In chapter 4 of this thesis, we studied the stability of capillary electrophoresis on microchips. Observations presented in the chapter revealed the limitations of the geometry of microchips and provided a basis for the future design of microchips and microchip operational protocols for cell manipulations.

We successfully demonstrated the separation of biological cells on microchips solely based on electrophoresis (Chapter 5). It was proved that the electrophoretic separation of and selective introduction cells on microchips was feasible and promising. Some preliminary studies towards selective identification of cells based on the specific binding of fluorescence-tagged antibody were also conducted (Chapter 6). We are among the first to demonstrate those techniques on microfluidic devices, and these have tremendous potential for the development of low-cost, high-efficiency, and portable devices in the field of life science and environmental monitoring.